

**Design and Analysis**  
**of a Hybrid Power System for Western Libya**

by

Fathi Mosbah

A Thesis submitted to School of Graduate Studies  
in Partial fulfillment of the Requirements  
for the degree of Master of Engineering

**Faculty of Engineering and Applied Science**  
**Memorial University of Newfoundland**

August 2018

St. John's, Newfoundland, Canada

## Abstract

Renewable energy systems are widely used in the world, as their prices are going down and efficiencies are improving every year. According to energy data from the General Electricity Company of Libya, electricity demand in Libya is growing by about 9 percent every year. An increasing number of power generators is needed to meet the electricity demand and prevent power outages. In this thesis, available renewable energy sources in Bani Walid, Libya, which is part of the western Libya power system, are studied to design a hybrid power system. Optimization results show that a large-scale 76.8 MW PV system with a backup generator and batteries for energy storage can provide reliable power in that area. A detailed system design, optimal location, and stability analysis of the system have been studied and the results are presented in this thesis. The system is sized using Homer ver. 2.68. Results of sensitivity analysis show that irradiance sensitivity of -5, 0, and +5 have more effect on PV sizing than on the batteries. Power system steady-state analysis and power flow calculation are done using PowerWorld. Designed system stability and fault analysis are done using ETAP. Results indicate that the expected maximum voltage drop is only 1.2%. Contingency analysis indicates that an outage of transformer T10 will lead to 130% overloading of T11 and an outage of transformer T13 can cause 108% overloading of T14. Transient analysis results indicate that after a trip, voltage can vary by  $\pm 4\%$ , with a peak variation of  $\pm 12\%$ . The system control methods and suggestions for further work are included in the thesis.

## **Acknowledgements**

First of all, I am grateful to Allah for the well-being and good health that were necessary to complete this research.

I would like to extend my sincere immense gratitude and appreciation to my supervisor Prof. Tariq Iqbal for his useful suggestions and guidance for my research and writing the thesis. I am deeply grateful for his help during my graduate program to pursue my M.Eng Degree.

I express my great gratitude to my mother, father, brother, and sisters for their love and support.

I also would like to express my gratitude to all employees in the General Electricity Company of Libya for providing me all the data needed to complete my research. Also, I take this opportunity to thank all my friends in Canada and Libya for their encouragement and help.

I would like to gratefully acknowledge my home country of Libya, which provided the scholarship that made continuing my master's degree possible.

## Contents

Abstract .....	ii
Acknowledgements.....	iii
Contents .....	iv
List of Tables .....	ix
List of Figures .....	x
List of Abbreviations and Symbols .....	xv
Chapter 1 .....	1
1 Introduction.....	1
1.1 Research on Mini-grid Systems.....	2
1.2 Mini-grid Design Standards .....	3
1.3 Mini-grid System Design Quality.....	4
1.4 Hybrid Mini-grid Systems.....	5
1.5 Libyan Energy Production .....	6
1.5.1 Renewable power sources in Libya .....	10
1.5.1.1 Libya's PV systems.....	10
1.5.1.2 Libya's wind energy.....	13
1.6 Literature review of mini-grid stability.....	14
1.7 Renewable energy system (RES) in Libya.....	21
1.8 Research objectives.....	25
1.9 Thesis Organization .....	26

Chapter 2	28
2 Steady-state analysis of power grid in Western Libya using PowerWorld	28
2.1 An overview of Bani Walid power grid	28
2.2 Power flow analysis at max average loads	30
2.3 Power flow analysis at peak loads	32
2.4 Q-V Curve Analysis	34
2.5 Improvement of power flow of the power grid	36
2.6 Contingency analysis	40
2.7 Chapter summary	41
Chapter 3	43
3 Sizing of a hybrid power system for Bani Walid, Libya	43
3.1 Introduction	43
3.2 Electricity situation in Libya	44
3.3 Electrical Loads in Bani Walid	44
3.4 Renewable Energy Sources in Bani Walid	45
3.4.1 Wind Energy	47
3.4.2 Solar Energy	48
3.5 System Sizing Using Homer	49
3.5.1 System Input Data	50
3.5.2 System Block Diagram	51
3.5.3 Optimized System	52

3.5.4	Economic Optimization Results and Financial Analysis.....	52
3.5.5	Electrical and System Simulation Results .....	55
3.5.6	Sensitivity Analysis .....	59
3.5.6.1	Levelized cost of energy (COE) .....	59
3.5.6.2	Optimal systems.....	62
3.5.6.2.1	Optimal PV system .....	62
3.5.6.2.2	Optimal battery storage.....	64
3.6	Proposed location.....	67
3.7	Conclusion.....	68
Chapter 4	.....	71
4	Impact of a large-scale PV system with ESS and generator sets on a distribution network in Bani Walid.....	71
4.1	Introduction .....	71
4.2	An Overview of the designed hybrid power system.....	71
4.2.1	PV Panels .....	72
4.2.2	PV array calculations .....	74
4.2.3	Required Area for PV Modules.....	78
4.2.4	Cables Sizing.....	80
4.3	Power Flow Analysis of the designed Hybrid Power System.....	84
4.3.1	Load flow analysis methods.....	84
4.3.1.1	Newton-Raphson Method.....	86
4.3.2	Simulation results of power flow.....	87

4.3.2.1	Voltages at Load Buses .....	87
4.3.2.2	Branches loading and losses .....	90
4.3.3	Control of power flow.....	91
4.3.3.1	On Load Tap Changer (OLTC).....	94
4.3.3.2	Control of power flow using automatic voltage-magnitude-regulating transformer.....	95
4.3.3.3	Simulation results.....	96
4.3.3.4	Branches loading and losses .....	100
4.4	Contingency Analysis .....	104
4.4.1	Contingency analysis results .....	105
4.5	Transient stability analysis of the designed hybrid power system .....	108
4.5.1	Control methods .....	111
4.5.2	Simulation results .....	112
4.5.2.1	Trip of utility grid.....	113
4.5.2.2	Trip of PV system .....	114
4.5.2.3	Three phase short circuit at Bus 1 results in tripping the utility grid.....	115
4.5.2.4	Three phase short circuit at Bus 29 results in tripping the PV system.....	117
4.5.2.5	Three phase short circuit at line 11 results in tripping the load No 10 (7.222 MVA) .....	119
4.5.2.6	Power system stabilizer (PSS) performance during transient stability on the designed connected hybrid power system .....	120
4.5.2.7	The performance of automatic voltage-magnitude-regulating transformer on the system during transient stability.....	121

4.6	Conclusion.....	123
Chapter 5 .....		124
5	Conclusion and Future Work .....	124
5.1	Conclusion.....	124
5.2	Contribution.....	126
5.3	Future Work .....	127
References .....		129
Appendix A: Parameters of the governor Woodward UG-8 (UG-8).....		135
Appendix B: Parameters of the exciter IEEE Type AC4 - High-Initial-Response Alternator- Supplied Controlled Rectifier Exciter (AC4).....		135
Appendix C: The parameters of power system stabilizer IEEE Type 1 PSS (PSS1A) .....		136

## List of Tables

Table 1.1 PV Systems and kWp in Libya to 2012.....	12
Table 2.1 Buses information at max average load power flow analysis.....	30
Table 2.2 Buses information at peak load power flow analysis .....	32
Table 2.3 Q-V curve information .....	35
Table 2.4 Power flow results before adding shunt capacitor to buses 8 and 9.....	37
Table 2.5 Power flow results after adding shunt capacitor to buses 8 and 9 .....	37
Table 2.6 Voltages and angles at load buses after improvement of power flows at peak loads	38
Table 2.7 Results of contingency analysis .....	40
Table 3.1 Monthly averaged wind speed at 10 m above the surface of the earth for terrain similar to airports (m/s).....	47
Table 3.2 Monthly averaged insolation incidence on a horizontal surface (kWh/m <sup>2</sup> /day) in Bani Walid at N31.8° E14° .....	48
Table 3.3 System input data .....	50
Table 3.4 Selected system components.....	52
Table 3.5 Cost summary .....	53
Table 3.6 Economics comparison between current case system and base case system .....	53
Table 3.7 Expected electrical output results.....	56
Table 3.8 Expected PV output results.....	57
Table 3.9 Sensitivity variable inputs.....	59
Table 4.1 Inverter specifications.....	74
Table 4.2 PV panel specifications.....	75

Table 4.3 11kV cables length from PV 11-kV substations to the 66-kV PV substation .....	82
Table 4.4 Load buses voltages at average max load and at peak load.....	88
Table 4.5 Transmission line loading and losses .....	91
Table 4.6 Number of steps and tapping steps [11] .....	94
Table 4.7 Regulated voltages at load buses.....	97
Table 4.8 Total losses at transformers for different cases.....	101
Table 4.9 Transmission line loading report after regulating voltages at load buses.....	102
Table 4.10 Cables loading report at average max load after regulating voltages at load buses .....	103
Table 4.11 Loading Violations .....	105
Table 4.12 Voltage Violations.....	106
Table 4.13 Losses during contingency analysis .....	107
Table 4.14 Performance index.....	108

## List of Figures

Figure. 1.1 GECOL power generation fuel percentages in 2012 .....	7
Figure 1.2. GECOL customer load percentages in 2012 .....	7
Figure 1.3 Electricity infrastructure in Libya .....	8
Figure 1.4. Electricity usage in Libya from 2003 to 2012 .....	9
Figure 1.5 Monthly peak loads in Libya in 2010.....	9
Figure 1.6 Libya’s global horizontal irradiance (GHI) .....	11
Figure. 1.7 Power system stability classifications .....	16
Figure 2.1 Bani Walid location.....	29
Figure.2.2. Transmission lines network in Bani Walid.....	29
Figure.2.3. Power flow analysis at max average load.....	31
Figure.2.4. Load flow analysis at peak loads .....	33
Figure 2.5 Q-V curve plot of load buses .....	35
Figure 2.6 Load flow analysis at peak loads with using shunt capacitor.....	39
Figure 3.1 Monthly average and peak loads in 2015 in Bani Walid .....	45
Figure 3.2 Bani Walid location.....	46
Figure 3.3: Average high and low temperature in Bani Walid.....	47
Figure 3.4: Average wind speed in Bani Walid.....	48
Figure 3.5 Global horizontal irradiance in Bani Walid region (GHI).....	49

Figure 3.6 Solar data resources.....	51
Figure 3.7 System block diagram in Homer.....	51
Figure 3.8 Optimization results .....	52
Figure 3.9 Cash flow summary.....	54
Figure 3.10 Comparison of optimal case system and base case system .....	54
Figure 3.11 Cash flows .....	55
Figure 3.12 Monthly average electric production.....	56
Figure 3.13 PV output.....	57
Figure 3.14 Generator sets output.....	58
Figure 3.15 Inverter and rectifier output .....	58
Figure 3.16 Battery bank state of charge .....	59
Figure 3.17 (a): COE at load sensitivities (0, 10, and 20%) and diesel price 0% .....	60
Figure 3.17 (b): COE at load sensitivities (0, 10, and 20%) and diesel price 10% .....	60
Figure 3.17 (c): COE at load sensitivities (0, 10, and 20%) and diesel price 20% .....	61
Figure 3.17 (d): COE at load sensitivities (0, 10, and 20%) and diesel price 30% .....	61
Figure 3.18 Optimal PV (a): At load sensitivities (0,10, and 20%) and diesel price 0% .....	62
Figure 3.18 Optimal PV (b): At load sensitivities (0,10, and 20%) and diesel price 10% .....	63
Figure 3.18 Optimal PV (c): At load sensitivities (0,10, and 20%) and diesel price 20% .....	63
Figure 3.18 Optimal PV (d): At load sensitivities (0,10, and 20%) and diesel price 30% .....	64
Figure 3.19 Optimal PV and Batter system sizing at diesel sensitivity 0%.....	65
Figure 3.20 Optimal battery (a): At load sensitivities (0,10, and 20%) and diesel price 0%...	65

Figure 3.20 Optimal battery (b): At load sensitivities (0,10, and 20%) and diesel price 10%	66
Figure 3.20 Optimal battery (c): At load sensitivities (0,10, and 20%) and diesel price 20%	66
Figure 3.20 Optimal battery (d): At load sensitivities (0,10, and 20%) and diesel price 30%	67
Figure 3.21 Proposed location for PV modules.....	68
Figure 4.1 Block diagram of the designed hybrid power system .....	72
Figure 4.2 PV module parameters .....	73
Figure 4.3 Configuration of PV arrays.....	77
Figure 4.4 Schematic circuit diagram of the 76.8 MW PV power station .....	78
Figure 4.5 (a): Arrangement of a large number of rows of fixed modules .....	79
Figure 4.5 (b): Configuration of fixed PV array.....	80
Figure 4.6 Field design for the proposed PV system .....	83
Figure 4.7 Power flow analysis of the hybrid power system .....	89
Figure 4.8 Generator Thevenin equivalent.....	93
Figure 4.9 Voltage-magnitude-regulating transformer .....	94
Figure 4.10 Load Tap changer.....	95
Figure 4.11 Load Flow analysis after automatic voltage regulation.....	98
Figure 4.12 Power flow at maximum average loads	
(a) Power flow at base case .....	99
(b) Power flow with automatic voltage regulator.....	99

Figure 4.13 Power flow at peak loads	
(a) Power flow at base case.....	100
(b) Power flow with automatic voltage regulator.....	100
Figure 4.14 Woodward UG-8 (UG-8).....	111
Figure 4.15 IEEE Type AC4 - High-Initial-Response Alternator-Supplied	
Controlled Rectifier Exciter (AC4) .....	111
Figure 4.16 IEEE Type 1 PSS (PSS1A).....	112
Figure 4.17 Trip of utility grid, (a) Bus 2 and Bus12 voltage (%) .....	113
Figure 4.17 Trip of utility grid, (b) Generators absolute power angle.....	114
Figure 4.18 Trip of PV system, (a) Generators absolute power angle.....	115
Figure 4.18 Trip of PV system, (b) Bus 2 and Bus12 voltage (%).....	115
Figure 4.19 Three phase short circuit at Bus 1, (a) Generators' absolute power angle .....	116
Figure 4.19 Three phase short circuit at Bus 1, (b) Bus 2 and Bus12 voltage (%).....	116
Figure 4.20 Three phase short circuit at Bus 29, (a) Generators' absolute power angle .....	117
Figure 4.20 Three phase short circuit at Bus 29, (b) Bus 2 and Bus12 voltage (%).....	118
Figure 4.20 Three phase short circuit at Bus 29, (c) Bus 2 and Bus12 frequency (%).....	118
Figure 4.21 Three phase short circuit at line 11, (a) Generators' absolute power angle .....	119
Figure 4.21 Three phase short circuit at Bus 29, (b) Bus 2 and Bus12 frequency (%).....	119
Figure 4.22 Generators' absolute power angle with and without PSS after three-phase short	

circuit at Bus 29.....	120
Figure 4.23 (a) Voltages at bus 2 and load bus 3 with automatic voltage-magnitude	
-regulating transformer .....	121
Figure 4.23 (b) Voltages at bus 2 and load bus 3 without automatic voltage-magnitude-	
regulating transformer .....	122
Figure 4.24 Voltage plot at all load buses after trip of utility grid .....	122

## **List of Abbreviations and Symbols**

AC	Alternating Current
BP-ANN	Back Propagation – Artificial Neural Networks
CF	Capacity Factor
CO <sub>2</sub>	Carbon dioxide
COE	Cost Of Energy
DC	Direct Current
DigSILENT	Digital Simulation and Electrical Network calculation program
DNI	Direct Normal Irradiance
ESS	Energy Storage System
ETAP	Electrical Transient Analysis Program
FF	Fill Factor
GECOL	General Electricity Company of Libya
GHI	Global Horizontal Irradiance
GPTC	General Posts and Telecommunications Company
HOMER	Hybrid Optimization Model for Electrical Renewable
I	Current
I <sub>sc</sub>	Short Circuit Current
kWp	kilowatt Peak
L	Length
MPP	Maximum Power Point
NASA	National Aeronautics and Space Administration
NEC	National Electric Code
NOCT	Normal Operating Cell Temperature
NPC	Net Percent Cost
OLTC	On Load Tap Changer
P	Active Power

pu	Per Unit
$P_{in}$	Input Power
$P_{max}$	Maximum Power
PSS	Power System Stabilizer
PV	Photovoltaic
Q	Reactive Power
R	Resistance
RES	Renewable Energy System
SCF	Solar Capacity Factor
SSM	Single Switch Master
T	Transformer
$T$	Temperature
UDM	User-Defined Dynamic Models
V	Voltage
VBA	Visual Basic for Applications
$V_D$	Voltage Drop
$V_{oc}$	Voltage at Open Circuit
$\eta$	Efficiency

## Chapter 1

### 1 Introduction

A mini-grid is a group or series of generators or other electrical sources that can operate either in tandem (i.e., interconnected) with micro-grids or independently (i.e., islanded), servicing local customers. Although these kinds of grids are generally networked to a larger distribution system and feature, some form of ESS (energy storage system), mini-grids can also be installed for only one customer, such as in a solar-powered domestic system, in which case no distribution system is required. In most instances, however, mini-grids are part of a larger grid system, as local generators cannot always satisfy local customer needs [1]. The normal operating condition for mini-grids usually means being connected to a main grid and only operating independently if there is an outage in the main grid; less common is the mini-grid operating mostly as an independent power source with infrequent interconnectivity with the main grid if local power generation is insufficient [2].

Mini-grid systems are especially useful in rural environments, where they have been found to increase living standards by improving agricultural productivity through reliability and decreased power costs [3]. The main advantages of using mini-grid systems are outlined below:

- Mini-grids can enhance power efficiency and reduce overall carbon emissions. Hybrid mini-grid systems are particularly attractive in this regard, as they typically use energy sources which are nearly 100% renewable.
- Mini-grid systems, including hybrids, are known for generating a reliable power supply due to a variety of factors (e.g., infrastructure being locally owned and maintained; a small-scale operation produces fewer complications).

- In developing nations, where grid systems are typically less developed, mini-grids can easily be implemented and operated by small- and medium-sized businesses. As the region's energy needs increase, these privately-owned systems can then later connect to an expanding grid.
- Both biomass gasifiers and biogas digesters have emerged as economically viable renewable power sources for mini-grid systems, due in large part to their high capacity as well as their adaptability to a grid.
- Issues around cost increases, resources' depletion and fossil fuel costs are further advantages for mini-grid systems. Moreover, renewable power resources have been significantly reducing in cost due to extensive R&D in the industry. While renewable energy installations do often need some subsidization, this is becoming less and less with each passing year and still remains cheaper than installation to the main grid [4].

### **1.1 Research on Mini-grid Systems**

According to the literature, the biggest hurdle facing the implementation of mini-grids today is their cost and available financing options [4]. Most mini-grids require a substantial investment compared to more traditional energy production methods in rural areas (e.g., diesel-powered generators). The main premise is that mini-grid projects must ultimately be financially self-sustaining while at the same time be affordable to customers. Mini-grid financing can be accomplished in a variety of ways, the most popular of which involve government-sourced subsidies and grants or industry-sourced assistance [4]. However, if these approaches are not available, this could act as a hindrance to the development of mini-grid systems.

In many developing countries today, rural areas would not have a viable electricity system were it not for mini-grids. Furthermore, because the mini-grids increase rural users'

access to power, their socio-economic circumstances have notably improved [4]. However, not all poor areas are being served even with micro-grids, due to customers in deeply impoverished areas being unable to pay for the service [4]. Urban areas, on the other hand, are usually always well-serviced with electricity even in destitute neighbourhoods, as their proximity to industry and financial centers guarantees them some level of electric supply from local urban utilities.

In poor rural areas which are situated outside the servicing area of the region's main grid, the provision of electricity takes on a decided community flair. Locals are forced to improvise small systems for themselves and their neighbours, and so usually fall back on traditional fuels such as diesel or hydropower. The motivation in building these micro-grid systems is to generate energy at the lowest possible cost, with reliability, safety and environmental concerns taking a back seat. Improvements to these systems are considered outside the realm of regional governments, so no overarching design standards are currently imposed [5].

## **1.2 Mini-grid Design Standards**

Mini-grid systems are often designed without any clear-cut standards to guide the builders. However, a few guiding principles could easily be incorporated into the system design for the benefit of the grid users, such as high efficiency and cost effectiveness, ease of expandability, and safety. These principles are explained below.

A mini-grid system design would be considered high efficient and cost effective if it could generate and provide power at a reasonable rate and in sufficient quantities to satisfy demand for the anticipated duration of the grid's service life. Efficiency might entail the use of higher quality materials in the design of the mini-grid, as lower quality materials might require more maintenance or even replacement. Efficiency could also mean building a larger grid than

current consumption patterns require, as it might be easier in the long-term to activate a grid where infrastructure is already present than to have to modify the design to add extra power to satisfy increased consumer demand. A larger system would also be more efficient if it prevented occurrences such as unwanted power losses and voltage drops [5].

A mini-grid system design would be considered safe when its operation posed no more problems or potential problems than typical larger grid systems, such as those found in urban areas. Using this definition as a guide, mini-grids could be designed with an eye to existing electrical standards and codes already applied to the region's other energy-producing infrastructure. However, using existing standards and codes as a guide does not mean that mini-grid design should not leave room for exceptions to those standards and codes. So, for instance, small conductors that might be inappropriate for larger grid usage (due to fire hazards) might be considered viable for mini-grids, as they would bring a substantial cost saving [5].

A mini-grid system design would be considered easily expandable if it lowered costs associated with the life of the equipment and components by including the ability to increase power production in the future. A good expansion design would, for instance, avoid the need for extensive rewiring or component replacement [5].

### **1.3 Mini-grid System Design Quality**

In the design of mini-grid hybrid systems, it is important to consider the quality of the components to be used as well as the type of power source, as both factors will affect not only the energy costs for users but also the reliability and durability of the system. The focus should be on long-term usability and affordability rather than options that will only benefit users in the short-term. Many rural communities in developing countries are often cash-strapped, so they look to building their power system as cheaply as possible, thinking from a short-term

perspective. This habit can be changed if the benefits of a long-term, good quality investment are presented to the users [6].

The same mindset (short-term usability and cheap cost) also influences the type of power source used in rural areas of developing nations. This, however, can benefit the implementation of mini-grid systems, as hybrid systems are cheaper to operate than grids that are run solely on diesel. Hybrid mini-grids also offer the option of using local resources, which provide a better guarantee of supplies being available when needed [6].

Two crucial measures that contribute to the design of mini-grid systems are efficiency and correct sizing. System efficiency is of major importance because it has a significant impact on the power load as well as on how much energy needs to be generated at any given time. Efficiency is also affected by sizing; if the system is too large or too small, the viability will be affected. Other measures include economic sustainability and issues around system operation, such as maintenance. Both governments and business interests can contribute to system implementation through subsidies and training, with the understanding that this is a long-term investment that should be sustain for several decades [6].

#### **1.4 Hybrid Mini-grid Systems**

In producing energy, hybrid mini-grids use a variety of technologies (i.e., minimally two types) as well as different kinds of RES (renewable energy sources) backed up by a diesel generator. The hybrid grids are able to feed power to local communities for use in communications systems, water treatment, general domestic usage, etc. In fact, a hybrid mini-grid operating independent of the national grid can be equally or even more efficient and reliable

than larger grids that supply urban areas. The mini-grids can also be hooked up to the national grid, should the need arise [6].

Research indicates that using a variety of technologies and power resources is superior to using just one technology or resource. In rural communities of developing countries, employing the use of a genset either as a back-up to or in combination with RES has been shown to offer the most economical and efficient means for energy provision. In general, the prices and availability of renewables are relatively consistent, as are diesel gensets, so combining RES with non-renewables makes hybrid mini-grids economically feasible [6].

At the same time, RES can be combined and substituted to suit seasonal changes in conditions as well as seasonal availability of power sources. Hence, during seasons with lower wind rates or hydro generation, solar PV collectors could be used, and when solar power is typically low (at night or during rainy seasons), batteries that have stored energy during peak solar energy production times can be used [6].

## **1.5 Libyan Energy Production**

In the northern African nation of Libya (population ~6 million), the government-run General Electric Company of Libya (GECOL) is charged with providing electricity for the entire country. The per capita average consumption of power in Libya has been estimated at 4,271 kWh [7], with around 98% of domestic households being supplied with power [8]. GECOL uses natural gas as the main fuel for energy production, as shown in Figure 1.1, although some areas of the country use heavy or light fuel oils in addition to the gas. Using natural gas is not only cheaper, it also cuts down on harmful CO<sub>2</sub> emissions, so Libya is moving towards using more natural gas in its production of energy [9].

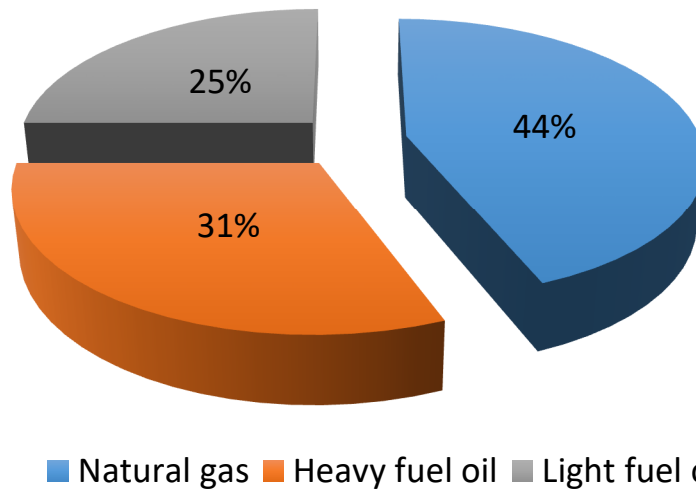


**Figure 1.1 GECOL power generation fuel percentages in 2012 [9]**

Power usage in Libya differs according to customer and area. Figure 1.2 illustrates the various main consumption sectors and types of load. As can be seen in the figure, the residential load has the highest power consumption rate in the northern African country [9].

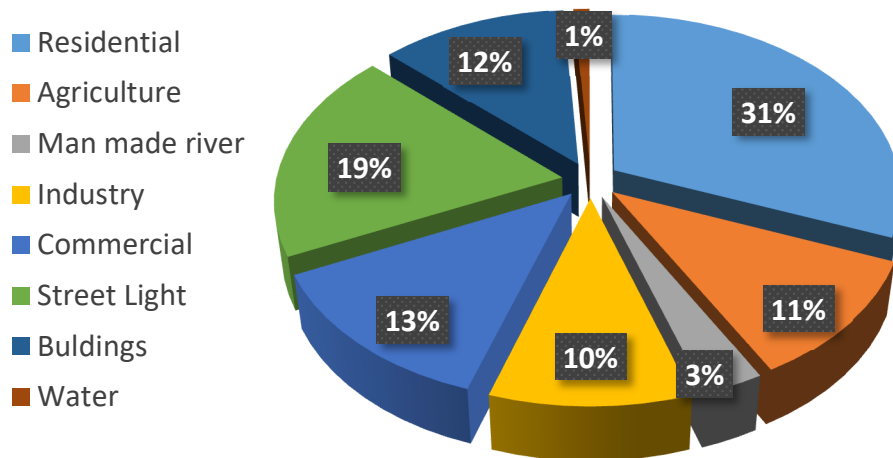


**Figure 1.2 GECOL customer load percentages in 2012 [9]**

The map in Figure. 1.3 below indicates that over half of the high-power infrastructure in Libya has been built near the coastal areas, as most of the population is concentrated there [10].

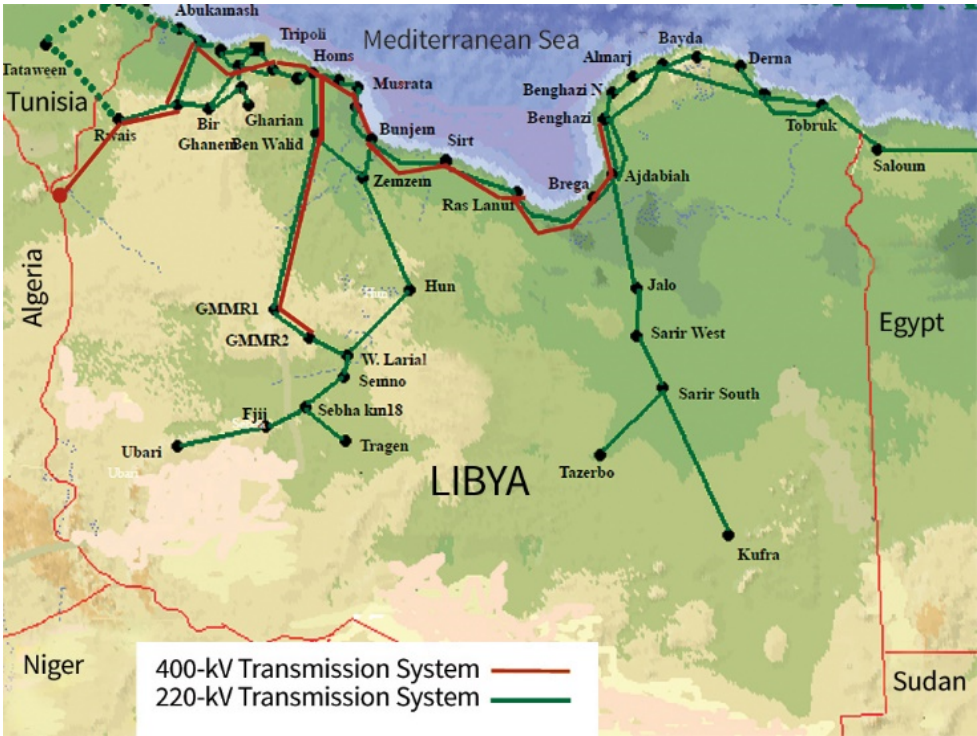


**Figure 1.3 Electricity infrastructure in Libya [10]**

Usage has most notably increased during summer months as more and more Libyans install air conditioning in their homes to keep cool (source: GECOL website). The steady rise in electricity demand has generally kept pace with the increase in power generation, but occasional spikes in load have resulted in power shortfalls leading to outages in urban areas where electricity usage is heaviest [12]. Figure 1.4 shows monthly average and peak loads for 2010, which was a year of heavy usage.

Figure 1.5 illustrates the increase in peak loads between 2003 and 2012. As can be seen in the figure, the steady growth in usage shows an annual increase of around 9%.

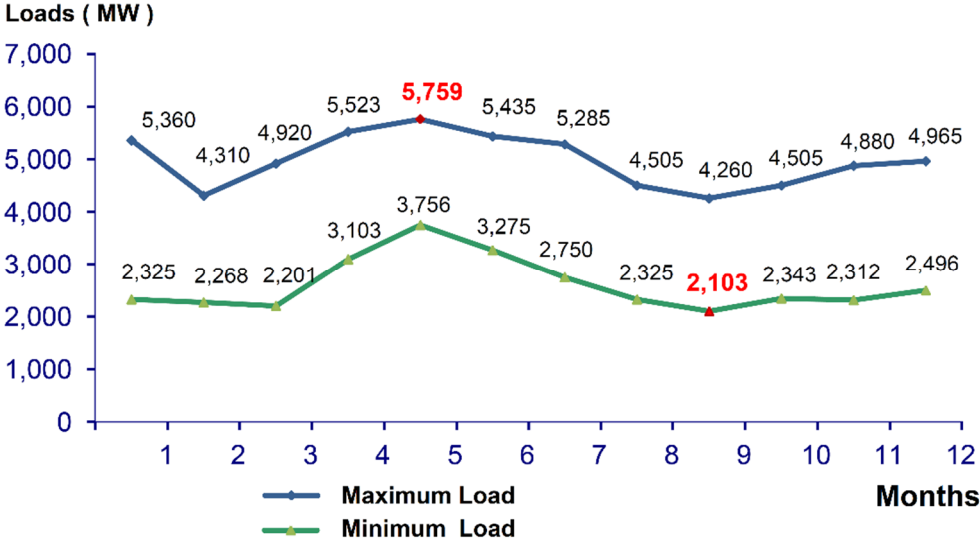


Figure 1.4 Monthly peak loads in Libya in 2010 [11]

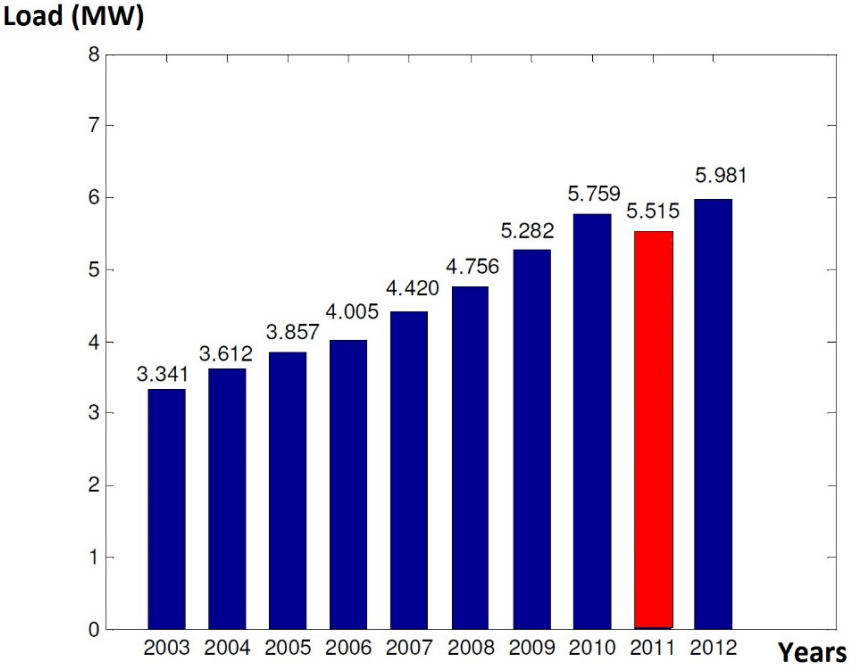


Figure 1.5 Electricity usage in Libya from 2003 to 2012 [9]

### **1.5.1 Renewable power sources in Libya**

Natural gas, crude oil, biofuels, and the burning of waste products provided Libyans with around 0.36 PW.h of power in 2011. By far, crude oil was responsible for producing the most power (80%) in the country, while waste and biofuels comprised significantly less (0.6%) and RES only 0.06% of overall production [8]. Since being adopted in Libya in the mid-1900s, a RES is primarily applied for specialized and rural needs (e.g., water pumping, communications components, and oil sites in remote locations) [13]. However, despite GECOL's ongoing heavy dependence on fossil fuel, alternative renewable energy sources like solar and wind are currently being piloted by the government [9].

Solar power in particular holds immense promise as a renewable energy source in Libya, given the country's dry and sunny climate. The rise of solar energy as an alternative source will help to offset rising demand for electrical power across the nation, including in rural areas. As mentioned in the previous paragraph, RES technology currently makes up only a very tiny portion of Libya's energy infrastructure, but interest in small- and mini-grid-connected PV (photovoltaic) systems is growing as demand for affordable, reliable and environmentally friendly energy sources increases across the country. Other options besides solar-powered systems include using wind-generated power from large-scale array farms. Along with benefitting Libyan consumers, an expansion of RES would provide the government the ability and incentive to share technology and related advances with the global community, thus potentially opening the country to new energy-related trade opportunities [9].

#### **1.5.1.1 Libya's PV systems**

Libya's hot, dry and sunny climate is ideal for solar power production. The country, which is situated along the coast of northern Africa, receives less than 150 mm of rain annually.

The mean yearly solar radiation is approximately 7.5 kWh/m<sup>2</sup>/day, while the mean annual sunshine hours number around 3,250. These dry and sunny conditions give Libya enormous potential for effective use of solar-based RES [9].

Within Libya, the region most conducive to expansion of the country's emergent solar power industry is in the south, in cities such as Sabha and Alkufra, which feature mean daily solar radiation measurements of 8.1 kWh/m<sup>2</sup>/day. The northern coastal urban areas (e.g., Misratah and Tripoli) are also fairly sunny, receiving on average 7.1 kW.h/m<sup>2</sup>/day (using the horizontal irradiance measurement tool). Considering that the country receives around 3250h of sunshine annually, this results in mean annual solar radiation of ~ 2.8 GWh/m<sup>2</sup>/year [8]. Figure 1.6 shows Libya's global horizontal irradiance (GHI) [14].

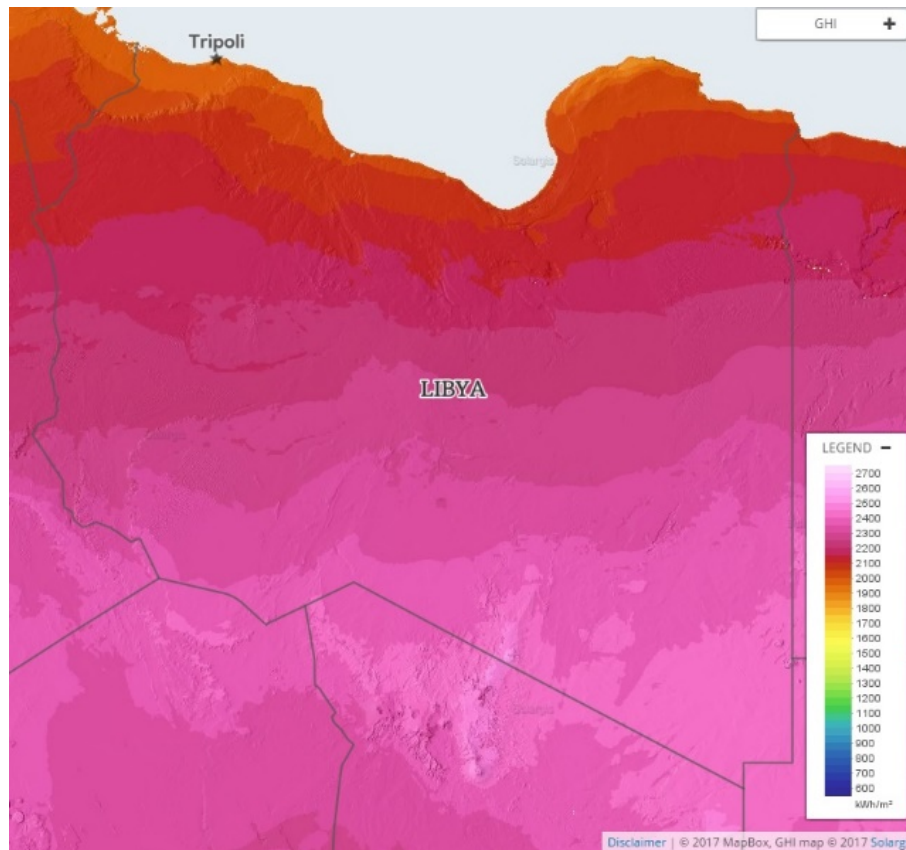


**Figure 1.6 Libya's global horizontal irradiance (GHI) [14]**

As mentioned above, solar power has been in use in Libya since the mid-1900s [8]. For example, in 1976, a PV system was employed for cathodic protection of the Port of Sedra pipeline project, while a few years later, PV technology assisted in water pumping systems near El-Agailat. PVs were also used for microwave repeaters in an installation in a remote section of southern Libya. By the turn of the century, PV systems were being installed for power provision in small rural villages that lay beyond the reach of the main grid. Table 1.1 presents a list of all the PV systems installed in Libya up to the year 2012 and their respective kWp [8].

**Table 1.1 PV Systems and kWp in Libya to 2012**

PV	kWp
PV (rural power)	725
PV (water pumps)	120
GPTC	850
Almadar	1500
Libyana	330
Oil Comp	120
Other	10
Total PV (communication systems)	2810
PV (street lights)	1125
Centralized PV system	110
PV (rooftop systems)	30

As shown in the table above, the installed power capacity for solar PV was 5MW in total. Some of the projects referenced in the table include the Wadi-Marsit project (a centralized system) that features a peak capacity of more than 67 kWp, as well as communication repeater stations (with a peak capacity of 950 kWp) and small-scale grid-connected PV systems (with a

peak capacity of around 42 kWp) [8]. Along with the country's enormous potential in relation to PV-based power production, Libya is also positioned to take advantage of PV infrastructure-related opportunities by becoming a regional leader in the manufacturing of PV components such as pods, panels, mounting systems and water tanks [8].

#### **1.5.1.2 Libya's wind energy**

An offshoot of direct solar energy is wind energy. Wind is produced by pressure and temperature differences in the atmosphere caused by solar radiation absorption over a specific region, which then induces various types of air movement [9]. Along with solar energy, wind power has gained a higher profile recently in Libya as a popular and cost-effective RES. In fact, the harnessing of the wind's power is not a new approach in Libya, as wind power has been used there for nearly 80 years already, mainly for irrigation and other needs related to water in desert areas of the country. The potential for applying wind power technology is immense, especially with Libya's famous "Ghibli", which are hot strong winds that blow in from the surrounding deserts every year from spring until fall. The only barrier to harnessing this wind potentiality on a large scale in Libya is the current lack of wind energy-related infrastructure in the country [8].

A few decades ago, GECOL began the process of educating Libyan engineers on the benefits of incorporating wind farms into their projects. Around the same time, GECOL also began a comprehensive program to introduce power from RES. Local engineers were tasked with the job of finding the best location for a large-scale (60 MW) wind farm in Libya. The farm would be a pilot project to showcase the country's potential for this type of energy production.

A group of professional engineers accepted the challenge, and one year later (in 2002) had already drawn up a list of promising sites for the pilot project. The engineers focused on the

coastal regions, where wind speeds averaged approximately 6-10 m/s (eastern region), 5-9 m/s (central region), and 4.5-9 m/s (western region) [8].

Five years later, in 2007, the wind farm project took another step forward with the creation of REAOL (Renewable Energy Authority of Libya). The ambitious target of REAOL at the time was for power sourced solely from RE to fulfill one-tenth of Libya's power demands by 2020. Of that one-tenth, 1GW would come specifically from wind. The pilot project finally became a reality in 2008 at Dernah, which is located in Libya's eastern coastal region. The farm boasted a 25 MW capacity. By 2009, RCREE, the Regional Centre for Renewable Energy and Energy Efficiency, tabled a report suggesting that the 2020 aim of one-tenth RE power was not feasible, to which REAOL responded by increasing the wind farm capacity to 60 MW in 2010; a plan was also made to add another 60 MW to the farm by 2012. These plans were, however, interrupted in 2011 by the revolution in Libya, after which REAOL shifted its focus from a specific goal and target date to exploring the potential development of different kinds of RE over the next decade [8].

## **1.6 Literature review of mini-grid stability**

Several research studies in the literature have investigated solar PV as an alternative to traditional power generation. Solar PV systems function differently than other power systems. Through the use of semiconductor solar cells, solar PV changes solar rays first to DC energy and then to AC energy by means of a DC-to-AC converter. Because of this conversion process, there is no inertia in solar PV, and the inverters' controls and characteristics determine the solar PV's dynamic behavior. The two main sizes in solar PV systems are large and small scale systems. Large-scale systems rate to around 1000 MW and usually connect through transmission

sites, whereas small-scale PV systems typically rate no higher than 20 MW and connect either at sub-transmission levels or through distribution networks [15].

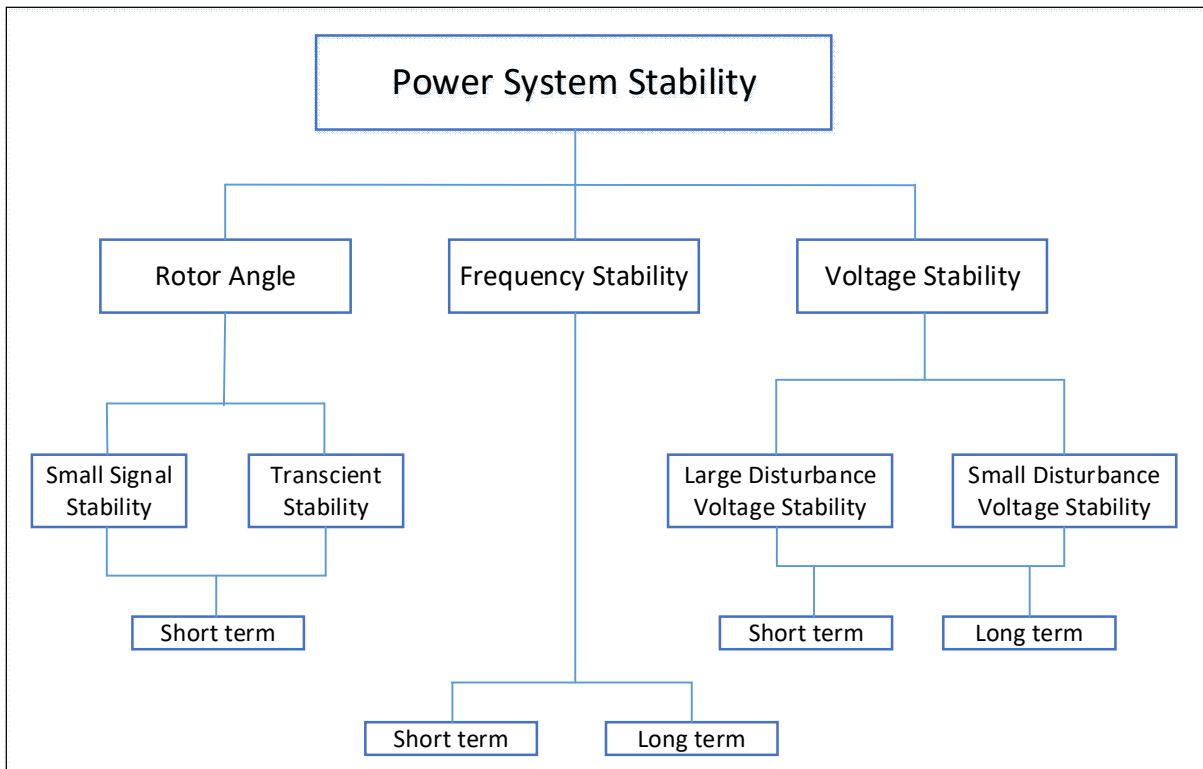
It can be challenging to integrate solar PV into a functioning electricity system as the design of most existing networks is not suited to the addition of DG (distributed generation). Problems that can arise through forced integration include issues around stability, quality, and overall operation. However, because small-scale solar PV has negative loads, neither the operation of the system nor its stability is affected. Indeed, system stability (i.e., being able to achieve and maintain equilibrium, even when disturbed) is a crucial factor in the overall functionality of power systems.

Figure 1.7 depicts the classification of power system stability. As can be seen in the figure, the main elements affected are stabilities related to voltage, frequency and rotor angle.

- *Voltage stability*: A power system that can achieve and hold steady voltages across every bus in the system even under disturbed conditions is considered to have voltage stability. On the other hand, a system which cannot maintain steady voltages is unstable and can result in transmission line faults, generator loss, load tripping, and even voltage collapse. Voltage disturbances can be either short- or long-term [13].

- *Frequency stability*: A power system that can achieve and hold steady frequency even under disturbed conditions such as load and generation imbalances is considered to have frequency stability. Conversely, a system that suffers from frequency instability will exhibit features such as inadequate generation reserves, insufficient equipment responses and substandard functioning in equipment used for protection and control of the system. Frequency stability can be either short- or long-term [15].

- *Rotor angle stability*: An interconnected power system that can achieve and hold synchronicity even under disturbed conditions is considered to have rotor angle stability. On the other hand, a system lacking in this kind of stability will be out of synch in relation to the other generators in the system. Rotor angle instability can be caused by unwanted increases in angular swings in one or more generators and, like rotor angle stability, can only be short-term [15].



**Figure 1.7 Power system stability classifications [15]**

A number of research studies have examined how PV affects the stability factor in energy systems, focusing on how stability is disturbed by high-penetration solar PV. For instance, in [15], the researchers show how a three-phase fault can result in transient stability, which can lead to the shut-down of inverters or a disconnection of the system. If a disconnection occurs, the system’s transient stability is negatively affected. The positioning of the dispatch

generator or the level of penetration of the PV generator can also cause transient stability in the system [15].

Also in [15], researchers looked into power system voltage instability caused by power generation. Aspects such as static and dynamic voltage stabilities were analyzed and indicated that voltage stability depends in large part on overall design factors as well as how the design is implemented and maintained. Moreover, how a PV system affects the stability of transmission/distribution systems was shown to be related to issues such as penetration level, meteorological conditions, shading, plant model type and plant site latitude [15].

In [16], researchers investigated how a distribution system's dynamic voltage is affected by a grid-connected PV generator, looking at factors such as line-tripping, penetration level and solar intermittency [16]. By performing DigSILENT simulations on voltage stability, the researchers found that heightened levels of PV penetration create better voltage stability in the system. An exception to this trend can occur when the load increases beyond 80%, at which stage voltage instability results (despite maximum PV penetration) and then ends in voltage collapse with the application of line outage. The researchers in [16] suggest that this occurs due to the PV generator being removed from the system, causing the PV-connected busbar voltage to plunge to the point where it can no longer function [16].

In [17], researchers modeled a PV mini-grid as a means to examine the stability of grids and to look at possible interactions between centralized diesel power sources and distributed PV. The study outcomes indicate only negligible effects on PV mini-grids quality of energy, including at extreme penetration levels [17].

In [18], researchers performed an analytical study on the Kythnos energy system, testing it for insolation disturbances at various penetration levels of PV [18]. The test outcomes showed

notable levels of instability during high penetration rates, although in some instances the systems were able to function even when nearing operational limits. The researchers also found that during cloud movement speeds that were considered slow ( $< 80$  km/hr), back-up generators could be initiated to prevent the onset of instability [18]. Sizeable penetrations of PV could also be handled with adjustments involving storage systems, inverters, grid management, load controllers, or non-critical load disconnection [18].

In [19], researchers presented a summary of control methods for achieving voltage and frequency stability for PV hybrid mini-grid systems [19]. The section below provides details on some of the main classifications:

- *Single-switched master (SSM) mini-grid*: This design features several different sources of AC (e.g., PV inverters, batteries and a generator) which are mini-grid-connected. This set-up is popularly applied for small local micro-grid systems [19].
- *Multi-master inverter-dominated mini-grid*: This design features several different AC sources as well, and is also mini-grid-connected. It is best applied in situations where there are multiple generators distributed across a wider network of power generation [19].
- *Multi-master rotating machine-dominated mini-grid*: This design is most often used in diesel-powered mini-grids and, like the mini-grids mentioned above, also uses several different types of AC sources, such as PV inverters, diesel generators, etc. This type of mini-grid is grid-connected but also supplies energy to the grid [19].

In current applications, the equipment used in conjunction with the control technology enables SSM systems to function at upper limits of around 200 kilowatts. However, SSM designs could

be applied to larger mini-grids if bigger 3-phase bi-directional inverters that could manage and dispatch several generators simultaneously were installed [19].

Coordinated control technology is needed for combining PV together with RE or non-RE generation sources [19]. There are two specific types of control technology: the first is primary control, which seeks to achieve and maintain the stability of the grid; the second type is termed secondary or supervisory control and involves making the best use of the alternative sources of generation being used [19]. The present research work focuses on primary control approaches for grid stability maintenance. With this strategy, the aim is to maintain frequency and voltage within the functional range by balancing both energy consumption and energy production using grid-forming units [19].

Issues affecting primary control are derived from the core features of PV (i.e., its intermittent and fluctuating nature) as well as the ever-changing load profiles that normally occur in mini-grids that are situated off the main line (e.g., in villages in remote areas). Because of these issues, choosing the optimal control approach involves understanding the design and functionality of hybrid mini-grid systems and their components. For instance, energy storage components along with secondary controllable loads are useful for helping to balance power. Furthermore, designs that feature centralization of components (e.g., storage systems, controllable loads and generators) enable faster communication of energy production and usage to relevant data centers, thus assisting stability and balance through real-time information sharing and timely action in relation to potential imbalance scenarios [19].

In contrast, and as mentioned briefly above, multi-master inverter-dominated design is decentralized. In this type of architecture, numerous sources of generation are based in different locations along the mini-grid but work together as one unit. In most cases, power sources in this

design use an electronic converter to connect with the grid. There is also an energy storage component in this design, but communication between the power sources is slow and thus not suitable for primary control purposes. Energy balance among the scattered resources is achieved using reactive power vs. voltage droop control and active power vs. frequency control. Other power management options in this design include grid frequency signaling, limiting power production when there is too much power or turning off dispatchable loads when there is insufficient power for customer demand [19]. The multi-master method has received significant attention recently, due mainly to its perceived ability to incorporate several mini-grids and include different power sources, thus making it less likely to experience single-point failures. Despite the theoretical success, these systems have as yet little or no actual field experience [19].

Overall, any one of the primary control approaches mentioned here can regulate the frequency and voltage of mini-grids to satisfy current energy demand. It is therefore up to individuals and organizations to choose which approach (centralized vs. decentralized; RES vs. diesel; dispatchable loads vs. ESS, etc.) best suits their needs, budget, and location. It is worth noting that the control methods mentioned above are best suited to relatively low-power mini-grids that feature centralized energy production. This is because increases in energy levels, of necessity, require an expanded area in which to operate and thus greater dispersion. Additional research should be carried out on commercial-grade control systems intended for use in larger distributed mini-grids [19].

## 1.7 Renewable energy system (RES) in Libya

In Libya, highly reliable stand-alone PV solar energy production has been provided for several decades for the purpose of water pumping, cathodic protection, communications and rural power supplies. The low cost has made this service even more attractive for users and producers alike, particularly in poor and remote regions of the country. Currently in Libya, solar PV's total installed peak power capacity has reached 1.5 MW, but this amount is likely to rise, given the excellent performance of the renewable resource and the willingness of the government to invest in solar PV technology, especially to supply electricity to remote areas [20].

In research published in 2007, Nassar and colleagues [21] devised a mathematical expression to represent surface cell temperature. This expression was then used to formulate PV cell surface temperature. However, such correlations can only be considered broadly general in nature, as they refer only to a specific locale, a specific solar radiation and a specific temperature, all of which can vary depending on geography and season. Keeping this in mind, the following formulation describes surface cell temperature [21]:

$$T_{cell} = T_{\infty} + 7.8 * 10^{-2} I$$

where  $I$  represents solar radiation intensity [Watt/m<sup>2</sup>] and  $T_{cell}$  refers to ambient air and surface cell temperatures [°C], respectively.

Within the framework of [21], the solar PV system is unsuited to play a key role in power production in southern Libya due to problems that arose during the experimentation (i.e., surface temperature increases). Instead, the researchers suggest that PV systems are better utilized in smaller formats, such as in home systems (islanded systems) or in small remote villages [21]. This suggestion does not take into consideration, however, that solar PV panels have improved

significantly since the study was performed. Additionally, cooling systems are now being designed specifically to combat efficiency losses in solar PV in extreme heat scenarios, such as those experienced in Libya. For example, a 50 MW PV energy production project was set up in Alkufra using a HIT PV. Early usage outcomes indicate a rise in efficiency rates of around 0.6%, with a predicted annual power generation of 114 GWh and an annual decrease in CO<sub>2</sub> pollution of 76,000 tons. This project is anticipated to take around 2.5 years to pay off [22].

According to researchers in [22], Libya is ready – financially, technologically, and ideologically – for the installation of these kinds of solar PV energy products on a large scale. Such plants [22] would help further diversify the country’s power generation fuel and also improve the environment with the increased use of RES. Power generation using this design has an annual output of around 114 GWh/year (with no cooling system) or around 119 GWh/year (with a cooling system). The mean efficiency of the modules that include a cooling system is 16.6%, whereas the mean efficiency in modules without a cooling system is 17.2% [22].

In [23], researchers analyzed a 50MW PV grid-connected energy producing plant located near Al-jagbob in Libya, acknowledged by REAOL for having abundant solar radiation. The plant incorporated an ultra-high-efficiency Sanyo HIT solar PV panel rated at 200W. REAOL also compiled data on the site’s long-term hourly ambient temperature, mean daily wind speed, mean daily global radiation and mean number of daily sunshine hours. The study [23] input the data in a Microsoft Excel-VBA program specifically developed by the research team to measure cell and sky temperatures, dew point and slope radiation. Also measured with the program’s software were panel efficiency and maximum power output in relation to tracking mechanisms.

The data for the site show total annual power output as 128.5 GWh, with maximum cell temperature as 51.8°C (noon in June) and minimum cell temperature as 5.4°C (early morning in January). The mean panel efficiency measured 16.5%. Additionally, the tracking system's values for the power production solar capacity factor (SCF) and capacity factor (CF) measured 70% and 29%, respectively. The plant's total cost payback timeframe is estimated at approximately four years [23].

In [24], researchers looked at performance levels of a grid-connected PV system made of tandem amorphous silicon thin film modules from fall 2009 to fall 2012. Their findings indicate the following:

- Mean PV power produced monthly: 3961.24KWh.
- Mean performance ratio monthly: 70%.

Their conclusion was that grid-connected PV systems could easily be integrated within Libya's existing transmission network, given that their test system exhibited an 86% performance ratio (extremely high) and mean monthly solar irradiation of 139.01 (kWh/m<sup>2</sup>/month) [24]. Moreover, grid-connected PV systems could also prove invaluable solutions for energy production in other Mediterranean nations [24], particularly if amorphous Si thin film modules were to be used.

The literature review of relevant studies on RES power generation using solar PV provides an important overview of an ES which is growing in popularity for commercial and domestic applications. From its beginnings in the 1970s as stand-alone PV systems supplying small-scale loads in remote locations to recent field tests of large-scale projects, solar PV is emerging as a viable energy source for larger projects. Despite the success of recent wind power sites in Derna and Al-Fatthaih in northern Libya [25], solar power usage has crept ever higher

in southern Libya. However, issues with heat and dust [26] have delayed wider implementation of the technology, as dust and dirt accumulations in solar panels can substantially lower energy output as well as efficiency [26]. Studies show that periodic (monthly) cleaning of the equipment is crucial to maintain the components in good working order [26].

Libya can benefit from the use of PV systems for energy production now and into the future. Currently, Libya mainly uses gas and oil for power production, but these resources are nonrenewable, highly polluting and expensive. As load demand rises, relying on fossil fuels will become too costly. Solar PV, on the other hand, is renewable, clean, and relatively cheap compared to fossil fuels. As more and more districts start to implement PV systems in their grids, people will become more aware of this type of RES and how it benefits the country's energy production [13].

Mean summer temperatures in Libya's central and northern areas are usually not as high as in the south, and dust is not as much of an issue. At the same time, the level of irradiance is lower compared to the south but slightly higher compared to the coast. Unlike the Sahara desert regions that dominate the southern portion of Libya, the central and northern sections of the nation are characterized by rocky and hilly landscapes. Most of this region is sparsely populated and could benefit from electricity provided by solar PV mini-grids either as stand-alone infrastructure or as an adjunct to the main grid.

Bani Walid is a city situated north of the Sahara. The rocky hills that characterize the region are a key feature in the relatively isolated town. The 30-meter-high hills perched above the deep valley run south to north. Because of this natural barrier between Bani Walid and the desert region, there is very little dust, making the area better suited for proper maintenance of solar PV modules than the desert.

Prior to Libya's revolution and civil war, electricity supplies were generally satisfactory. Outages occurred on average once a month and only for an hour, usually due to maintenance requirements or a dust storm. However, electricity outages after 2011 significantly increased in frequency, becoming almost a daily occurrence for several hours at a time. For example, by the summer of 2017, outages were not only happening daily but lasting up to seven hours. These problems were mainly the result of the increases in demand for power being greater than the actual supply. In fact, electricity demand in Libya has grown nearly 10% annually over the past decade, even though the infrastructure has been only slightly expanded. As a result, GECOL has to prioritize certain areas (e.g., major urban areas and military zones) for supply while cutting energy from areas that are less critical to the functioning of the country (e.g., remote towns and villages).

This piecemeal approach to power provision is not a long-term solution, however. The ever-increasing demand for electricity needs a more permanent strategy that takes advantage of the country's main renewable natural resources – sun and wind. To that end, Libya could develop hybrid power systems to satisfy the growing demand while at the same time maintaining the electricity service without interruptions or outages.

## **1.8 Research objectives**

The five main research objectives of the present study are as follows:

1. Propose a hybrid power system for use near Bani Walid Libya to provide reliable electricity.
2. Analyze steady state stability of the Bani Walid power grid using PowerWorld Simulator and the real power grid data and loads in Bani Walid, Libya.

3. Complete a sizing of the hybrid power system to suit the proposed site at Bani Walid and analyze the economic and technological feasibility of the system if battery storage were employed. Rescale the design approach to accommodate a range of situations and then investigate the effects of these different situations in relation to the system sizing.
4. Based on the specifications of the proposed hybrid power system, the effects of a hybrid grid-connected energy-generating system are determined using ETAP (Electrical Transient Analysis Program) to study the effects of having added a large scale PV system with energy storage system to a distribution network in Bani Walid. Various analyses are performed (e.g., power flow analysis, contingency analysis, transient stability analysis). Further, control of the power flow is proposed and performed in this study to improve power flows.
5. Contribute to the enhancement, increase and refocus of energy production across western Libya through the application of hybrid energy-producing systems and by exploiting the benefits of local renewable energy systems in cities like Bani Walid.

## **1.9 Thesis Organization**

This thesis is divided into 5 chapters, structured as follows:

Chapter 1 presents the introduction to the mini-grid power system, hybrid mini-grid power system and technical and financial issues in general. It also introduces electricity in Libya, (e.g., current electricity generation resources, electrical network, loads, and renewable energy in Libya). Mainly, photovoltaic and current wind energy are presented. Next, an overview of stability of mini-grids which gives a classification of power system stability. The results of previous focusing on the PV mini-grid are also presented in this chapter.

In chapter 2, steady state analysis of the existing power grid in Bani Walid grid is carried out using PowerWorld Simulator and real data of the grid and loads to ensure stability of the grid in different scenarios, and a Q-V curve analysis is performed before designing a hybrid power system for that grid. Improvement of power flows of the grid is also presented in chapter 2.

Chapter 3 presents a study of available renewable energy sources in Bani Walid as well as the electricity situation in that location and the proposed location for the PV system. The proposed hybrid power system is sized using the Homer software tool. Economic analysis and technological feasibility of different optimization results are discussed and the design approach has been scaled for different cases in chapter 3.

In chapter 4, an overview of the designed hybrid power system is presented. This includes configurations of the PV system and field design of the PV system for cable sizing. This hybrid grid-connected power system is analyzed based on the specifications of the proposed hybrid power system to study the impact of a large-scale PV system with an energy storage system in a distribution network in Bani Walid by using ETAP (Electrical Transient Analysis Program). The analysis includes power flows and control of power flows, contingency and transient stability analysis. Solutions are also proposed in chapter 4.

Chapter 5 concludes this thesis by describing the study findings and detailing the major contribution of the thesis. Future work is also presented in chapter 5.

## **Chapter 2**

### **2 Steady-state analysis of power grid in Western Libya using PowerWorld**

An overview of the selected grid in western Libya is presented in this chapter. Data of the power grid and loads have been collected from the General Electricity Company of Libya (GECOL).

The investigation of steady-state stability on the real grid power system has been carried out for the selected grid power system using PowerWorld Simulator. Simulator solves the power flow equations using a Newton-Raphson power flow algorithm.

PowerWorld Simulator is a power system simulation software which enables easy high voltage transmission system modeling. Power flow is a numerical analysis tool to determine the voltage magnitude and angle at each bus as well as the active and reactive power flow in each power line of a given system. These values are obtained for steady state operation only, and depend on the scheduled generation and demand profiles [27].

Power flow analysis is performed in two scenarios, at max average loads and at peak loads. Q-V Curve analysis determines voltage stability at load buses and the improvement of the power flow of the grid. Contingency analysis is also carried out using PowerWorld Simulator to determine system security under contingencies.

#### **2.1 An overview of Bani Walid power grid**

The proposed hybrid power system is in Bani Walid, located about 180 km in the southeast of Tripoli, as shown in Figure 2.1. The main substations at that location are 220/66

kV and 66/11 kV. The transmission lines network in Bani Walid is shown in Figure 2.2. The blue lines represent 220 kV lines and red lines represent 66 kV lines.



Figure 2.1 Bani Walid location

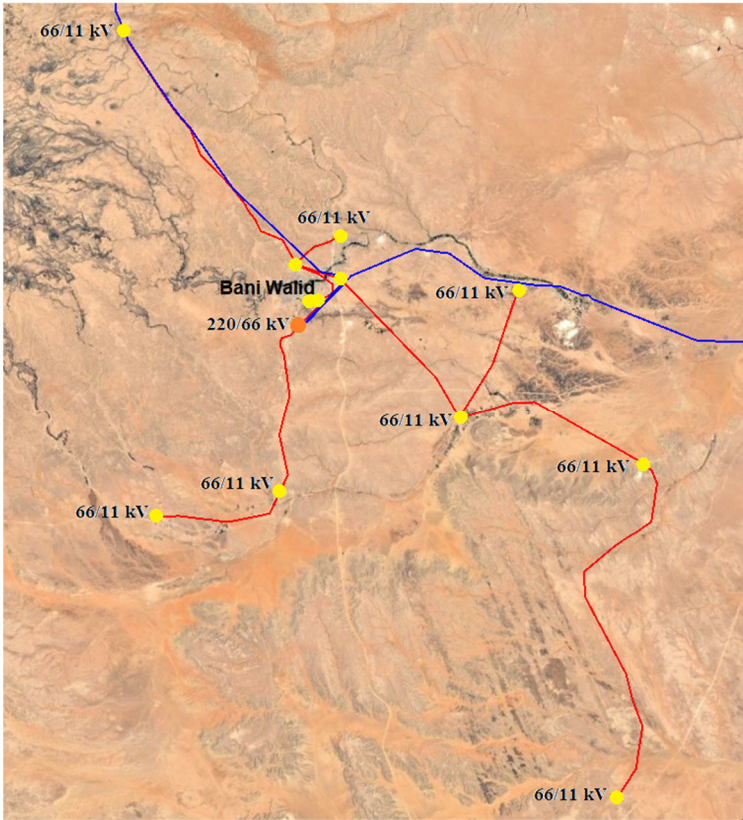


Figure 2.2 Transmission lines network in Bani Walid

## 2.2 Power flow analysis at max average loads

Simulation results can be seen in Figure.2.3, with voltages and phase angles of each bus, as well as the branch loading in percent. Some buses' voltages are below their permitted limits. Bus voltages should be from 0.95 to 1.05 pu, the minimum bus voltage is bus 13 with 0.934 p.u. The maximum branch loading of 62% is for transformers between bus 8 and 9. Most of the branches are loaded below or around 30%. The total load of the grid is 63MW and the loss of the grid is 1.04 MW. Buses voltage, angles, and loads can be seen in Table.2.1. The power flow analysis shows no violation of branches loading on the grid.

**Table 2.1 Buses information at max average load power flow analysis**

Bus Number	Load Name	Nom kV	PU Volt	Angle (Deg)	Load MW	Load Mvar
3	Bani Walid	11.00	0.976	-2.55	2.00	0.969
5	Eshmikh	11.00	0.974	-2.76	0.50	0.242
7	Tininai	11.00	0.974	-2.84	1.50	0.726
9	Al Soof	11.00	0.945	-5.22	22.00	10.655
11	Boyot Al Shabab	11.00	0.960	-3.67	2.50	1.211
13	Khermani	11.00	0.934	-5.90	18.50	8.960
15	Foguha	11.00	0.948	-4.52	1.00	0.484
17	Weshtata	11.00	0.946	-4.55	0.50	0.242
18	Weshtata	11.00	0.946	-4.65	1.00	0.484
20	Shemalya	11.00	0.940	-5.07	6.50	3.148
22	Sof Al Jeen	11.00	0.945	-4.97	1.50	0.726
24	Al Mardom	11.00	0.939	-5.45	4.00	1.937
26	Saddadah	11.00	0.945	-5.11	1.00	0.484
28	Gerza	11.00	0.945	-5.32	0.50	0.242

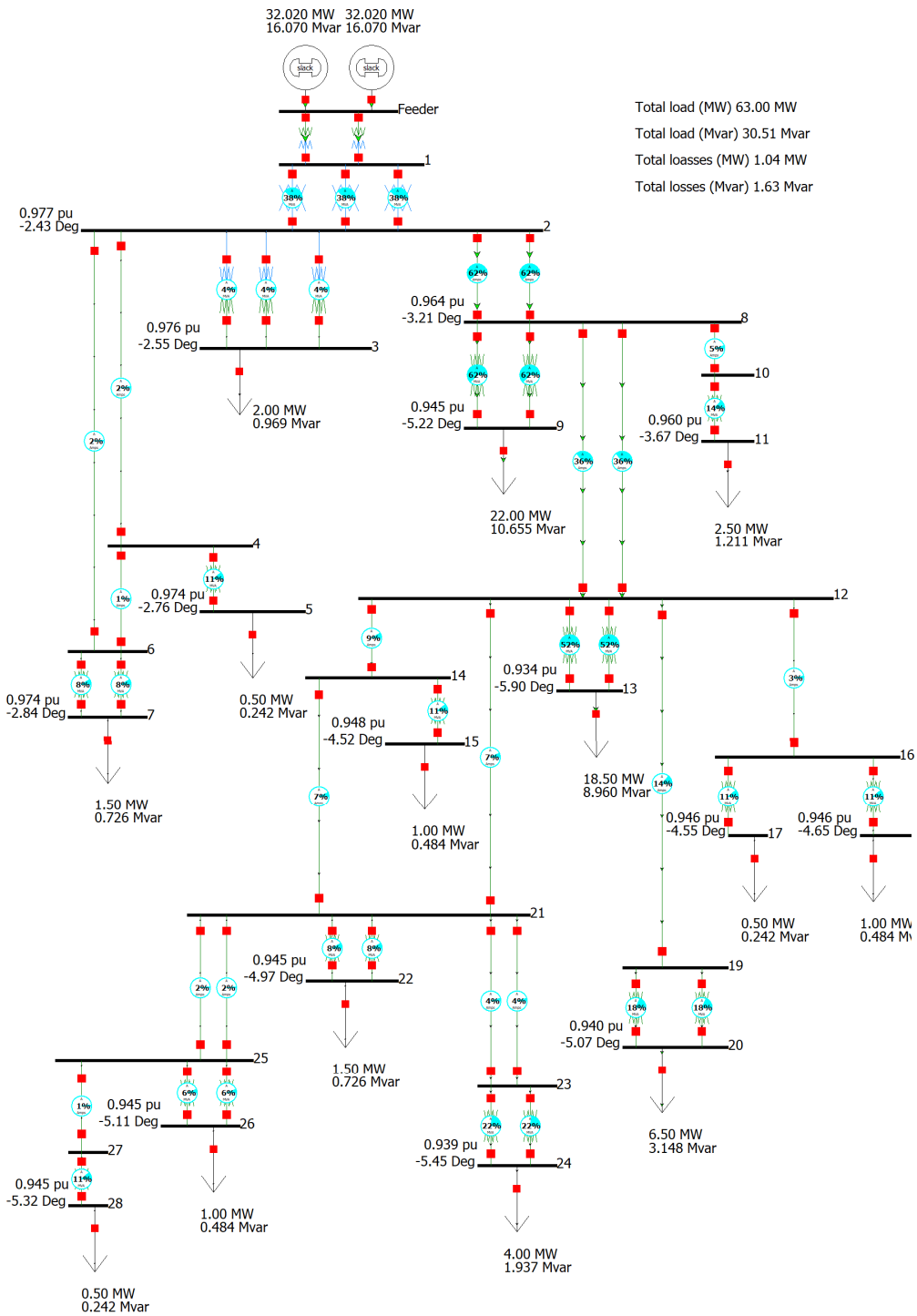


Figure 2.3 Power flow analysis at max average load

### 2.3 Power flow analysis at peak loads

The peak load of the entire grid was 85 MW in 2015 [11]. Power flow analysis at peak load shows that branches between bus 2 and 8 and transformers between bus 8 and 9 are loading at 83% and 85% respectively. Branches loading, bus angles, buses voltage, total load and total loss can be seen in Figure 2.4. The lowest bus voltage is bus 13 operating at 0.903 pu. Table 2.2 shows power flow results. Power flow analysis shows most load buses operating under voltage, which is under 0.95 p.u.

**Table 2.2 Buses information at peak load power flow analysis**

Bus Number	Load Name	Nom kV	PU Volt	Angle (Deg)	Load MW	Load Mvar
3	Bani Walid	11.00	0.963	-3.49	2.698	1.307
5	Eshmikh	11.00	0.961	-3.78	0.675	0.327
7	Tininai	11.00	0.959	-3.89	2.024	0.980
9	Al Soof	11.00	0.919	-7.24	29.683	14.376
11	Boyot Al Shabab	11.00	0.940	-5.05	3.373	1.634
13	Khermani	11.00	0.903	-8.22	24.960	12.089
15	Foguha	11.00	0.922	-6.22	1.349	0.653
17	Weshtata	11.00	0.920	-6.27	0.675	0.327
18	Weshtata	11.00	0.919	-6.41	1.349	0.653
20	Shemalya	11.00	0.911	-7.02	8.770	4.247
22	Sof Al Jeen	11.00	0.916	-6.84	2.024	0.980
24	Al Mardom	11.00	0.908	-7.53	5.397	2.613
26	Saddadah	11.00	0.915	-7.02	1.349	0.653
28	Gerza	11.00	0.914	-7.30	0.675	0.327

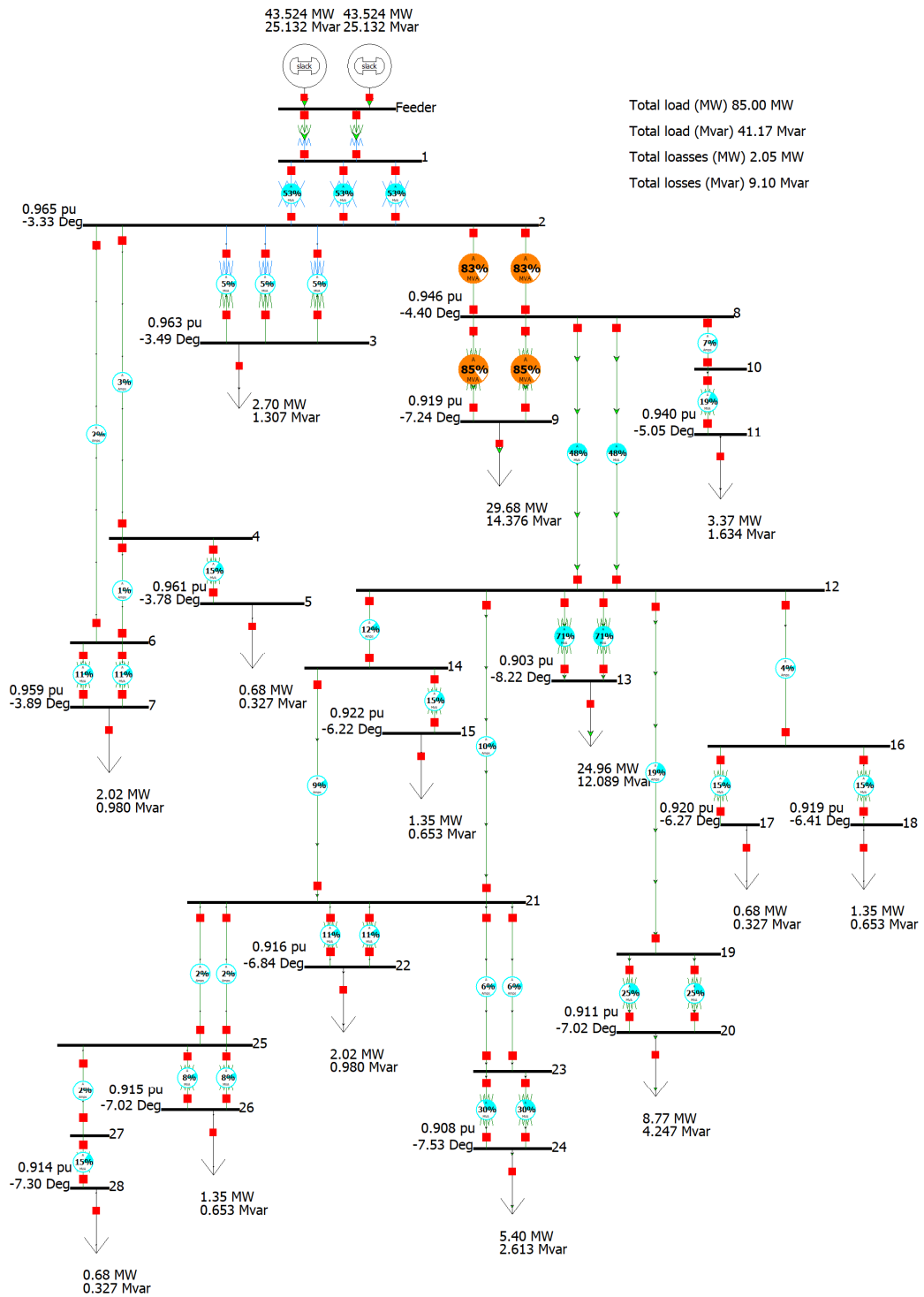


Figure 2.4 Load flow analysis at peak loads

## 2.4 Q-V Curve Analysis

The Q-V curve method is widely used to investigate voltage instability problems in power systems during the post transient period. The knee point or critical point of the characteristics corresponds to the voltage where  $dQ/dV$  becomes equal to zero. If the knee point of the Q-V curve is above the horizontal axis, then the system is reactive power deficient. To prevent voltage collapse, additional reactive power sources are needed. Buses have a positive V-Q sensitivity if the Q-V curves are below the horizontal axis. There may still what are called stiff buses, depending on the nose points of the buses [28].

The Q-V curve analysis is done on the system to study how the variation of reactive power affects the voltage in the system; all load buses are monitored to determine bus voltage stability. The Q-V curve shows the sensitivity and variation of bus voltages with respect to reactive power absorptions or injections. The system is considered voltage stable if V-Q sensitivity is positive for every bus and voltage unstable if the V-Q sensitivity is negative for at least one bus. All control systems (e.g., generators Var, transformers Taps, ...etc) assume that increasing Var will increase voltage; therefore, if there is a negative V-Q sensitivity, the control systems will behave incorrectly and cause the system to collapse, because they will increase Var injection, driving the voltage in the wrong direction.

Q-V curves of all load buses can be seen in Figure. 2.5. All buses have positive sensitivities. Bus 3 is much stable while bus 28 is less stable. The nose point or critical point and the operating point for each bus can be seen in Table 2.3. The column ( Q at VMax ) indicates how much Mvar of the shunt capacitor could be connected individually to the corresponding bus to achieve 1 p.u voltage.

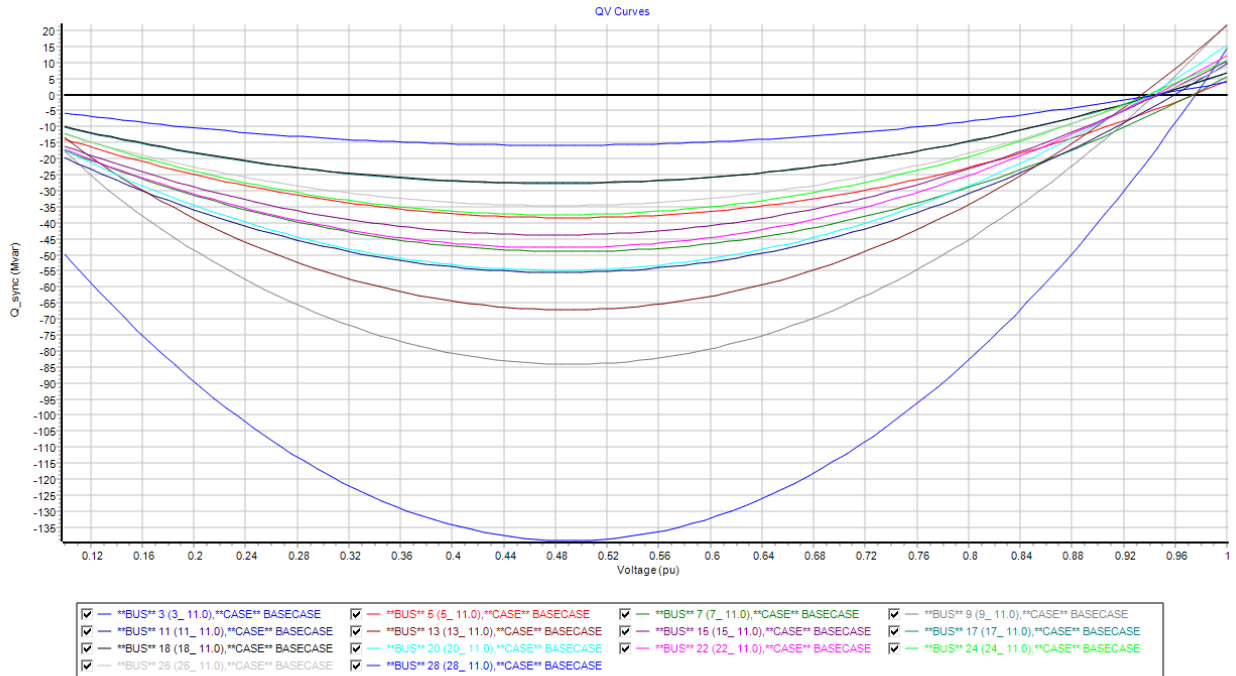


**Figure 2.5 Q-V curve plot of load buses**

5/2016

**Table 2.3 Q-V curve information**

Bus No	Nom kV	V at Q0	Vmax	Q at VMax	Qinj at Vmax	V at Qmin	Qmin	Vmin	Q at Vmin
3	11.00	0.98	1.0000	14.31	14.31	0.4958	-139.18	0.1000	-49.86
5	11.00	0.97	1.0000	4.17	4.17	0.4945	-38.43	0.1000	-13.89
7	11.00	0.97	1.0000	5.53	5.53	0.4936	-48.98	0.1000	-17.32
9	11.00	0.94	1.0000	21.90	21.90	0.4946	-84.15	0.1000	-17.66
11	11.00	0.96	1.0000	9.81	9.81	0.4797	-55.48	0.1000	-19.63
13	11.00	0.93	1.0000	21.43	21.43	0.4840	-67.09	0.1000	-13.33
15	11.00	0.95	1.0000	10.30	10.30	0.4778	-43.82	0.1000	-16.04
17	11.00	0.95	1.0000	6.75	6.75	0.4764	-27.77	0.1000	-10.19
18	11.00	0.95	1.0000	6.85	6.85	0.4756	-27.62	0.1000	-9.95
20	11.00	0.94	1.0000	15.32	15.32	0.4802	-54.81	0.1000	-17.44
22	11.00	0.94	1.0000	12.17	12.17	0.4846	-47.75	0.1000	-17.03
24	11.00	0.94	1.0000	10.75	10.75	0.4790	-37.54	0.1000	-12.21
26	11.00	0.95	1.0000	8.74	8.74	0.4751	-34.66	0.1000	-12.46
28	11.00	0.95	1.0000	3.98	3.98	0.4752	-15.82	0.1000	-5.71

## 2.5 Improvement of power flow of the power grid

Power flow at peak load shows violation of voltages and branches loading. Four branches are loaded over 83% and 85%, as shown in Figure 2.4. This percentage loading is according to MVA limits of the branches. Controlling of Mvar flows could reduce branch a loading and improve bus voltages and power flow. Shunt capacitors are designed appropriately to improve power flow of the grid. The Q-V curve information at average load in Table 2.3 shows that the nominal Mvar of the shunt capacities that could be connected to bus 8 and bus 9 to achieve maximum voltage 1 p.u are 36.85 Mvar and 21.9 Mvar, while the nominal Mvar shunt capacities that could be connected at peak load are 54.12 Mvar and 31.48Mvar. However, the maximum voltage 1 p.u could be achieved at the corresponding bus if only one capacitor is connected, because they effect on each other if they are connected at the same time. Since the main goal is to reduce losses at specific branches and study the effect on the total system losses, the shunt capacities adjusted manually after entering the nominal values to achieve a lower loss on the overloaded branches and highest voltage at the corresponding buses. The optimal values of the shunt capacitors are 34.9 Mvar and 14.7 Mvar, which are connected to bus 8 and bus 9 respectively. The results show that the shunt capacitor reduced MVA loading of the transmission lines between bus 2 and 8 from 83% to 74%, and the loading of transformers between bus 8 and 9 from 85% to 74%. Bus voltages are also improved. All load buses operated close to the nominal value of 1 pu. Total MW losses on the system are reduced from 2.05 MW to 1.62 MW. Table 2.4 shows the results before adding a shunt capacitor to buses 8 and 9, and table 2.5 shows the results after adding appropriate shunt capacitors 34.9 and 14.7 Mvar to buses 8 and 9 respectively. Table 2.6 shows voltages and angles at load buses after improvement of power

flows at peak loads. Figure 2.6 shows the power flow results after using shunt capacitors at bus 8 and bus 9.

**Table 2.4 Power flow results before adding shunt capacitor to buses 8 and 9**

Branch	From bus No	To bus No	Loading MW (%)	Loading Mvar (%)	Loading MVA (%)	Total system losses (MW)	Total system losses (Mvar)
Lines	2	8	74	39	83	2.05	9.1
transformers	8	9	75	41	85		

**Table 2.5 Power flow results after adding shunt capacitor to buses 8 and 9**

Branch	From bus No	To bus No	Loading MW (%)	Loading Mvar (%)	Loading MVA (%)	Total system losses (MW)	Total system losses (Mvar)
Lines	2	8	74	5	74	1.62	5.18
transformers	8	9	74	3	74		

**Table 2.6 Voltages and angles at load buses after improvement of power flows at peak loads**

Bus No	Name	Nom kV	PU Volt	Angle (Deg)	Load MW	Load Mvar
3	Bani Walid	11.00	0.999	-3.47	2.698	1.307
5	Eshmikh	11.00	0.997	-3.74	0.675	0.327
7	Tininai	11.00	0.995	-3.84	2.024	0.980
9	Al Soof	11.00	0.993	-7.13	29.683	14.376
11	Boyot Al Shabab	11.00	0.990	-5.13	3.373	1.634
13	Khermani	11.00	0.955	-7.97	24.960	12.089
15	Foguha	11.00	0.973	-6.19	1.349	0.653
17	weshtata	11.00	0.971	-6.24	0.675	0.327
18	weshtata	11.00	0.970	-6.36	1.349	0.653
20	Shemalya	11.00	0.963	-6.91	8.770	4.247
22	Sof Al Jeen	11.00	0.968	-6.75	2.024	0.980
24	Al Mardom	11.00	0.960	-7.37	5.397	2.613
26	Saddadah	11.00	0.968	-6.92	1.349	0.653
28	Gerza	11.00	0.967	-7.17	0.675	0.327

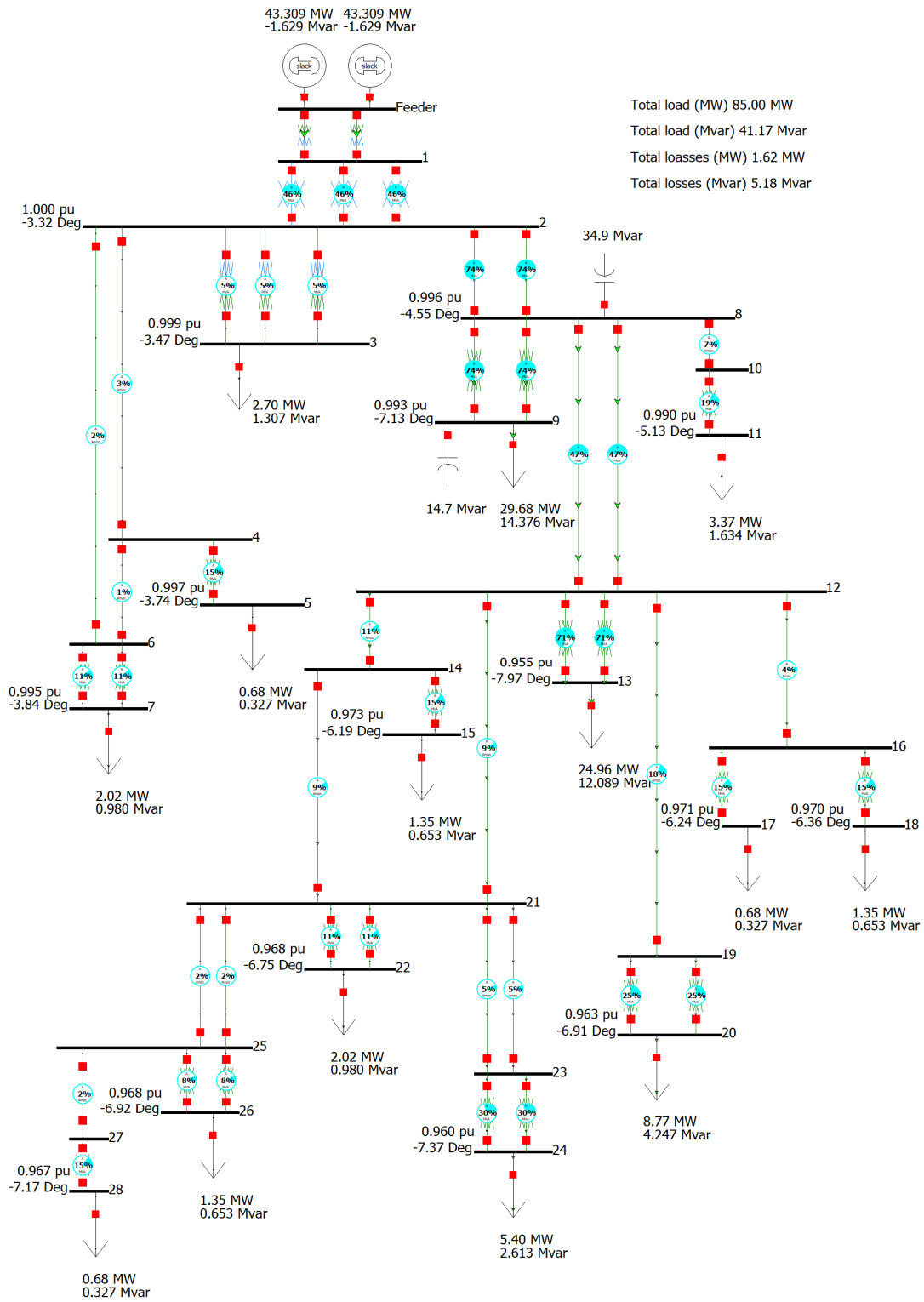


**Figure 2.6 Load flow analysis at peak loads with using shunt capacitor**

## 2.6 Contingency analysis

Power systems are operated so that overloads do not occur either in real time or under any statistically likely contingency. This is often called maintaining system security, and a system that meets this criterion should be secure. Contingency analysis can be automatic or manually performed with the PowerWorld Simulator. Contingencies can consist of several different actions or elements, including a simple example such as the outage of a single transmission line or transformer, or could be more complex, such as outage of several lines, several generators, and the closure of a normally open transmission line.

The simple contingency analysis N-1 is carried out in the simulation and automatically performed for transmission lines and transformers to determine the stability of the grid during contingencies. Six contingencies cause overloading of six branches. Transformers between bus 8 and 9, and bus 12 and 13 overloaded 127.79% and 106.74 respectively; lines between bus 2 and 8 overloaded 122.55%. The results show no voltage violations for the system. Ten contingencies cause load islanding at buses 5, 11, 15, 17, 18 19, and bus 28. Table 2.7 shows the results of contingency analysis.

**Table 2.7 Results of contingency analysis**

Actions	From bus No.	To bus No.	Violations	Max % Loading Cont.
Open transformers	8	9	1	127.79
Open transformers	8	9	1	127.79
Open line	2	8	1	122.55
Open line	2	8	1	122.55
Open transformers	12	13	1	106.74
Open transformers	12	13	1	106.74

## 2.7 Chapter summary

Power flow analysis of the selected power grid is performed in chapter 2 using the PowerWorld Simulator in two scenarios, at average max loads and at peak loads, to determine the stability of the power grid. The results are presented and described. At max average load, the results show no overloading violations. The lowest load bus voltage in the system is for bus 13 operating at 0.934 pu. At peak loads, two transmission lines between bus 2 and bus 8 are overloaded of 83% and two transformers between bus 8 and bus 9 are overloaded 85%. Q-V curve analysis is performed for load buses to determine voltage stability of the load buses; the results show that all load buses have positive Q-V sensitivities. The compensation of reactive power is designed with appropriate parameters to improve voltage stability and reduce total system losses. The results show no voltage violations and the system losses are reduced from 2.05 MW to 1.62 MW at peak loads.

Increasing capability of transmission lines can be done by connecting a series capacitors but needs high experience because connecting capacitors could cause resonance in the system and destroy the generators.

The results of the N-1 contingency analysis show six alerts of loading violations. The following solutions can be done to make it N-1 secure:

- (a) Replacing the transformers between bus 8 and bus 9 with higher rated MVA. The 100% loading is considered as a critical loading in PowerWorld for this simulation. The transformers loading should be less than 100% during a contingency. Therefore, the minimum capacity for each transformer which assumed to be loaded of 99% during the contingency can be calculated as:

$$\text{Minimum capacity} = \frac{127.79}{99\%} * 20 \text{ MVA} = 25.816 \text{ MVA} \approx 26 \text{ MVA}$$

Similarly, the minimum capacity for each transformer between bus 12 and bus 13 can be calculated as:

$$\text{Minimum capacity} = \frac{106.74}{99\%} * 20 \text{ MVA} = 21.563 \text{ MVA} \approx 22 \text{ MVA}$$

where the 20 MVA is the rated capacity of previous installed transformer.

- (b) Replacing the transmission lines between bus 2 and bus 8 with higher ampere limit transmission lines. The minimum rated loading can be calculated as:

$$\text{Minimum capacity} = \frac{122.55}{99\%} * 480 \text{ A} = 594.182 \text{ A} \approx 595 \text{ A}$$

## Chapter 3

### 3 Sizing of a hybrid power system for Bani Walid, Libya

#### 3.1 Introduction

A hybrid power system is an independent grid that merges at least two different types of energy for power generation and distributes electricity to consumers. It functions as an autonomous entity and can provide almost the same service and quality as a national grid. Moreover, with appropriate arrangements, a hybrid power system can, in fact, be connected to a national grid [6].

Recently, the price of solar panels has dropped by 45% or more, which makes the entire system much more affordable [29]. In addition, a study in [30] shows that the installation capacity of large-scale PV systems reduces both the amount of generated electricity and subsequent CO<sub>2</sub> emissions. The amount of total electricity generated and CO<sub>2</sub> emission reduction by the installation capacity in Liaoning is more than 2.7 times larger than for other regions in that study [30]. North Africa has a great potential of solar energy as reported by the Solar Atlas. A comparison between measurements and Atlas data in the Algerian south area (Ghardaia region) shows the relative error between the annual accumulated global solar radiation is only 0.6%, whereas it is about 2% for DNI solar radiation [31]. Both cloud cover and the dust accumulation on the surface of the solar module have a great impact on photovoltaic solar performance. The effect of cloud cover is immediate, with a drop in global solar irradiance and subsequently in power output for a short time, while the effect of dust accumulation has a long-term effect [32]. Feasibility and optimal design of a stand-alone photovoltaic energy system for an orphanage has been presented in [33]. It shows that the optimal design of a PV

with a battery storage system has been carried out, minimizing the net present cost by varying the size of the batteries until a configuration that produces the desired power needs of the orphanage is achieved. Selected components and generation sources for a hybrid power system will have a real influence on the lifetime of the system and its affordability to end-users. To increase cost saving and efficiency, sizing the system appropriately should be the priority [29]. This chapter presents the electricity situation in Libya, proposes a large hybrid power system and shows that a hybrid power system could be the best solution for that part of the world.

### **3.2 Electricity situation in Libya**

In Libya, there are many remote areas and villages with small populations. Even though most of these areas are located far away from the central power plants and the national grid, 99.8% of Libyan people have access to electricity. Due to a high economic growth and greater investment in the oil and natural gas sectors, electricity generation has more than doubled from 2000 to 2010. However, because the growing power demand has been greater than gains in installed generation capacity, electricity shortfalls have occurred regularly, even before the civil war of 2011 [34]. From 2011 to 2017, power outage has occurred daily for about 3 hours up to 12 hours due to load shedding, which increases during summer and winter seasons. In some remote areas, the power outage lasts more than one day when there is a fault on the grid plus load shedding. GECOL schedules load shedding daily to maintain stability of the grid.

### **3.3 Electrical Loads in Bani Walid**

Most of the loads in Bani Walid are residential in addition to commercial loads. The average load in Bani Walid in 2015 was 35.98 MW. The maximum average load and peak load were 47.8 MW and 85MW respectively in August, mainly due to operating a number of air

conditioners. Moreover, the insulation systems in homes are inefficient, which leads to operation of the air conditioners most of the time. The minimum average load and minimum peak load were 26.2 MW and 46 MW in March because of the mild weather in March, as shown in Figure 3.1. Load data have been collected from GECOL.

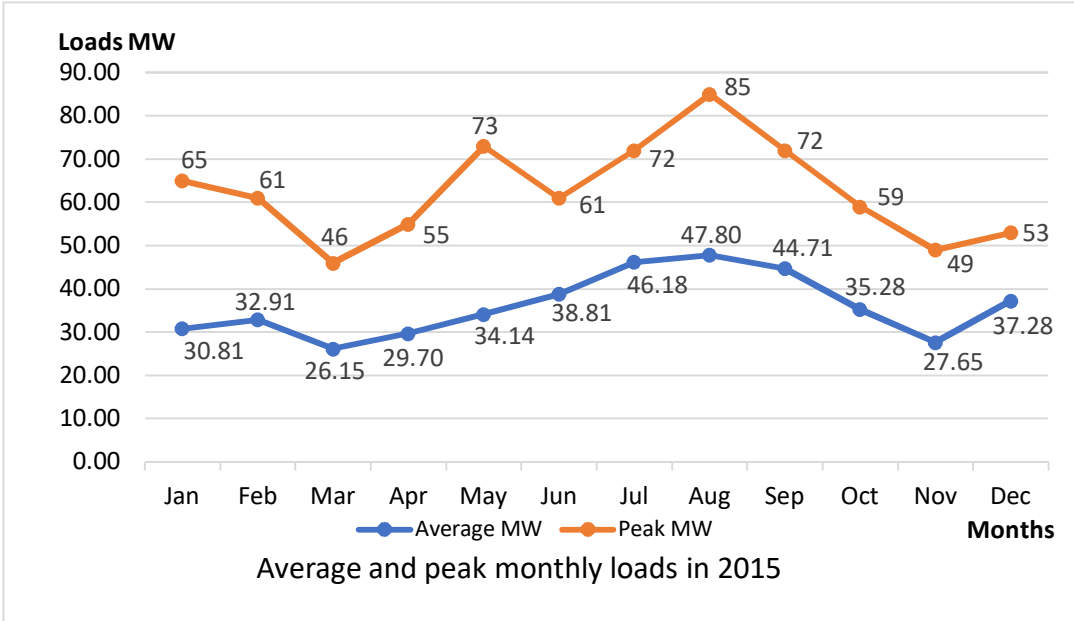


**Figure 3.1 Monthly average and peak loads in 2015 in Bani Walid**

**3.4 Renewable Energy Sources in Bani Walid**

The renewable energy sector in Libya planned a number of projects in the last decade. The proposed projects are mainly solar energy and wind energy systems, which are the best alternatives for renewable energy in Libya [35].

Bani Walid is about 180 km southeast of Tripoli at latitude 31° 45’ E and longitude 13° 59’ E, as shown in Figure 3.2. The summers are long, arid, sweltering and clear and the winters are cold, windy, dry, and mostly clear. During the year, the temperature typically varies from

39°F (3.8°C) to 101°F (38.3°C) and is rarely below 33°F (0.6°C) or above 112°F(44°C). Figure 3.3 shows the average high and low temperature during a year in Bani Walid [36]. Temperature has a significant effect on the electrical performance and power generation efficiency of the photovoltaic module. Online modelling and calculation for operating temperature of Silicon-Based PV modules based on BP-ANN has been presented in [37].



**Figure 3.2 Bani Walid location**

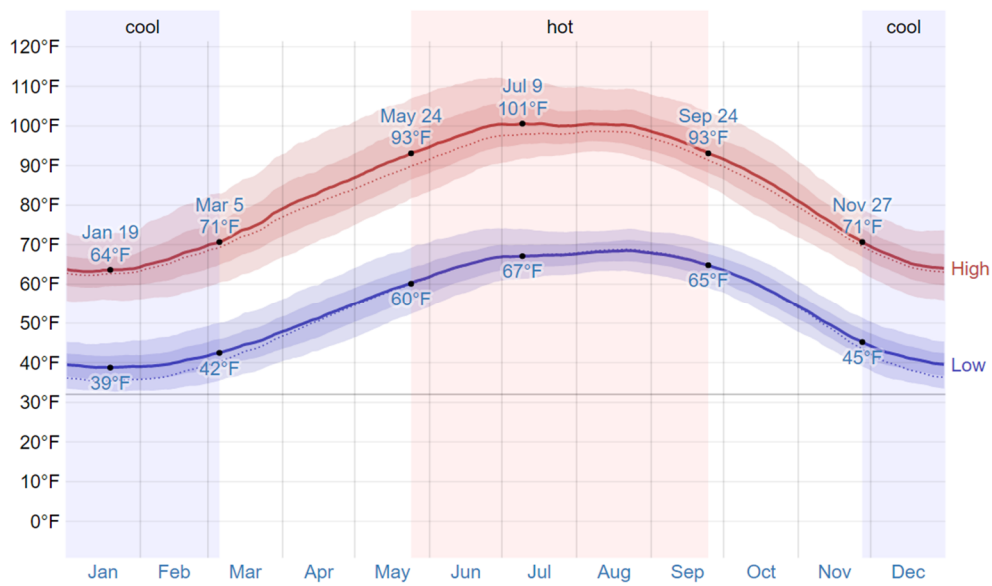


**Figure 3.3 Average high and low temperature in Bani Walid**

### 3.4.1 Wind Energy

The average yearly wind speed at latitude  $31.8^{\circ}$  N and longitude  $14^{\circ}$  E is 3.96 m/s and the average monthly wind speed is shown in Table 3.1 [38]. The windiest day was usually in February with an average speed of 10.3 miles per hour (4.6 m/s.) (as measured at 10 meters above the ground). The average hourly wind speed in Bani Walid experiences mild seasonal variation during the year, as shown in Figure 3.4 [36].

**Table 3.1 Monthly averaged wind speed at 10 m above the surface of the earth for terrain similar to airports (m/s)**

Jan.	Feb.	Mar.	Apr.	May	Jun.	Jul.	Aug.	Sep.	Oct.	Nov.	Dec.
3.92	4.28	4.22	4.27	4.35	4.2	3.6	3.66	3.69	3.81	3.73	3.78

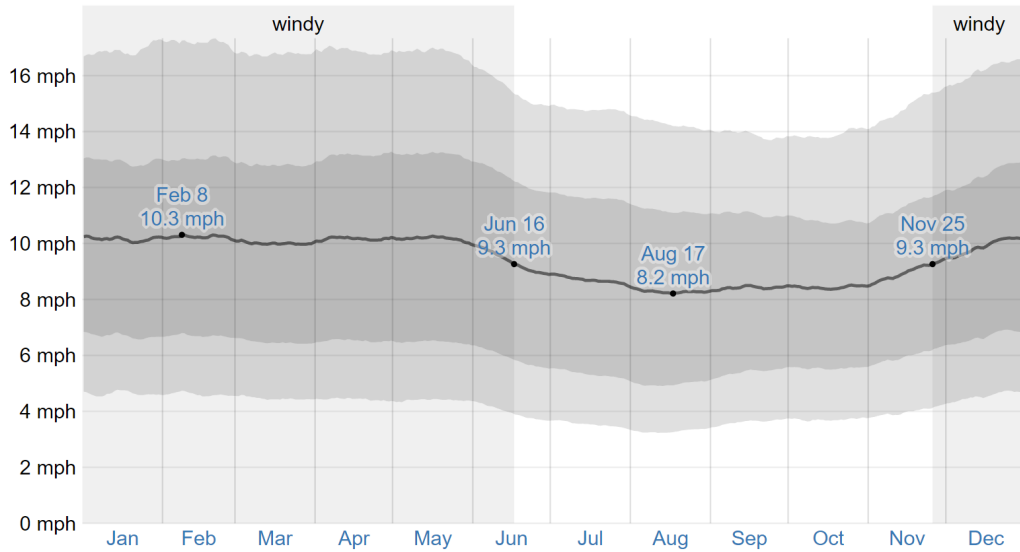


**Figure 3.4 Average wind speed in Bani Walid**

### 3.4.2 Solar Energy

According to data from NASA surface meteorology and the Solar Energy Corporation, the average insolation incident on a horizontal surface in July is 8.03 kWh/m<sup>2</sup>/day at latitude 31.8° N and longitude 14° E (the selected location for a PV in Bani Walid). This makes Bani Walid very good potential place for solar energy production. Table 3.2 shows monthly averaged insolation incidence on a horizontal surface (kWh/m<sup>2</sup>/day) [38]. Figure 3.5 shows the global horizontal irradiance in Bani Walid region (GHI) [14].

**Table 3.2 Monthly averaged insolation incidence on a horizontal surface (kWh/m<sup>2</sup>/day) in Bani Walid at N31.8° E14°**

Jan.	Feb.	Mar.	Apr.	May	Jun.	Jul.	Aug.	Sep.	Oct.	Nov.	Dec.
2.95	4.10	5.32	6.46	7.19	7.83	8.03	7.24	5.74	4.41	3.19	2.65

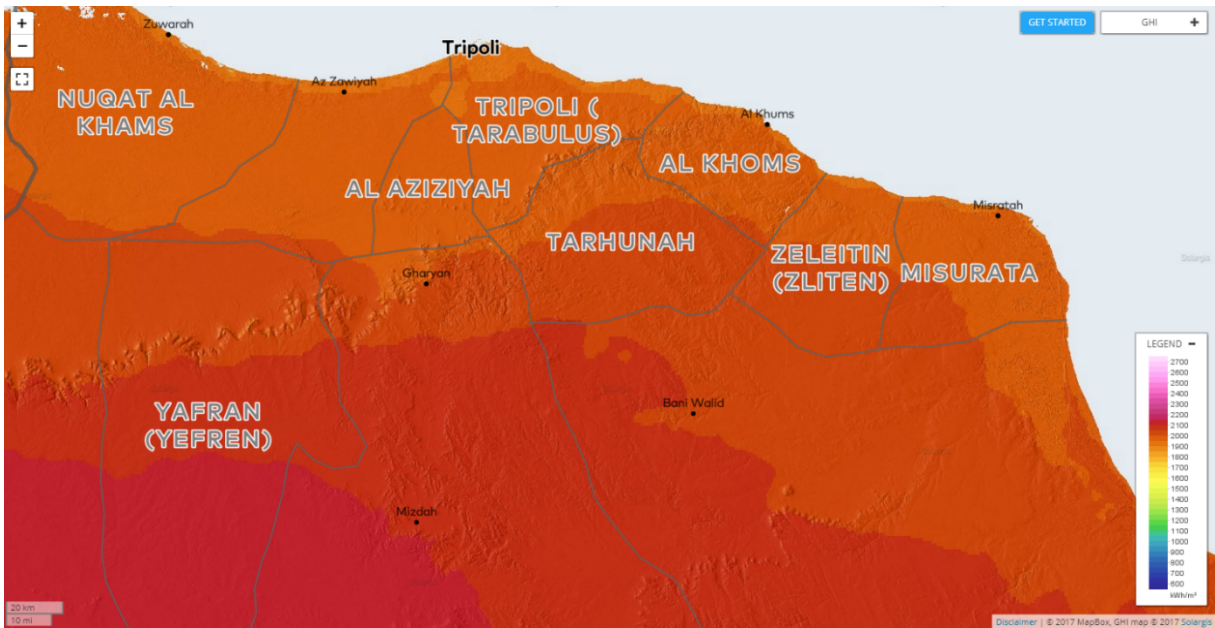


**Figure 3.5 Global horizontal irradiance in Bani Walid region (GHI)**

### 3.5 System Sizing Using Homer

Evaluation of the technical feasibility and economics of many technology options and accountability for variations in technology costs and energy resource availability, could easily be carried out using the hybrid optimization model for an electrical renewable (HOMER). A power system designer can use HOMER to provide an important overview that compares the cost and feasibility of different configurations and evaluates the technical performance of the power system [39]. In this study Homer ver 2.68 is used, which is a free software from the National Renewable Energy Lab [nrel.gov].

### 3.5.1 System Input Data

The system components for the sizing are the photovoltaic system, diesel generator sets, and batteries for energy storage. System input data with costs are shown in Table 3.3.

**Table 3.3 System input data**

PV System			
Size (kW)	Capital (\$)	Replacement (\$)	O&M (\$/yr)
12	22,473	13,620	150
Generator			
Size (kW)	Capital (\$)	Replacement (\$)	O&M (\$/hr)
2,600	2,475,000	1,500,000	52
Batteries			
Quantity	Capital (\$)	Replacement (\$)	O&M (\$/yr)
24	53,987	32,719	240
Converter			
Size (kW)	Capital (\$)	Replacement (\$)	O&M (\$/yr)
100	31,755	19,246	120

The selected PV module is Panasonic HIT VBHN240SJ25, with output power of 240 W, solar efficiency of 19%, NOCT of 44°C, and a lifetime of 25 years. Temperature effect is considered in the system. The selected battery is Hoppecke 26 OPzS 4700 Ah, 9.4 kWh with life cycle 20 years. Solar resources input and location are shown in Figure 3.6.

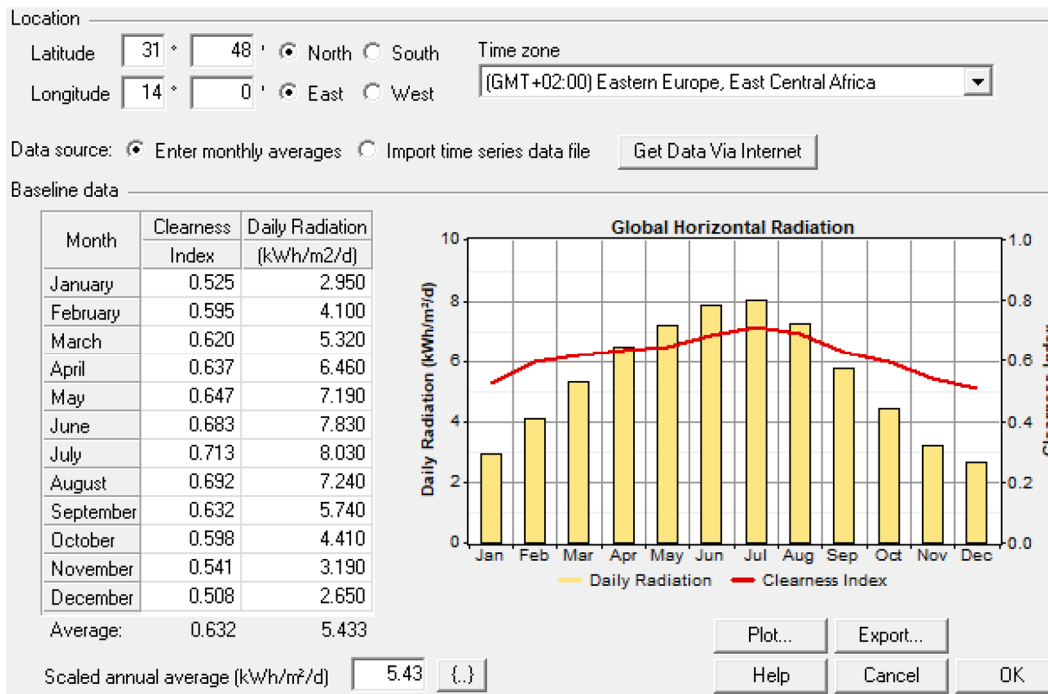


Figure 3.6 Solar data resources

### 3.5.2 System Block Diagram

The block diagram of the designed system is shown in Figure 3.7, where the primary load is 864 MWh/d, connected to the AC bus.

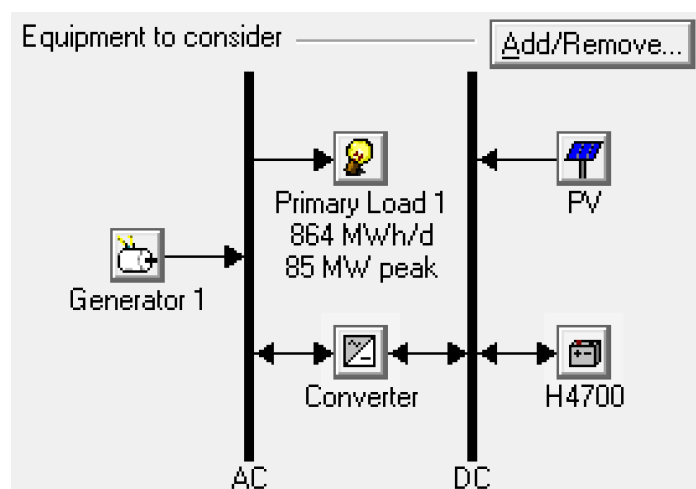


Figure 3.7 System block diagram in Homer

### 3.5.3 Optimized System

The optimization result shows the first ranking of the system with large scale 76.8 MW PV, with all other power sources in the system having levelized cost of energy (COE) of 0.213 \$/kWh and total net present cost (NPC) of \$856,859,008. The highest cost in the last ranking of the categorized system is without battery storage with a (COE) of 0.253 \$/kWh, as illustrated in Figure 3.8. A list of system components is provided in Table 3.4.

	PV (kW)	Gen1 (kW)	H4700	Conv. (kW)	Initial Capital	Operating Cost (\$/yr)	Total NPC	COE (\$/kWh)	Ren. Frac.	Diesel (L)	Gen1 (hrs)	Batt. Lf. (yr)
   	76800	62400	3360	55000	\$ 228,250,624	49,173,968	\$ 856,859,008	0.213	0.32	71,004,416	6,897	20.0
  		62400	4560	20000	\$ 76,008,528	61,106,280	\$ 857,151,872	0.213	0.00	90,582,080	8,554	20.0
 		70200			\$ 66,825,000	67,978,608	\$ 935,819,840	0.232	0.00	99,838,216	8,760	
  	100800	70200		55000	\$ 273,063,456	58,314,064	\$ 1,018,512,896	0.253	0.34	83,226,944	7,441	

**Figure 3.8 Optimization results**

**Table 3.4 Selected system components**

PV	76,800 kW
Generator sets	62,400 kW
Inverter	55,000 kW
Rectifier	55,000 kW
Batteries	3,360

### 3.5.4 Economic Optimization Results and Financial Analysis

Cost summary results of the optimized system are shown in Figure 3.9 and Table 3.5. The highest net present cost is from generator sets throughout the lifetime of the system (25 years); the lowest net present cost is batteries. The total system cost is \$856,859,328 with a COE of 0.213 \$/kWh, while for the case with only generator sets (base case system) the COE is 0.232

\$/kWh. The comparison of net percent costs indicates the differences in percent worth of \$78,960,928 between the two cases. Thus, the optimized system saves money over the project lifetime in comparison with the base case system, which proves the feasibility of using a renewable energy system in this project. The simple payback period is 9.02 years, as illustrated in table 3.6. Figure 3.10 demonstrates the cash flow (\$) throughout the project lifetime of the two cases, while Figure 3.11 shows the cash flow details of the optimized system.

**Table 3.5 Cost summary**

Component	Capital (\$)	Replacement (\$)	O&M (\$)	Fuel (\$)	Salvage (\$)	Total (\$)
PV	143,827,200	0	12,272,030	0	0	156,099,232
Generator 1	59,400,000	66,368,568	110,032,224	440,222,464	-5,782,452	670,240,960
Hoppecke 26 OPzS 4700	7,558,180	1,428,273	429,521	0	-800,467	8,615,506
Converter	17,465,250	4,416,880	843,702	0	-822,121	21,903,710
System	228,250,624	72,213,720	123,577,496	440,222,464	-7,405,040	856,859,328

**Table 3.6 Economics comparison between current case system and base case system**

Metric	Value
Present worth	\$ 78,960,928
Annual worth	\$ 6,176,854/yr
Return on investment	11.6 %
Internal rate of return	10.8 %
Simple payback	9.02 yrs
Metric	Value

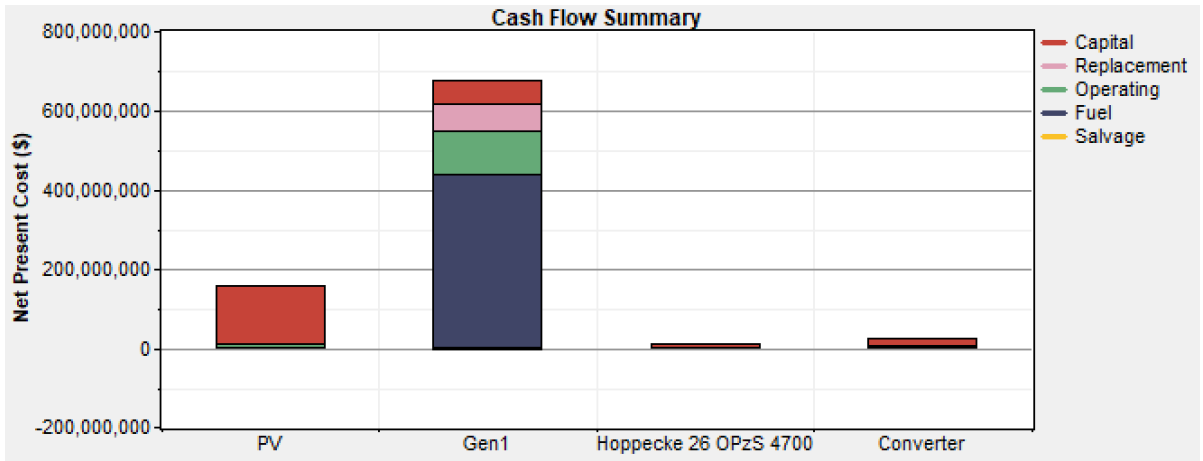


**Figure 3.9 Cash flow summary**

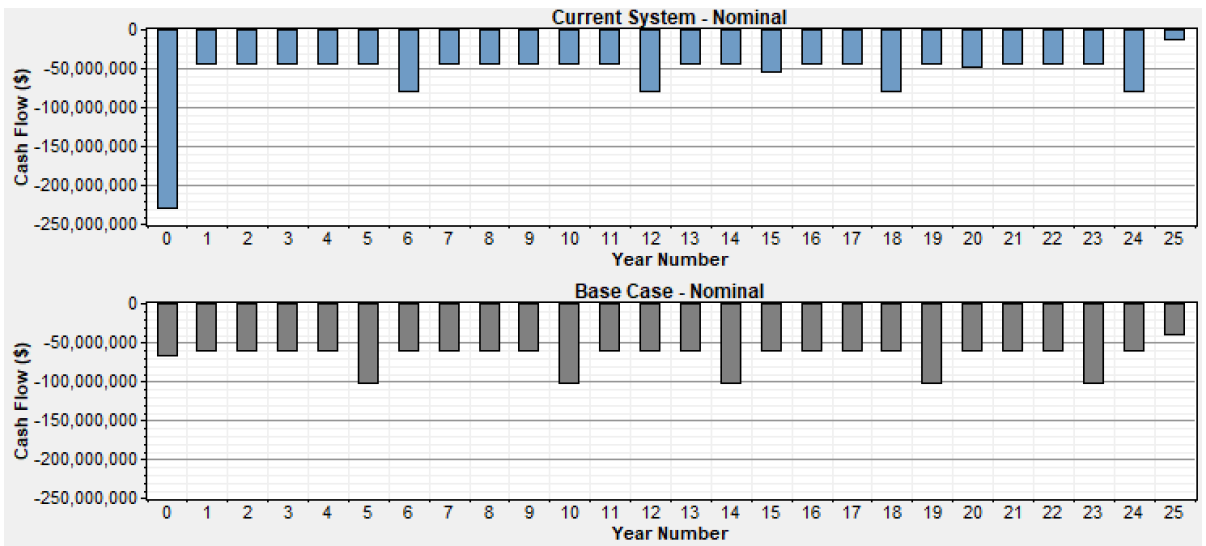


**Figure 3.10 Comparison of current case system and base case system**

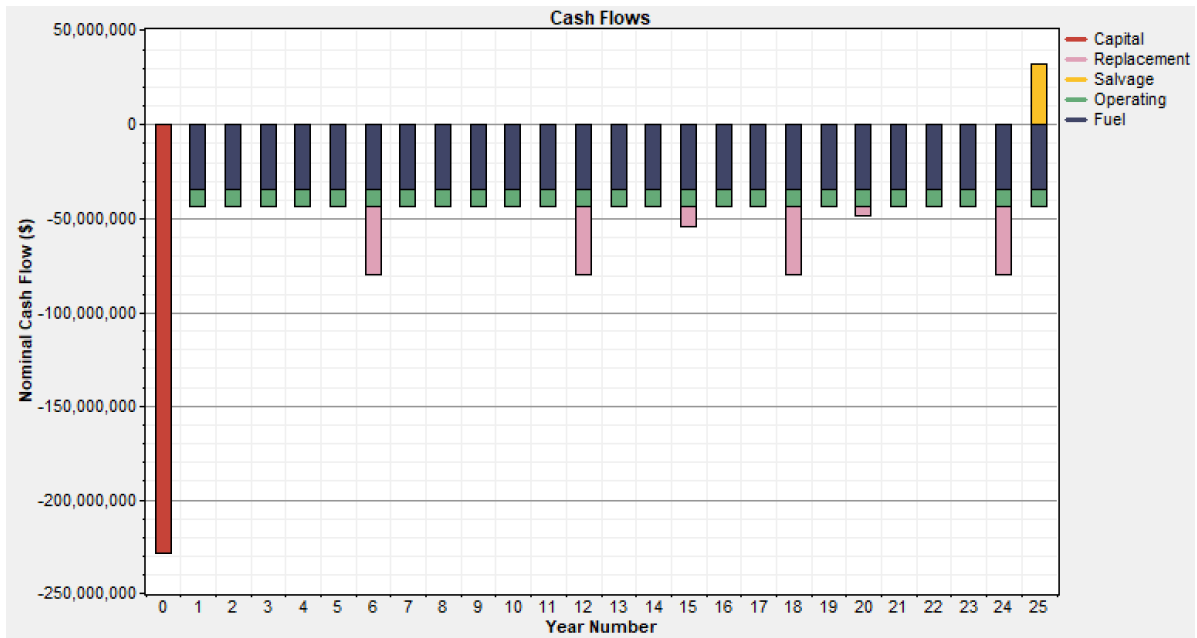


**Figure 3.11 Cash flows**

### 3.5.5 Electrical and System Simulation Results

Simulation results show that PV energy production will be 32%, with a penetration of 40.8%. The excess energy of the system is 21.9% which could be sold to the grid, with 0% unmet electrical load, as illustrated in table 3.7. Table 3.8 shows the expected PV output results. Average electric production from the PV modules and the generator sets are high during the summer season to meet the load demand, as shown in Figure 3.12. Figure 3.13 shows PV output in kW. Maximum PV production is around noon time, the modules have no track system. The maximum generator sets' production is during nighttime in summer and winter, while production during daytime is less, because PV system and batteries are supplied plenty of energy to the loads, as demonstrated in Figure 3.14. Since the generator sets supply most of the load

during nighttime, inverters work mostly during daytime while rectifiers work mostly during the night for charging batteries, as illustrated in Figure 3.15. The batteries state of charge is mostly 86% to 100%, as illustrated in Figure 3.16.

**Table 3.7 Expected electrical output results**

Production	kWh/yr	%
PV array	128,497,000	32
Generator 1	278,850,944	68
Total	407,347,936	100
Quantity	kWh/yr	%
Excess electricity	89,393,936	21.9
Unmet electric load	35,640	0.0
Capacity shortage	186,770	0.1

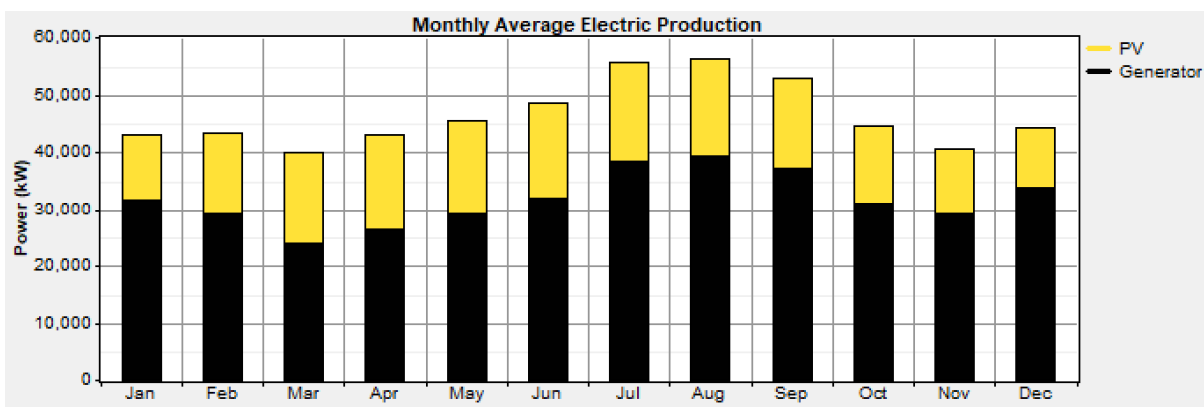


**Figure 3.12 Monthly average electric production**

**Table 3.8 Expected PV output results**

Quantity	Value	Units
Rated capacity	76,800	kW
Mean output	14,669	kW
Mean output	352,047	kWh/d
Capacity factor	19.1	%
Total production	128,497,000	kWh/yr
Quantity	Value	Units
Minimum output	0	kW
Maximum output	74,559	kW
PV penetration	40.8	%
Hours of operation	4,385	hr/yr
Levelized cost	0.0950	\$/kWh

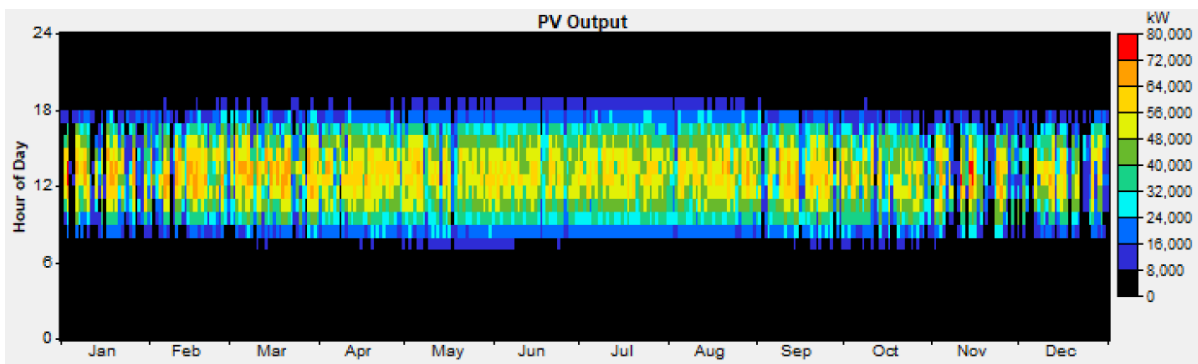


**Figure 3.13 PV output**

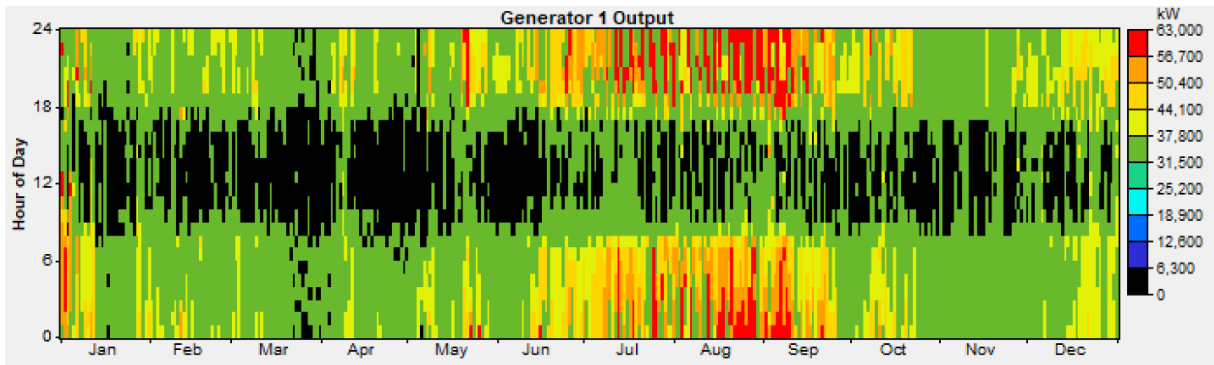


**Figure 3.14 Generator sets output**

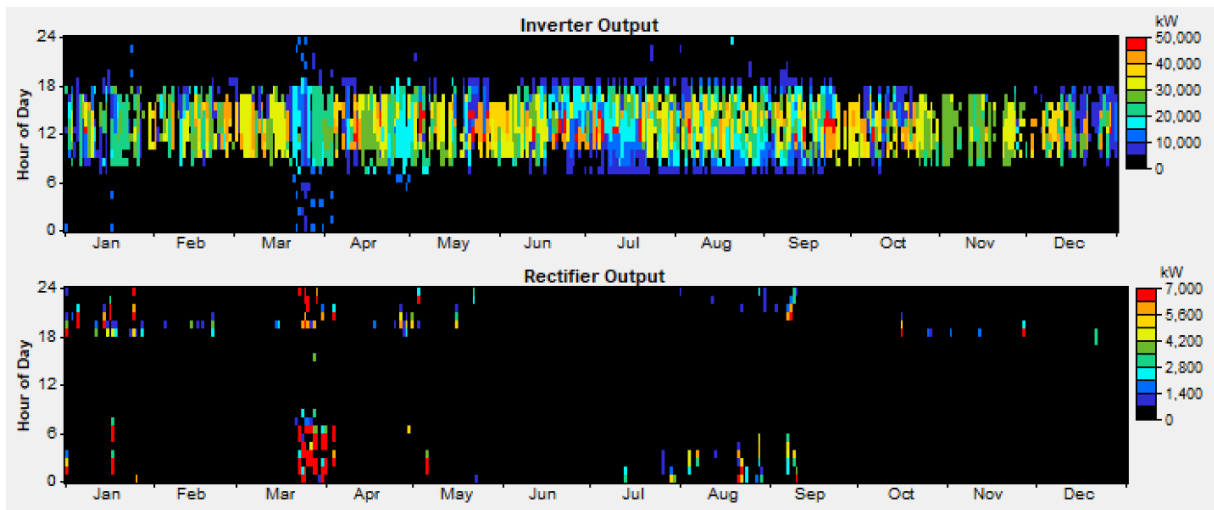


**Figure 3.15 Inverter and rectifier output**

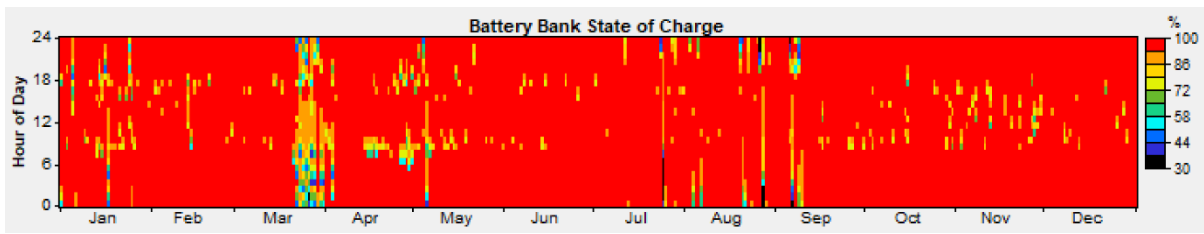


**Figure 3.16 Battery bank state of charge**

### 3.5.6 Sensitivity Analysis

The results are affected by variable inputs such as solar radiation, increasing loads and prices of the components. Therefore, the design approach can be scaled or translated for different cases. In this study, the considered sensitivity variables are shown in table 3.9.

**Table 3.9 Sensitivity variable inputs**

Diesel price	0%	10%	20%	30%
Load	0%	10%	20%	
Solar radiation	-5%	0%	5%	

#### 3.5.6.1 Levelized cost of energy (COE)

The levelized cost of energy (COE) is important for designing a power system. It is unreliable to design a power system with a very high COE.

Figure 3.17(a), (b), (c), and (d) demonstrates that the levelized cost of energy (COE) is increasing with increasing loads and decreasing irradiance. COE also increases with increasing diesel price, while it decreases with decreasing loads and increasing irradiance.

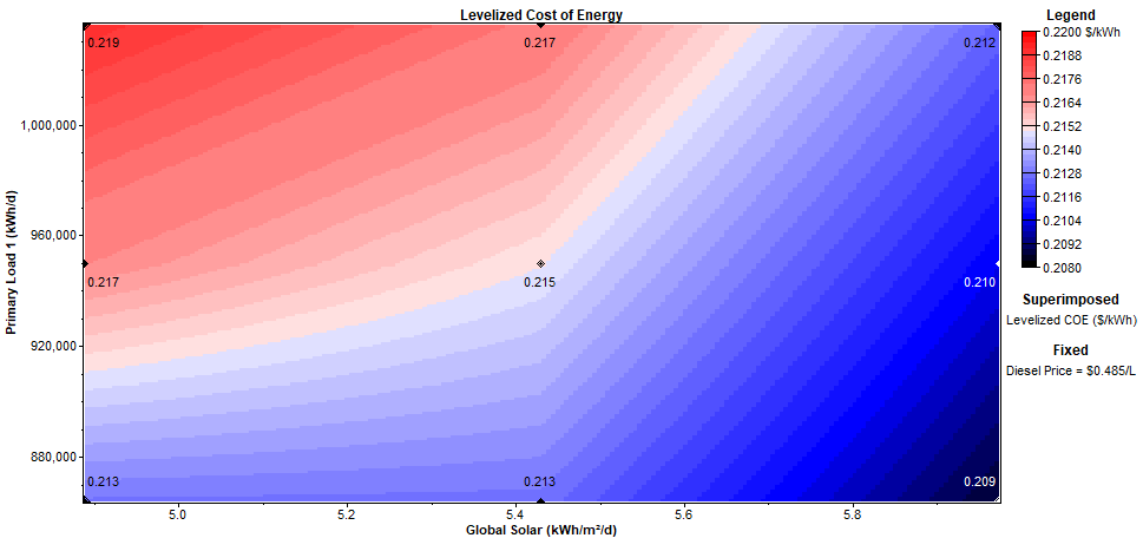


Figure 3.17 (a): COE at load sensitivities (0, 10, and 20%) and diesel price 0%

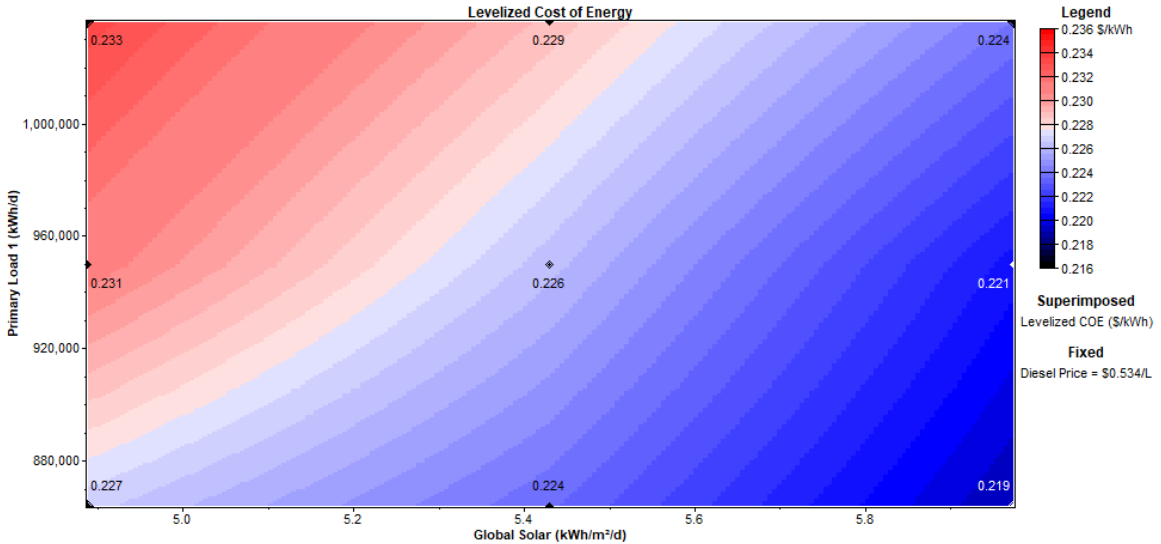
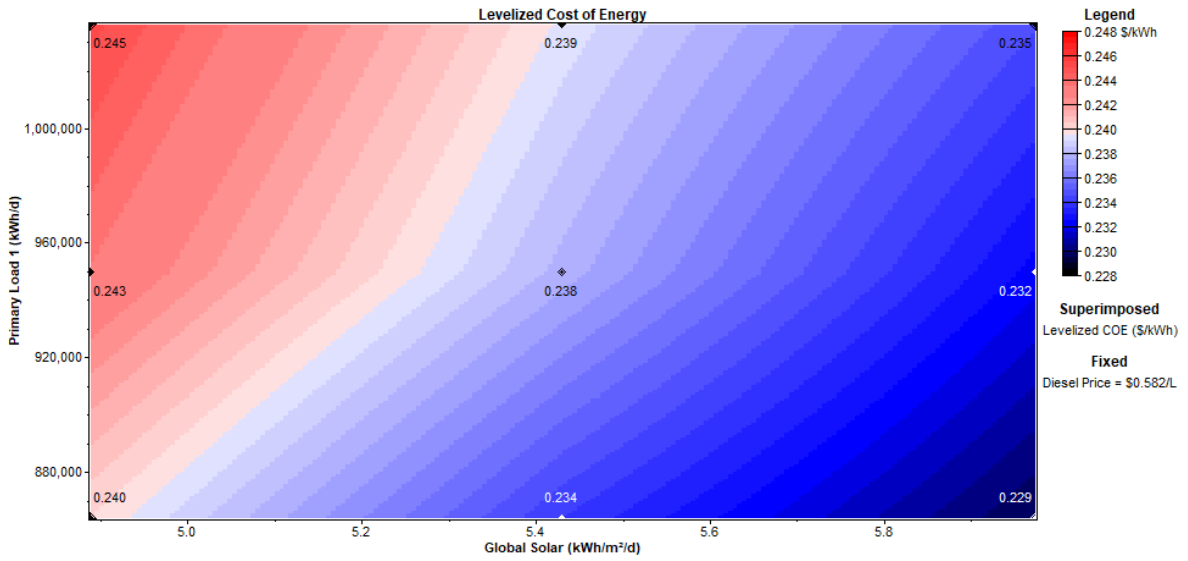
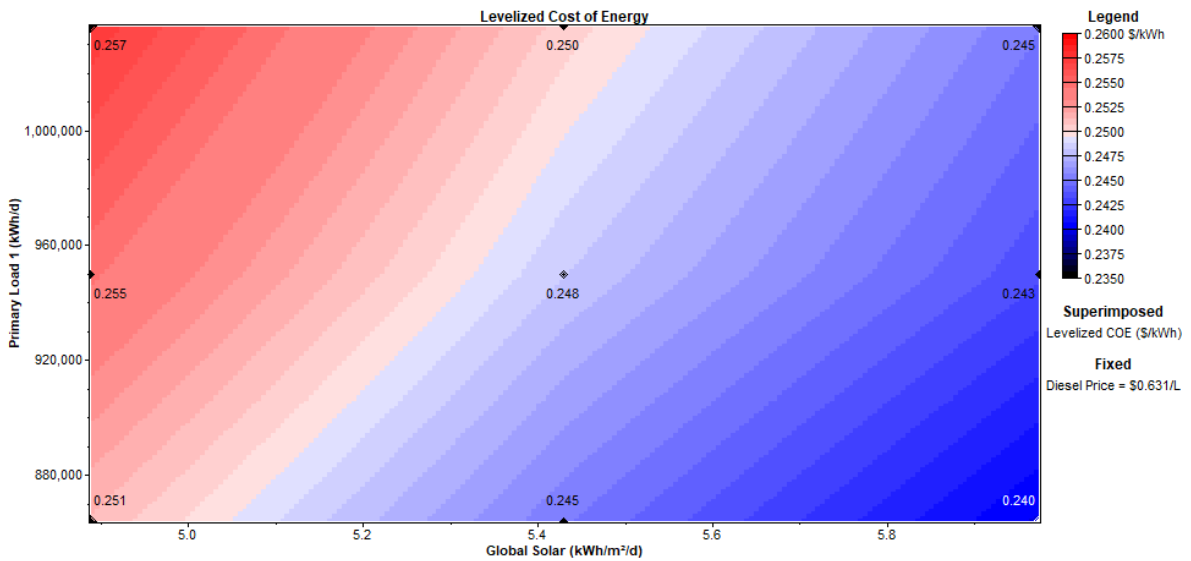


Figure 3.17 (b): COE at load sensitivities (0, 10, and 20%) diesel price 10%



**Figure 3.17 (c): COE at load sensitivities (0, 10, and 20%) and diesel price 20%**



**Figure 3.17 (d): COE at load sensitivities (0, 10, and 20%) and diesel price 30%**

### 3.5.6.2 Optimal systems

#### 3.5.6.2.1 Optimal PV system

The results of optimal PV system for variable sensitivity inputs can be seen in Figure 3.18(a), (b), (c), and (d). At diesel price sensitivities of 0% and 10%, the PV system capacity decreases significantly with decreasing the irradiance -5%.

With increasing the diesel price to 20% and 30%, the sizing shows that using a PV system is reliable at all irradiance sensitivities, the highest capacity of PV is at high loads and low irradiance after increasing diesel price to 30%, as shown in Figure.3.18 (d)

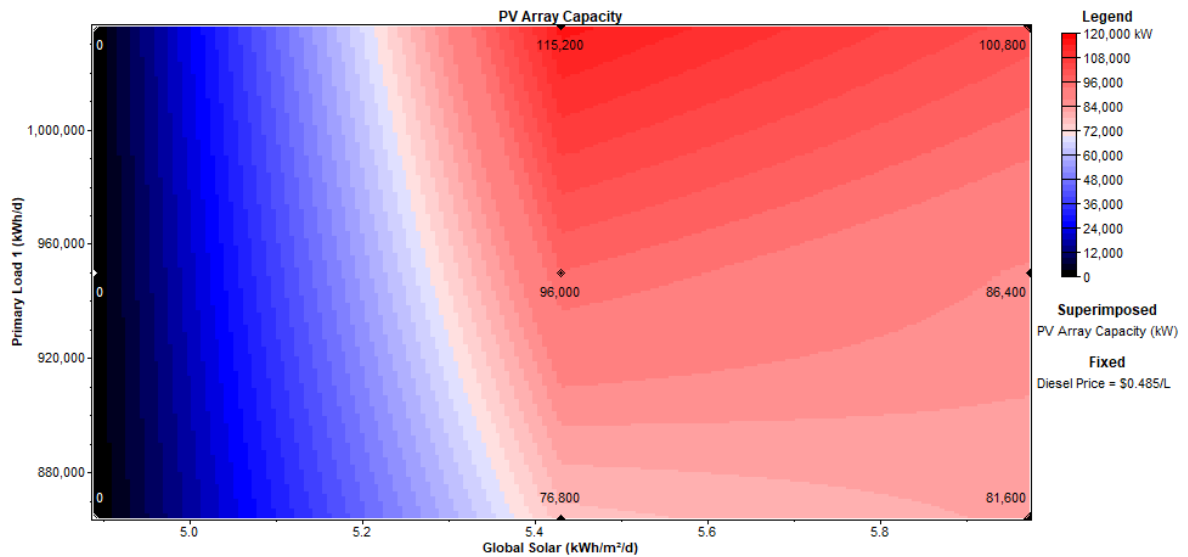
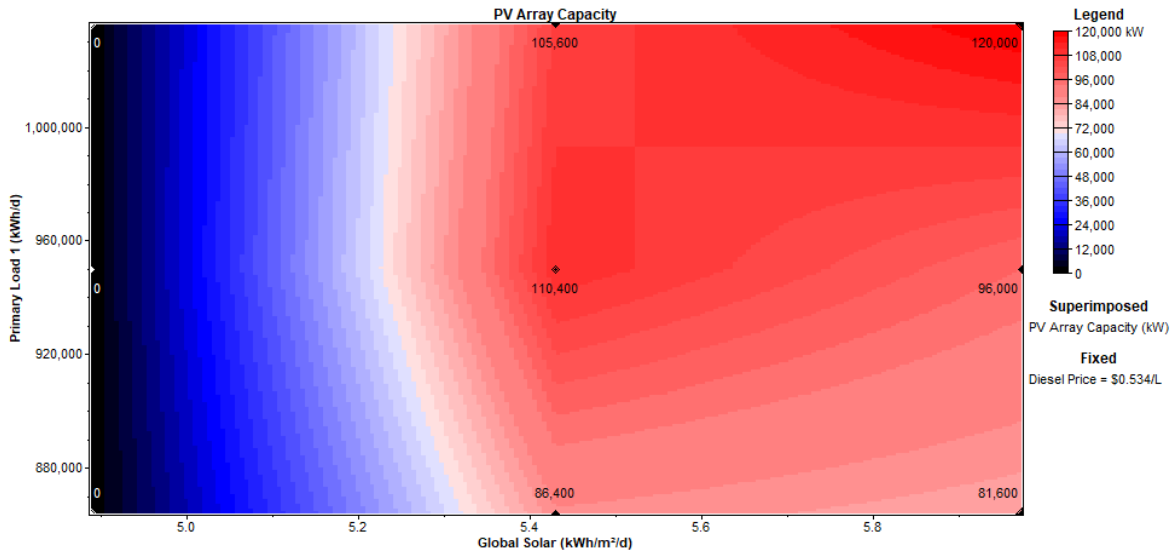
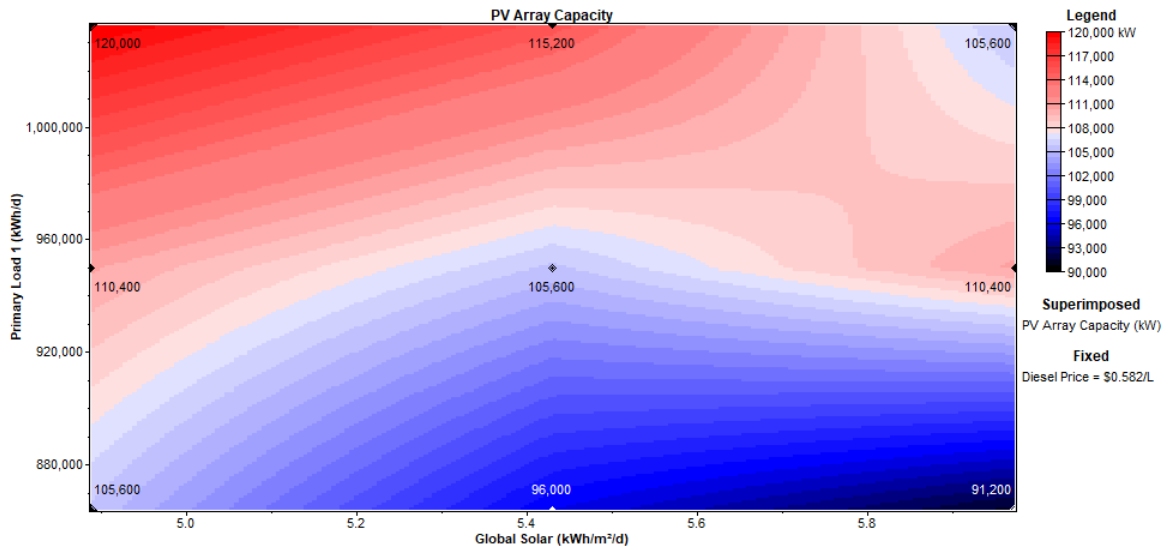


Figure 3.18 Optimal PV (a): At load sensitivities (0,10, and 20%) and diesel price 0%



**Figure 3.18 Optimal PV (b): At load sensitivities (0,10, and 20%) and diesel price 10%**



**Figure 3.18 Optimal PV (c): At load sensitivities (0,10, and 20%) and diesel price 20%**

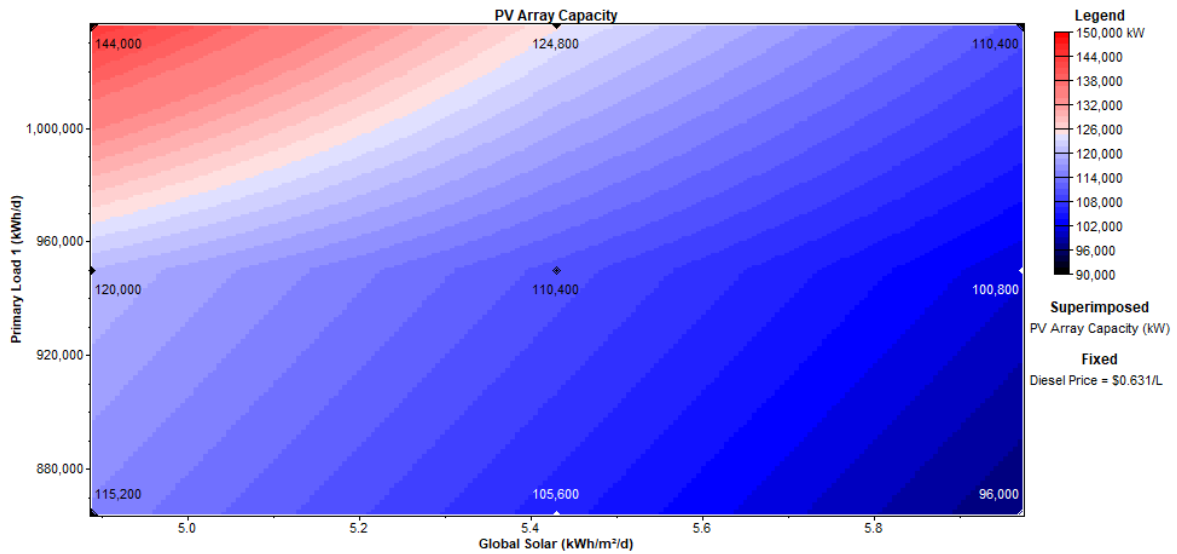


**Figure 3.18 Optimal PV (d): At load sensitivities (0,10, and 20%) and diesel price 30%**

### 3.5.6.2.2 Optimal battery storage

Sensitivity analysis shows that the hybrid power system is required more batteries at the very low capacity of the PV system, as shown in Figure.3.19. The irradiance sensitivities of 0% and 5% do not have much effect on battery sizing. At the diesel price sensitivity of 30% it can be seen clearly in Figure 3.20(d) that load growth affects battery sizing while irradiance sensitivities do not affect battery sizing in such a large power system, due to the high price jump of a large battery string.

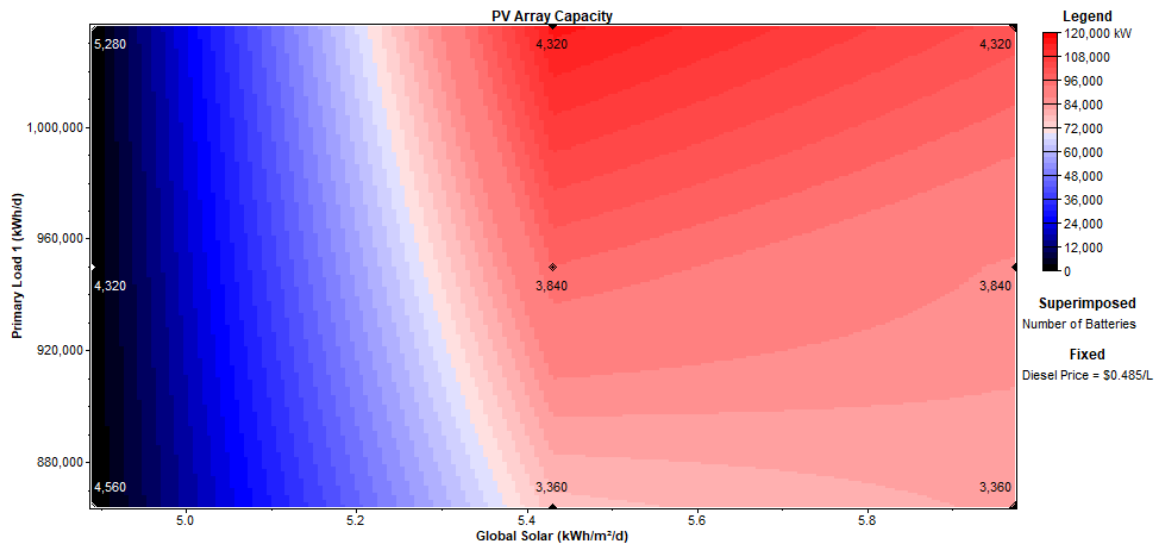


**Figure 3.19 Optimal PV and Battery sizing at diesel sensitivity of 0%**

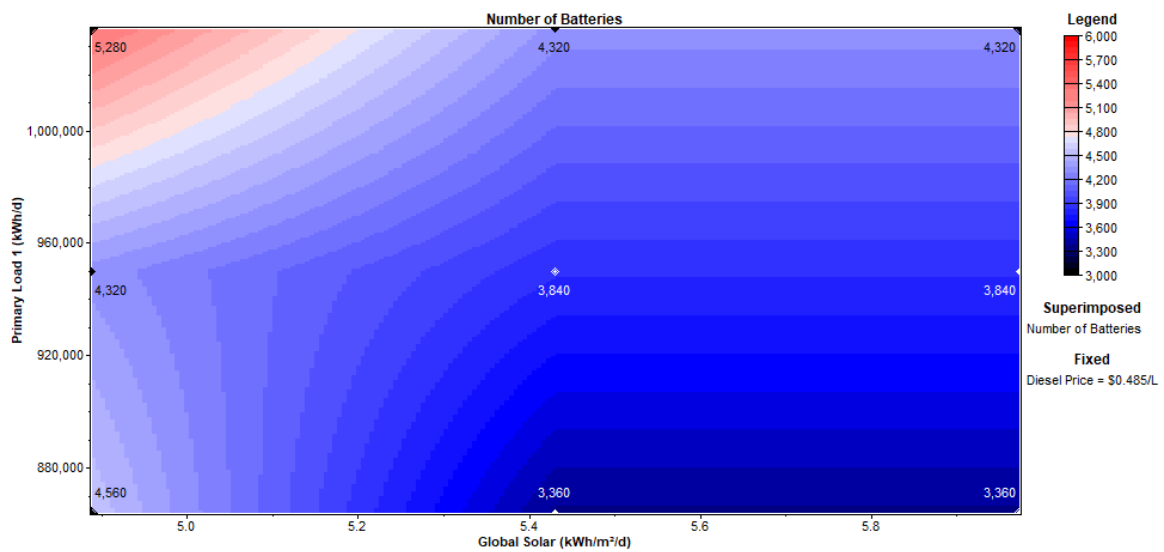


**Figure 3.20 Optimal battery (a): At load sensitivities (0,10, and 20%) and diesel price 0%**

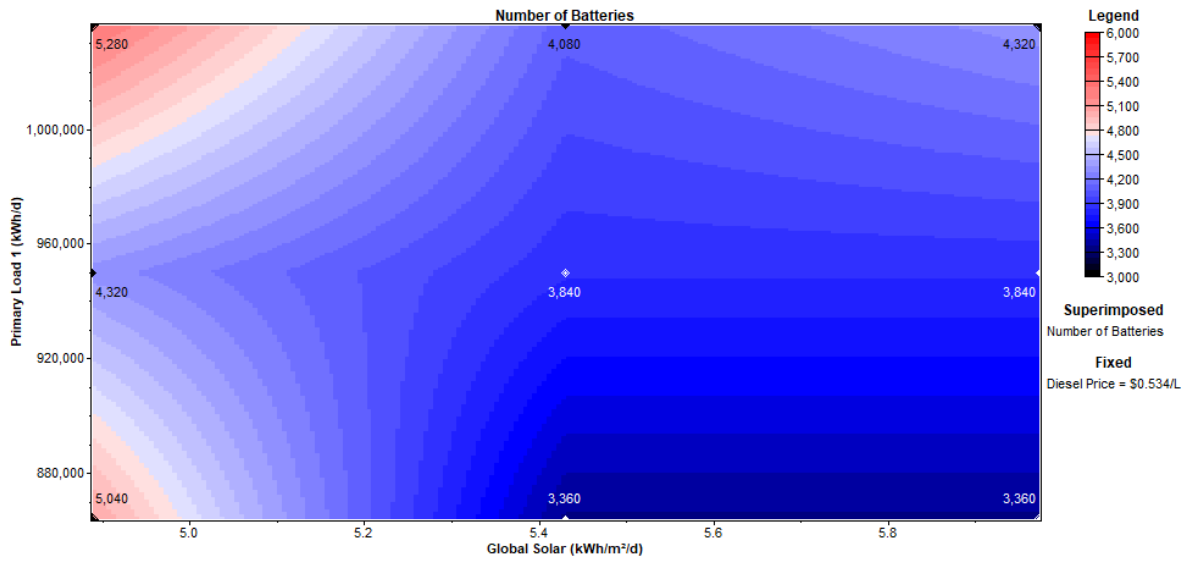


**Figure 3.20 Optimal battery (b): At load sensitivities (0,10, and 20%) and diesel price 10%**

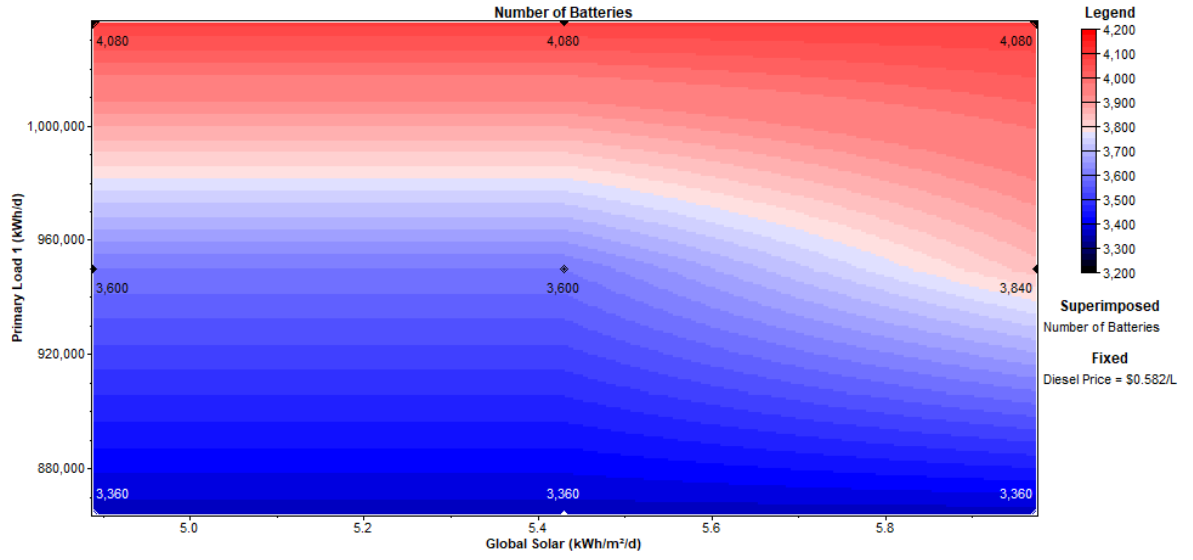


**Figure 3.20 Optimal battery (c): At load sensitivities (0,10, and 20%) and diesel price 20%**

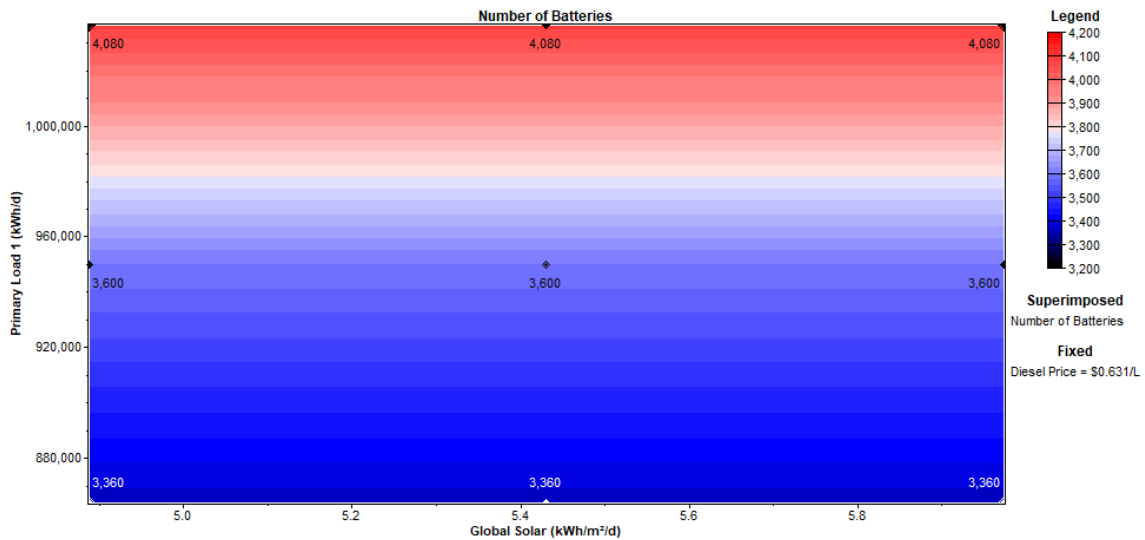


**Figure 3.20 Optimal battery (d): At load sensitivities (0,10, and 20%) and diesel price 30%**

### 3.6 Proposed location

The proposed location as shown in Figure 3.22 is at latitude  $31.8^{\circ}$  N and longitude  $14^{\circ}$  E, which is in the north of Bani Walid valley and very close to a distribution station, to avoid losses in the transmission lines. In addition, this station is located almost in the center of most loads. Thus, overload on the existing transmission lines is avoided, tested using the PowerWorld tool. This area is also characterized by high altitude and almost covered by rocks. Therefore, it has less dust compared to the southern cities in Libya. The red lines in Figure 3.22 represent the existing 66kV transmission lines.

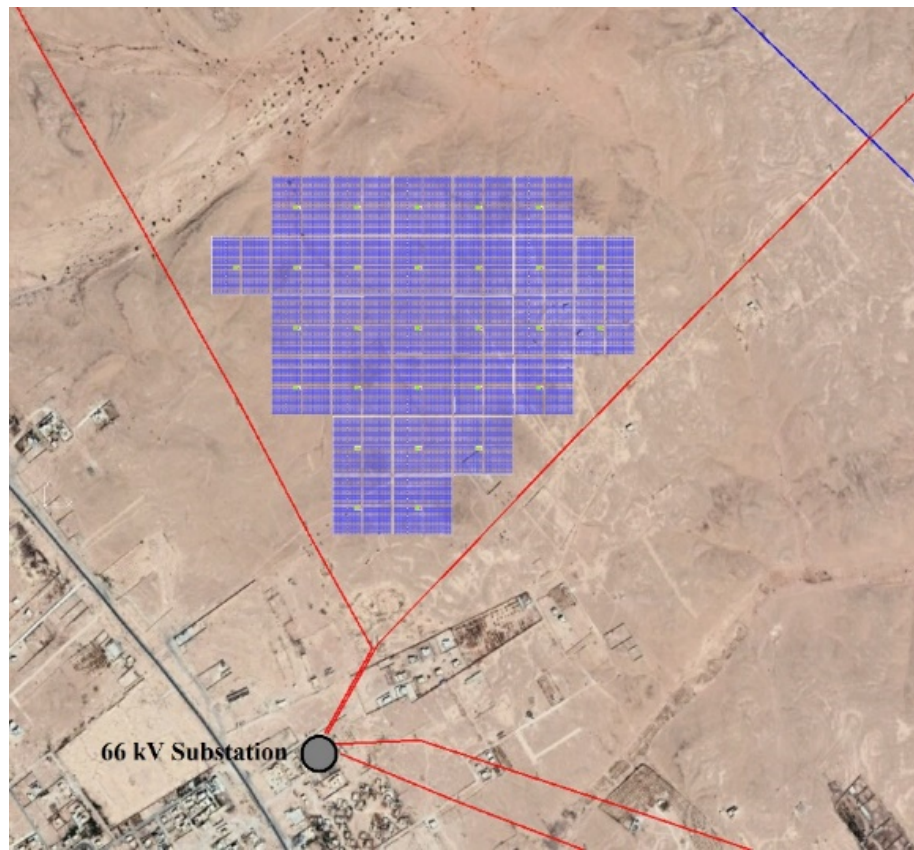


**Figure 3.21 Proposed location for PV modules**

### **3.7 Conclusion**

The design of any hybrid power system with renewable energy is based on the availability of renewable energy sources at that location as well as the prices of components to design a feasible hybrid power system with different renewable energy sources.

Libya has potential solar and wind energy. However, the wind energy in Libya depends significantly on the location. The main goal of this study is to investigate the available renewable energy sources in Bani Walid and optimize the hybrid grid power system, considering the effect of temperature in that area. The design approach is scaled for different cases. Based on this study, Bani Walid has a great potential for the use of solar energy, while wind energy is less

reliable with a yearly average wind speed of only 3.96 m/s and a maximum monthly average in May of a wind speed of 4.35 m/s. The windiest day is in February, with an average speed of 4.6 m/s.

The optimized system shows that the lowest COE ,0.213 \$/kWh, is with PV, generator sets, and battery storage, while with only generator sets is 0.232 \$/kWh. Comparison of these two cases shows that the present worth is \$78,960,928. The simple payback is 9.02 years with an annual worth of \$6,176,854. The payback indicates how long it would take to recover the difference in investment costs between the optimized system with renewable energy (optimized system) and the case with only generator sets (base case system). In addition, the emissions are reduced by 29 per cent as compared to the optimized system.

The optimization results illustrate that using renewable energy in a hybrid power system could lower the COE as the prices of renewable energy components have decreased recently. Furthermore, it reduces emissions up to 29 percent during the project lifetime.

The backup batteries play a major role to lower COE; the optimized system shows that the system without battery storage has highest COE.

The designed approach has been scaled for different cases, as the optimization results are affected by variable inputs such as solar radiation and increasing loads. From sensitivity analysis, it can be concluded that load growth and decreasing irradiance raise the COE. Sensitivity analysis shows load growth effect on PV and battery sizing, while irradiance sensitivities effect PV sizing but do not significantly affect battery sizing. At a sensitivity of diesel price 30%, the irradiance sensitivities do not affect the battery sizing, due to the high jump of the large string price in such a large hybrid power system.

This innovative design could be implemented in Libya and in neighboring countries in that part of the world to produce renewable energy.

## **Chapter 4**

### **4 Impact of a large-scale PV system with ESS and generator sets on a distribution network in Bani Walid**

#### **4.1 Introduction**

The main objective of this chapter is to analyze the designed hybrid grid connected power system and study the impact of a large PV system with a generator and energy storage system on the existing power grid in western Libya. Data has been collected from the General Electricity Company of Libya including load data, power transformers, transmission lines length, conductors and towers' parameters for that existing grid.

The analysis includes power flow analysis and the improvement of power flow by using control of power flow, contingency analysis, and transient stability analysis of the designed hybrid power system, using the Electrical Transient Analysis Program (ETAP).

An overview of the designed hybrid power system is presented in this chapter. Analysis and solutions are also proposed in this chapter.

#### **4.2 An Overview of the designed hybrid power system**

There is excess energy and a deficit of energy at certain times in any hybrid renewable energy system. Any excess energy produced by the hybrid system can be stored. Similarly, when the power demand is more than the energy produced by renewable sources, the storage system should supply loads with plenty of energy [40]. In this chapter, the hybrid grid-connected power system is designed as a stand-alone hybrid power system and can be connected to the central grid, so that any excess energy can be absorbed by the utility grid.

The components of the system are the PV system, generator sets, and energy storage system, which will help to stabilize the grid and provide dispatchable renewable energy in the western Libyan power grid.

All the power sources in this simulation are based on the results from the sizing in chapter 3. The rated power of generator sets is 62.4 MW and they are assumed to be operating as a voltage control, PV system at their full rated capacity, which is 76.8 MW. The battery bank operates as a swing to supply the load if there is not enough power from the other sources. The generator set is provided with an auxiliary device, which is a power system stabilizer (PSS) to help with system stability. Figure 4.1 below shows a system block diagram. Details are explained in the next section.

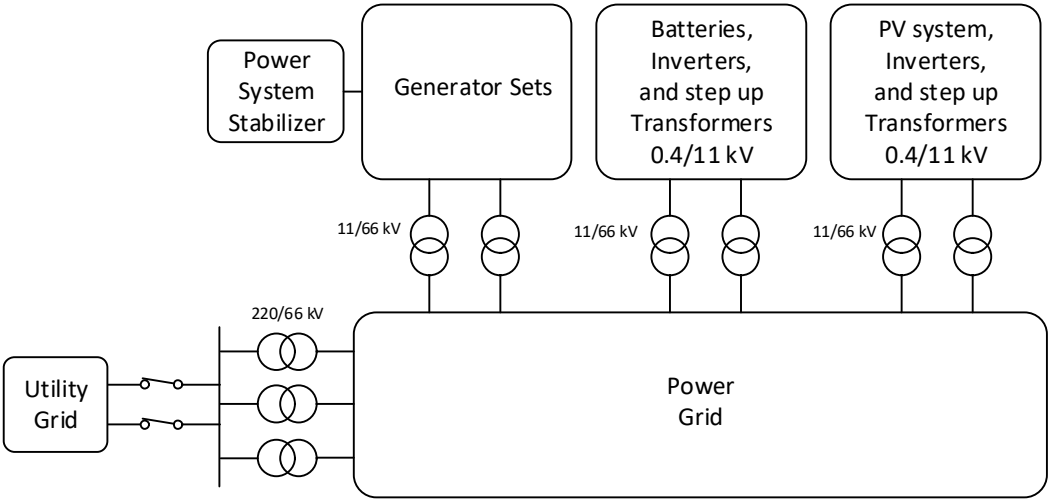


**Figure 4.1 Block diagram of the designed hybrid power system**

**4.2.1 PV Panels**

The irradiance has been calculated by using ETAP at maximum irradiance during the day in July 2017 for the PV location at latitude 31.8° N and longitude 14° E. PV input data for

the Panasonic VBHN240SJ25 PV module at a base temperature of 25 °C are shown in Figure 4.2 with a calculated fill factor (FF) of 78.29 %, which is an important value that determines the power conversion efficiency of an organic solar cell. FF can be calculated as:

$$FF = \frac{P_{max}}{I_{SC}V_{OC}} \dots\dots\dots (4.1)$$

where  $P_{max}$  is the maximum power generated,  $I_{SC}$  is the short circuit current, and  $V_{OC}$  is the open circuit voltage of the PV panel. FF depicts the “squareness” of the I–V curve while at the same time indicating whether or not the effort required to remove photo-generated carriers from a PV component could be considered easy or difficult. If the I–V curve is a rectangle, the FF has an ideal value of 100%. Here, the module efficiency is expressed as shown in [41]:

$$\eta = \frac{P_{max}}{P_{in}} = \frac{I_{SC} V_{OC} FF}{P_{in}} \dots\dots\dots (4.2)$$

where  $P_{in}$  is the light power incident on the PV panel.

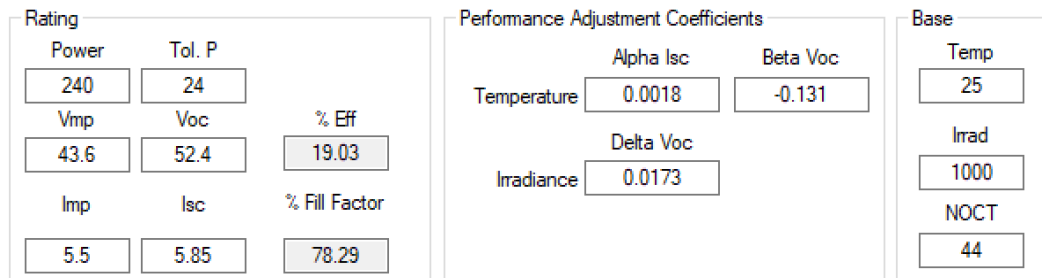


**Figure 4.2 PV module parameters**

#### 4.2.2 PV array calculations

The PV array has been calculated based on the minimum and maximum voltage and current of the installed inverter and PV module. The maximum open-circuit voltage and voltage at MPPT is at minimum temperature while the minimum voltage is at maximum temperature. The voltage range should be at limited values of the installed inverter. Table 4.1 shows the specifications of the inverter and Table.4.2 shows the specifications of the PV Module.

**Table 4.1 Inverter specifications**

Min. input voltage ( $V_{dc \text{ min}}$ )	460 V
Nominal input voltage ( $V_{dc,r}$ )	460 V
Feed-in start voltage ( $V_{dc \text{ start}}$ )	475 V
Max. input voltage ( $V_{dc \text{ max}}$ )	950 V
MPP voltage range ( $V_{mpp \text{ min}} - V_{mpp \text{ max}}$ )	460 V- 820 V
Max. input current ( $I_{dc \text{ max}}$ )	227A
Max. array short circuit current	340.5 A
Output Power	100 kW, Max = 100kVA

**Table 4.2 PV panel specifications**

Temperature (NOCT) [°C]	44 °C
Temp. coefficient of P <sub>max</sub> [%/°C]	-0.29 %/°C
Temp. coefficient of V <sub>oc</sub> [V/°C]	-0.131 V/°C
Temp. coefficient of I <sub>sc</sub> [mA/°C]	1.76 mA/°C
Open circuit voltage (V <sub>oc</sub> ) [V]	52.4 V
Max. power voltage (V <sub>mp</sub> ) [V]	43.6 V

The temperature variations modify the behaviour of the I-V curve of the photovoltaic devices. The voltage decreases and current increases when temperature rises. These variations are approximately linear with temperature.

The output voltage of the solar at temperature T is expressed by [42]:

$$V_{oc@T} = V_{oc@T_r} * \left( 1 + \frac{\beta V_{oc} * (T - T_r)}{100} \right) \dots \dots \dots (4.3)$$

$$V_{mp@T} = V_{mp@T_r} * \left( 1 + \frac{\beta V_{mp} * (T - T_r)}{100} \right) \dots \dots \dots (4.4)$$

$\beta V_{oc}$  and  $\beta V_{mp}$  are respectively the temperature coefficient variation in a percentage of the open circuit and maximum power point;  $T_r$  is the reference temperature. The maximum and minimum voltages of the system can be given by:

$$(V_{oc})_{@-40^{\circ}C} = 52.4 * \left[ 1 + (-0.131) * \left( \frac{-40 - 25}{100} \right) \right] = 56.86 V \dots \dots \dots 4.5$$

$$(V_{oc})_{@90^{\circ}C} = 52.4 * \left[ 1 + (-0.131) * \left( \frac{90 - 25}{100} \right) \right] = 47.94 V \dots\dots\dots 4.6$$

$$(V_{MPP})_{@-40^{\circ}C} = 43.6 * \left[ 1 + (-0.131) * \left( \frac{-40 - 25}{100} \right) \right] = 47.31 V \dots\dots\dots 4.7$$

$$(V_{MPP})_{@90^{\circ}C} = 43.6 * \left[ 1 + (-0.131) * \left( \frac{90 - 25}{100} \right) \right] = 39.89 V \dots\dots\dots 4.8$$

Minimum number of modules per string in series:

$$\frac{V_{MPP \text{ inverter}}}{V_{MPP @90^{\circ}C}} = \frac{460}{39.89} = 11.53 \approx 12 \text{ modules} \dots\dots\dots 4.9$$

Maximum number of modules per string in series:

$$\frac{V_{MPP \text{ inverter}}}{V_{oc @-40^{\circ}C}} = \frac{820}{56.86} = 14.42 \approx 14 \text{ modules} \dots\dots\dots 4.10$$

The minimum number of strings in the series is 12 strings and the maximum number of strings is 14 strings. Since the lowest temperature in Libya throughout a year is above -4 °C, the output voltage is less than the voltage at -40 °C. Selected optimum strings in the series are 12 modules.

Maximum arrays can be connected in parallel, given as follows:

$$\text{Modules per inverter} = \frac{100 \text{ kW}}{0.24 \text{ kW}} = 416.67 \text{ modules} \approx 416 \text{ modules} \dots\dots\dots 4.11$$

The output power of the string should not exceed the maximum power of the installed inverter. Maximum strings per module can be connected in parallel as:

$$\frac{\text{Modules per inverter}}{\text{Modules per strings}} = \frac{416}{12} = 34.67 \approx 34 \text{ strings} \dots \dots \dots 4.12$$

The output power of 35 strings exceeds the maximum power of the installed inverter;  
therefore, the selected strings number 34. and the number of modules per one inverter will be:

$$34 * 12 = 408 \text{ modules} \dots \dots \dots 4.13$$

Figure.4.3 shows the configuration of PV arrays. Each each of the 28 inverters is connected to a 5MW 0.4/11kV step up transformer. The output of all 5 MW transformers is divided into two groups for reliability and connected to two transformers of 50 MW 11/66 kV for reliability, as shown in Figure.4.4.

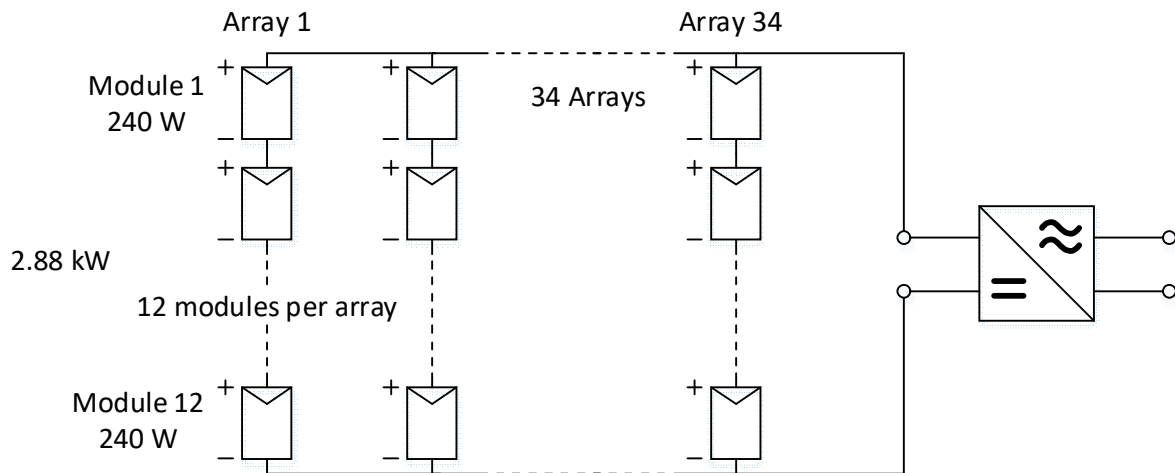


**Figure 4.3 Configuration of PV arrays**

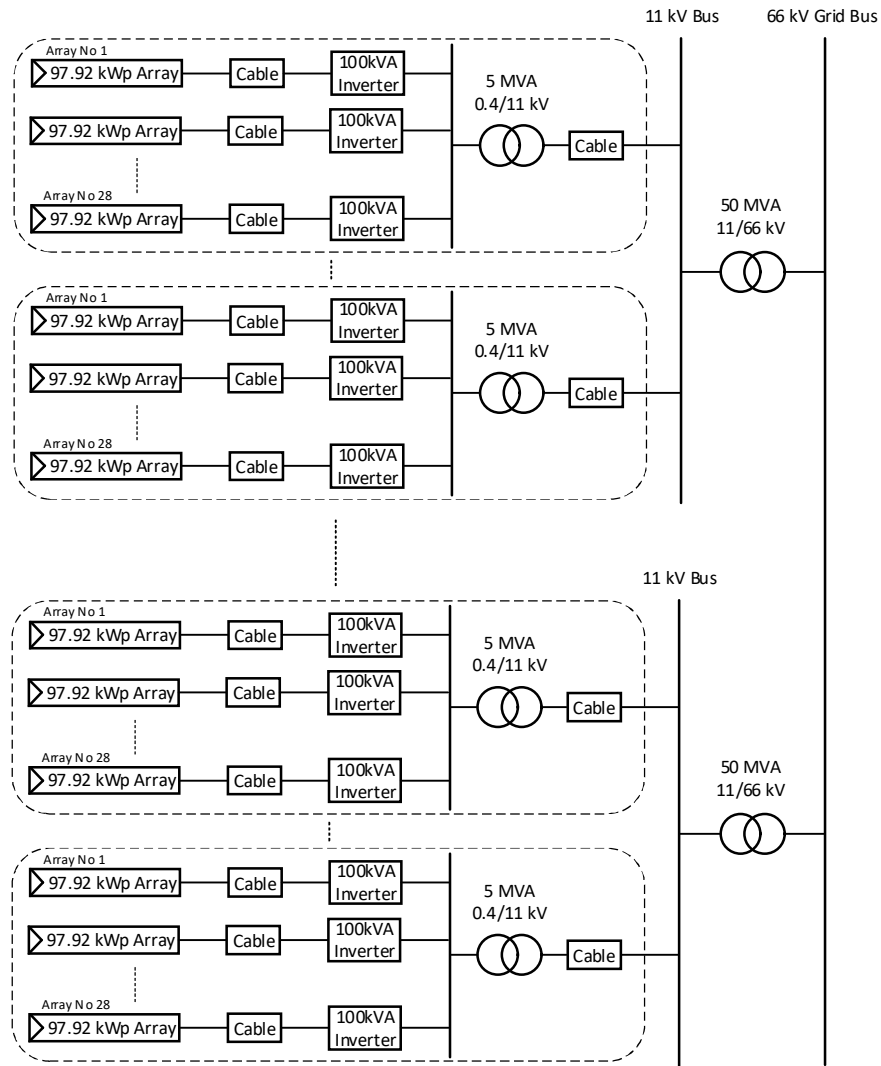


**Figure 4.4 Schematic circuit diagram of the 76.8 MW PV power station**

### 4.2.3 Required Area for PV Modules

A fixed array has been used in this study. Only the sun's apparent motion across the sky needs to be considered to optimize the distance between rows of modules. An adaptive

photovoltaic topology to overcome the shading effect in PV systems has been presented in [43]. To avoid excessive shadowing, the arrays should be spaced by a distance “d”, as illustrated in Figure 4.5 (a), in relation to the module width “a” [44]

$$\frac{d}{a} = \cos \beta + \frac{\sin \beta}{\tan \varepsilon} \dots \dots \dots (4.14)$$

where  $\varepsilon$  can be calculated by the geographical latitude  $\phi$  and the ecliptic angle  $\delta = 23.5^\circ$

$$\varepsilon = 90^\circ - \delta - \phi \dots \dots \dots (4.15)$$

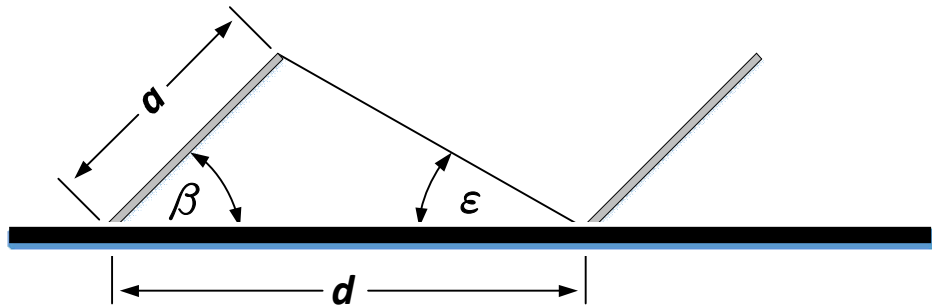


**Figure 4.5 (a): Arrangement of a large number of rows of fixed modules**

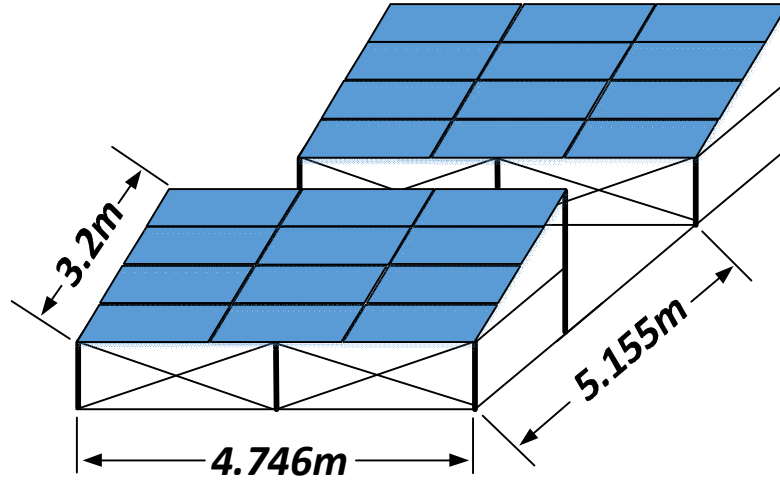


**Figure 4.5 (b): Configuration of fixed PV array**

The required area for one PV module (2.88 kW) is 12.995 m<sup>2</sup>, while the required area for one a PV module with land is 24.466 m<sup>2</sup>. The required area for one PV substation of 2,741.76 kW, including land, is 24,980.56 m<sup>2</sup>.

#### **4.2.4 Cables Sizing**

Based on the NEC (National Electric Code) [210.19 A (1)] FPN number 4 and [215.2 A (3)] FPN number 2, the allowable voltage drop for feeders is 3% and the acceptable voltage drop for the final sub circuit and branch circuit is 5% for proper and efficient operation. [45].

It is necessary to maintain the voltage at which it is supplied within certain limits to reduce voltage drop and power losses.

The voltage drop for single-phase and DC circuits can be expressed as:

$$V_D = I \frac{(2 L R)}{1000} \dots \dots \dots (4.16)$$

Voltage drop for three phase systems is expressed by:

$$V_D = \sqrt{3} I L \frac{(R)}{1000} \dots\dots\dots (4.17)$$

where  $V_D$  is voltage drop in volt,

$I$  is wire current in amperes,

$R$  is wire resistance in ohms ( $\Omega/\text{km}$ ), and

$L$  is wire distance in meters.

The average calculated distance for PV and inverter is 81m, and the calculated distance for 11kV cables to the 66-kV substation using AutoCAD software is shown in Table 4.3. However, it is worth noting that voltage drop formulations represent approximate calculations only, which means that the outcomes should not be assumed to rigidly adhere to the formulation. There are numerous factors that could affect the outcomes, including weather changes, temperature spikes and drops, a material’s resistivity, cables, conductors, and so on [45].

Sizing cables for this simulation are based on the rated current of the system and cables datasheet from the manufacture.  $I_{SC}$  of the PV array is 198.9A. Maximum allowable current flow through the cable from the PV array to the inverter is:

$$I_{\text{cable}} = (198.9\text{A}) (1.25) = 248.625 \text{ A} \dots\dots\dots 4.18$$

where 1.25 is a factor for security reasons. From ETAP, the maximum current of the 70mm<sup>2</sup>-cable is:

$$(269 \text{ A})_{\text{Base}} (92.94\%)_{\text{Derating Factor}} = 250.5 \text{ A} \dots\dots\dots 4.19$$

where 92.94% is the derating factor for that cable. Maximum allowable current flow through the cable from the PV station to the step up transformer of 11/66 kV is:

$$I_{\text{cable}} = [(198.9) (28)]/27.5 = 202.52 \text{ A} \dots\dots\dots 4.20$$

$$(202.52 \text{ A}) (1.25) = 253.15 \text{ A} \dots\dots\dots 4.21$$

**Table 4.3 11kV cables length from PV 11-kV substations to the 66-kV PV substation**

Cable No.	Length (m)	Cable No.	Length (m)
1	1659	15	1172
2	1172	16	1334
3	1334	17	1496
4	1496	18	1011
5	1658	19	1173
6	685	20	1335
7	847	21	1497
8	1009	22	1669
9	1171	23	1337
10	1333	24	1499
11	1495	25	1661
12	686	26	1823
13	848	27	1662
14	1010	28	1824

where 28 is the number of inverters connected to the same Bus, 27.5 is the transformer ratio of 0.4/11 kV, and 1.25 is a factor for security reason. From ETAP, the maximum current of 95 mm<sup>2</sup>-cable is:

$$(255 \text{ A})_{\text{base}} (89.22\%) = 227.5 \text{ A} \dots\dots\dots 4.22$$

where 89.22% is the derating factor for that cable. Figure.4.6. shows an overall field design for the proposed PV system.

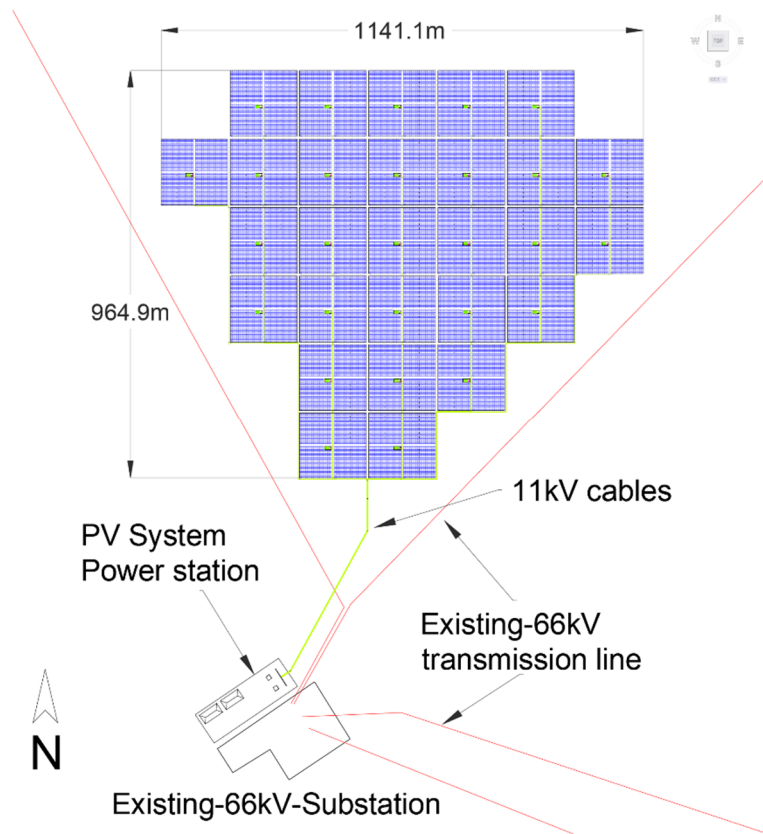


**Figure 4.6 Field design for the proposed PV system**

**4.3 Power Flow Analysis of the designed Hybrid Power System**

The following requirements are needed for successful power system operation in the normal balanced three-phase steady state condition:

- Generation supplies the loads and losses.
- Generation should operate within specified real and reactive power limits.
- Transmission lines and transformers should not be overloaded.
- Bus voltage magnitude should remain close to the rated values [46].

The simulation has been done using ETAP software to investigate these requirements and the control of power flow is proposed and performed in this study.

**4.3.1 Load flow analysis methods**

Performance equation solutions for computer-aided electrical energy system analysis (such as the analysis of load flow) are based on the numerical analysis of algebraic simultaneous equation solutions. So, in carrying out an analysis of load flow, input data from the transformer and transmission line must be used in order to find the Y-bus admittance. The expression below shows how we can formulate a power system network’s nodal equation can be formatted by applying the Y bus [47]:

$$I = Y_{BUS} V \dots \dots \dots (4.23)$$

The nodal equation can be written in a generalized form for an n bus system.

$$I_i = \sum_{j=1}^n Y_{ij} V_j \text{ for } i = 1,2,3,n \dots \dots \dots (4.24)$$

The complex power delivered to bus *i* is:

$$P_i + jQ_i = V_i I_i^* \dots \dots \dots (4.25)$$

$$I_i = \frac{P_i - jQ_i}{V_i^*} \dots \dots \dots (4.26)$$

Substituting for  $I_i$  in terms of  $i$  &  $i$  P Q, the equation yields:

$$\frac{P_i - jQ_i}{V_i^*} = V_i \sum_{j=1}^n y_{ij} - \sum_{j=1}^n y_{ij} V_j \quad j \neq i \dots \dots \dots (4.27)$$

The proceeding uses iterative techniques to solve load flow problems.

With closer investigation of Newton-Raphson and Gauss-Seidel, algorithms in the context of power-flow research, several instances where Gauss-Seidel and Jacobi diverge and Newton-Raphson converges can be observed. A close study also reveals that the number of iterations in the convergence remains independent of the number of buses  $N$  in the Newton-Raphson construct, even as it rises along with  $N$  in Gauss-Seidel and Jacobi. Previously, the main benefit in using the Gauss-Seidel and Jacobi approaches is that they demand low amounts of memory storage and have fewer computations per iteration compared with other methods; this benefit, however, has all but vanished with the requirement for solving power-flow problems using several thousands of buses and with the radical increases in computer memory. Nowadays, it is easier to use the Newton-Raphson, Fast Decoupled and “DC” Power Flow, given that the Q-V equation can be completely left out due to the extension of fast coupled power flow [46].

A comparison between Gauss-Seidel, Newton-Raphson, and Fast-Decoupled iterations has been done in [47]. MATLAB was used to perform the test simulations, which were then applied to IEEE 9-bus, IEEE 30-bus and IEEE 57-bus cases of Fast Decouple, Newton-Raphson,

and Gauss-Seidel. The latter approach took the longest. Specifically, Gauss-Seidel iteration times increased in tandem with bus increases (i.e., mathematical progression), while Newton-Raphson's rose quadratically and the fast decouple's rose geometrically. In [47], the findings indicate that Gauss-Seidel is likely the best approach for developing a small power system with reduced computational complexity, while the Newton-Raphson approach can be considered the most efficient and reliable overall, due to its ultra-fast convergence and higher levels of accuracy [47].

The methods that are used in ETAP software are Adaptive Newton-Raphson, Newton Raphson, Fast-Decoupled, and Accelerated Gauss-Seidel. For the Newton-Raphson and adaptive Newton Raphson methods, a few Gauss-Seidel iterations are made first, to establish a set of sound initial values for the bus voltages (since convergence of the Newton-Raphson Method is highly dependent on the initial bus voltages).

**4.3.1.1 Newton-Raphson Method**

Equation (4.21) is expressed in a polar form, in which  $j$  includes bus  $i$ :

$$I_i = \sum_{j=1}^n |Y_{ij}| |V_j| < \theta_{ij} + \delta_j \dots \dots \dots (4.28)$$

The real and reactive power at bus  $i$  is:

$$P_i - jQ_i = V_i^* I_i \dots \dots \dots (4.29)$$

Substituting equation (4.25) from Equation (4.26) for  $I_i$ :

$$P_i - jQ_i = |V_i| < -\delta_i \sum_{j=1}^n |Y_{ij}| |V_j| < \delta_{ij} + \delta_j \dots \dots \dots (4.30)$$

The real and imaginary parts are separated:

$$P_i = \sum_{j=1}^n |V_i| |V_j| |Y_{ij}| \cos(\theta_{ij} - \delta_i + \delta_j) \dots \dots \dots (4.31)$$

$$Q_i = \sum_{j=1}^n |V_i| |V_j| |Y_{ij}| \sin(\theta_{ij} - \delta_i + \delta_j) \dots \dots \dots (4.32)$$

Equations (4.28) and (4.29) constitute a set of non-linear algebraic equations in terms of |V| in per unit and δ in radians [47].

**4.3.2 Simulation results of power flow**

Load flow analysis has been carried out in this simulation for power flow analysis using ETAP, Adaptive Newton-Raphson, which is effective, most reliable, and widely used for solving non-linear equations.

**4.3.2.1 Voltages at Load Buses**

Loads modeling is performed by considering 80% motor loads in addition to 20% static loads. Table 4.4 shows the voltages at load buses at max average load and at peak load with ETAP alerts for under voltage buses. There are four marginal alerts at average max load, as shown in Table 4.4, are bus 9, 11, 13, and 20. The lowest voltage is at load bus 9, operating at 0.954 pu. Marginal alerts have been set above 0.95 pu and below 0.98 pu, while critical alerts have been set below 0.95 pu. ETAP load flow alerts at peak load flow can be clearly seen in Table 4.4 with two buses operating under voltage, which are bus 9 and bus 13, operating at 0.9368 pu and 0.94.91 pu respectively, while bus 5, 7, 11, 15, 17, 18, 20, and bus 24 operate at marginal alerts. Bus 3, 26 and bus 28 operate at normal voltage level during peak load.

The voltages' magnitude and power angles on buses can be seen in Figure.4.7. All power angles are not too large. The total power loss of the system is 1.433 MW, while at peak load the loss is 1.51 MW.

**Table 4.4 Load buses voltages at average max load and at peak load**

ID	Load name	Terminal Bus	Nominal kV	Voltage% at average max load	Voltage % at peak load
Lump1	Bani Walid	Bus3	11	98.53	98.1
Lump2	Eshmikh	Bus5	11	98.48	97.89
Lump3	Tininai	Bus7	11	98.55	97.97
Lump4	Al Soof	Bus9	11	95.4	93.68
Lump5	Boyot Al Shabab	Bus11	11	97.84	97.09
Lump6	Khermani	Bus13	11	96.36	94.91
Lump7	Foguha	Bus15	11	98.58	97.92
Lump8	Weshtata	Bus17	11	98.43	97.73
Lump9	Weshtata	Bus18	11	98.43	97.73
Lump10	Shemalya	Bus20	11	97.82	96.94
Lump11	Sof Al Jeen	Bus22	11	98.78	98.01
Lump12	Al Mardom	Bus24	11	98.05	96.99
Lump13	Saddadah	Bus26	11	99.12	98.33
Lump14	Gerza	Bus28	11	99.15	98.22

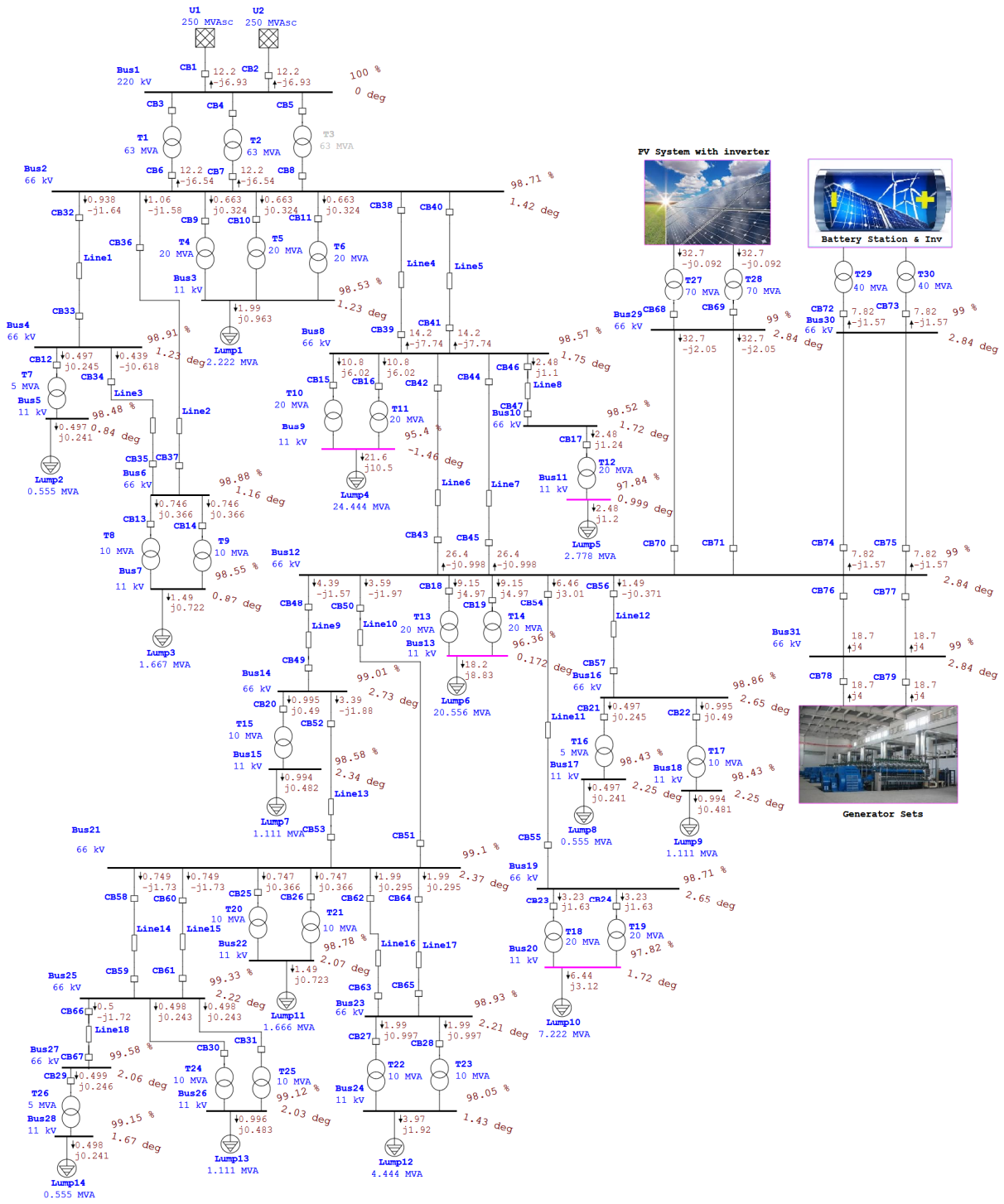


Figure 4.7 Power flow analysis of the hybrid power system

#### 4.3.2.2 Branches loading and losses

The marginal alert has been set at 95% while the critical alert has been set at 100%. All transformers are loaded under the permitted limit. The maximum loaded transformers are T10 and T11, loaded at 62 percent at max average load. T10 and T11 also have maximum loading at peak load, loaded at 84.2 percent. Total loss of all transformers is 641.299 kW, whereas at peak load the total loss is 767.963 kW.

All transmission lines are loaded below their permitted values. The maximum loaded transmission lines are line 6 and line 7, are loaded at 48.7 percent each. Also, at peak load, lines 6 and 7 have maximum loading with 43.7 percent. Maximum kw losses are founded on transmission lines 6 and 7 at both maximum average load and at peak load, with 133.3 kW and 107.6 kW respectively. The total loss of transmission lines is 353.911 kW while at peak load the total loss is 302.333 kW. The reason for decreasing total loss and losses at lines 4,5,6, and 7 at peak load is that more energy flows to loads and less energy flows to the central grid via line 4,5,6, and 7. Transmission line load flow and losses at average max load and at peak load are shown in table 4.5. All cables are loaded under permitted loading limits; the maximum loading of cables at 54.9 percent.

**Table 4.5 Transmission line loading and losses**

Load flow at max average load						Load flow at peak load				
ID	MW Flow	Mvar Flow	% Loading	kW Losses	kvar Losses	MW Flow	Mvar Flow	% Loading	kW Losses	kvar Losses
Line1	0.938	-1.643	3.5	1.39	-1270.2	1.263	-1.46	3.6	1.69	-1258.8
Line2	1.055	-1.584	3.5	1.61	-1656.9	1.421	-1.381	3.7	2.25	-1640.5
Line3	0.439	0.659	1.5	0.142	-1277	0.591	0.731	1.7	0.266	-1264.9
Line4	14.208	-7.736	29.9	25.05	-72.63	7.312	-9.16	21.8	13.2	-115.3
Line5	14.208	-7.736	29.9	25.05	-72.63	7.312	-9.16	21.8	13.2	-115.3
Line6	26.424	-0.998	48.7	133.3	163.1	23.533	0.102	43.7	107.6	70.6
Line7	26.424	-0.998	48.7	133.3	163.1	23.533	0.102	43.7	107.6	70.6
Line8	2.481	1.24	4.9	0.604	-135.6	3.338	1.688	6.7	1.12	-132.4
Line9	4.391	-1.571	8.6	2.39	-185.9	5.911	-0.72	11	3.97	-178.2
Line10	3.595	-1.965	7.5	8.43	-946.5	4.838	-1.254	9.2	13.51	-916.8
Line11	6.451	3.255	13.3	8.2	-247	8.677	4.443	18.1	15.17	-218.3
Line12	1.492	0.735	3.1	1.44	-1106.3	2.009	0.996	4.2	2.73	-1090.4
Line13	3.394	-1.876	7.1	6.13	-760.2	4.567	-1.206	8.7	9.71	-737.7
Line14	0.749	-1.729	3.5	1.23	-1113.6	1.008	-1.57	3.5	1.32	-1097.9
Line15	0.749	-1.729	3.5	1.23	-1113.6	1.008	-1.57	3.5	1.32	-1097.9
Line16	1.989	0.997	4.1	1.77	-702.2	2.674	1.358	5.6	3.36	-686.3
Line17	1.989	0.997	4.1	1.77	-702.2	2.674	1.358	5.6	3.36	-686.3
Line18	0.5	-1.717	3.3	0.875	-1962.8	0.672	-1.601	3.2	0.957	-1933.5

### 4.3.3 Control of power flow

There are several different ways to control power flow. Some of these approaches include: switching static var systems, shunt reactors and shunt capacitor banks, controlling any regulating and tap-changing transformers, and employing excitation/prime mover control over generators. Figure 4.8 shows a Thevenin equivalent model depicting a generator in a steady-state condition, with  $V_t$  indicating generator terminal voltage,  $E_g$  excitation voltage,  $\delta$  power

angle, and  $X_g$  positive-sequence synchronous reactance. In this case, the reactive and real powers can be expressed as:

$$P = Re S = \frac{V_t E_g}{X_g} \sin \delta \dots \dots \dots (4.33)$$

$$Q = Im S = \frac{V_t}{X_g} (E_g \cos \delta - V_t) \dots \dots \dots (4.34)$$

From Equation (4.33), real power, P, rises to reflect increases in power angle  $\delta$  can be seen. The functional progression proceeds as follows: if there is an increase in power to the generator from the prime mover, there is a subsequent increase in rotor speed, even as the excitation voltage remains constant. The increase in rotor speed also causes an increase in power angle  $\delta$ , which then leads to a boost of the generator real power output P.

From Equation (4.34), a reduction of reactive power output Q can be observed. This occurs if  $\delta$  remains below  $15^\circ$ , in which case the reduction in Q is much smaller than the rise in P. Regarding power flow, any rise made in prime-move power is related to rises in P occurring at the generator-connected constant-voltage bus. In this case, the slight alteration in Q along with the increase in d are tabulated by the power-flow program.

Also in Equation (4.34), increases in excitation voltage,  $E_g$ , leading to rises in reactive power output Q can be seen. This occurs because there is a rise in rotor current caused by the prime-mover power remaining constant, even as the generator exciter output rises. Rotor current increases lead to excitation voltage  $E_g$  increases, which then result in a rise in generator reactive power output ,Q. It is worth noting that, in (4.33), a slight reduction in  $\delta$  is needed to retain P as a constant [47].

In this power-flow formulation, the rise in generator excitation reflects the rise in the generator-connected voltage magnitude for the constant-voltage bus. The slight change in  $\delta$  as well as the rise in the generator-supplied reactive power  $Q$  are automatically formulated in the power-flow program [46].

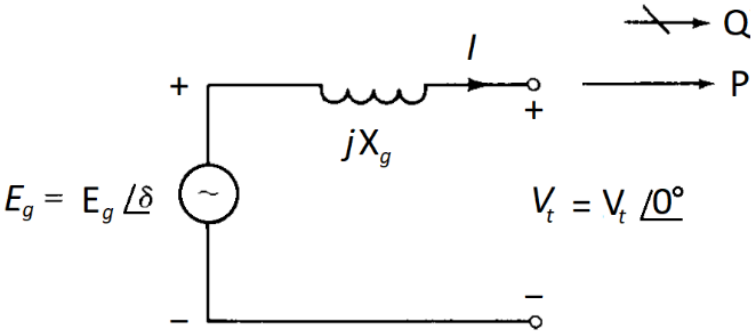


Figure 4.8 Generator Thevenin equivalent [46]

Tap-changing and voltage-magnitude-regulating transformers are used to control bus voltages. Therefore, 3-phase regulating transformers (Figure 4.9) can be built along the lines of transformers that feature turns-ratios which are off-nominal. In a voltage-magnitude-regulating transformer, the adjustable voltages  $\Delta V_{an}$ ,  $\Delta V_{bn}$ , and  $\Delta V_{cn}$  that exhibit the same magnitudes as  $\Delta V$  and are considered to be in-phase like phase voltages  $V_{an}$ ,  $V_{bn}$ , and  $V_{cn}$  can be inserted between buses  $a-a'$ ,  $b-b'$ , and  $c-c'$  of the series link. Thus, when designed to be a transformer that features an off-nominal turns-ratio, we can write  $c = (1 + \Delta V)$  can be written for an increase in voltage-magnitude in terms of bus abc; however, for the same type of increase in terms of bus  $a'b'c'$ ,  $c = (1 + \Delta V)^{-1}$  would be written[46].



**4.3.3.2 Control of power flow using automatic voltage-magnitude-regulating transformer**

An automatic voltage-magnitude-regulating transformer is used in ETAP to control and regulate voltages at load buses. Each transformer that is connected to a load bus performs the OLTC function for its connected load bus. The selected number of taps is 17 taps and the upper and lower band limits are 0.625% as shown in Figure 4.10. Only T10, T11, T22, and T23 are set at 0.625% for the upper band and 1.25% for the lower band, to avoid getting into cycles of transformers LTC adjustment in ETAP.

Regulated Bus		
Bus ID	Bus3	

Voltage Control		
Voltage	100	%
Upper Band	0.625	%
Lower Band	0.625	%

Tap		# of Taps
% Tap	kV Tap	
Min.	-10	59.4
Max.	10	72.6
Step	1.25	0.825
		17

Time Delay	
Initial	3
Operating	1

**Figure 4.10 Load Tap changer**

ETAP calculates number of taps and % step according to the following formula:

$$\# \text{ of Taps} = 1 + \frac{\%Max \text{ Tap} - \%Min \text{ Tap}}{\%Step} \dots \dots \dots (4.35)$$

$$\% \text{ Step} = \frac{\% \text{Max Tap} - \% \text{Min Tap}}{\# \text{ of Taps} - 1} \dots \dots \dots (4.36)$$

The rated voltage of the power transformers that used for voltage regulation is 66 kV and the tapping range is  $\pm 10\%$ . Therefore, the min voltage tap is 59.4 kV and max voltage tap is 72.6 kV. The location of OLTC is on the high voltage winding (primary winding) due to the higher current flowing through the secondary winding than through the primary winding.

#### 4.3.3.3 Simulation results

Simulation results illustrate that voltages are improved at all buses, as shown in Figure 4.11. The minimum bus voltage is bus 10 with 0.9851 pu and maximum voltage is at load bus 28 with 1.004 pu. Voltages at load buses clearly can be seen in Table 4.7. The minimum voltage is 0.993 pu at bus 24 while the maximum voltage is 1.004 pu at load bus 28. Total power loss of the system is reduced to 1.422 MW compared to the base case which was 1.433 MW.

Load flow results during peak load shows no voltage violation at all buses. The minimum bus voltage is at bus 10 operating at 0.9801 pu. while the maximum bus voltage is bus 3, operating at 1.0062 pu. Total power losses were also reduced during peak load to 1.489 MW, compared to the base case power flow at peak load, which was 1.51 MW.

**Table 4.7 Regulated voltages at load buses**

ID	Load name	Bus ID	Nominal kV	Voltage% at average max load	Voltage % at peak load
Lump1	Bani Walid	Bus3	11	99.78	100.62
Lump2	Eshmikh	Bus5	11	99.73	100.41
Lump3	Tininai	Bus7	11	99.8	100.49
Lump4	Al Soof	Bus9	11	99.32	99
Lump5	Boyot Al Shabab	Bus11	11	100.36	99.6
Lump6	Khermani	Bus13	11	100.28	100.22
Lump7	Foguha	Bus15	11	99.82	100.44
Lump8	Weshtata	Bus17	11	99.67	98.96
Lump9	Weshtata	Bus18	11	99.67	98.96
Lump10	Shemalya	Bus20	11	100.35	99.46
Lump11	Sof Al Jeen	Bus22	11	100.03	100.52
Lump12	Al Mardom	Bus24	11	99.3	99.51
Lump13	Saddadah	Bus26	11	100.36	99.56
Lump14	Gerza	Bus28	11	100.4	99.46

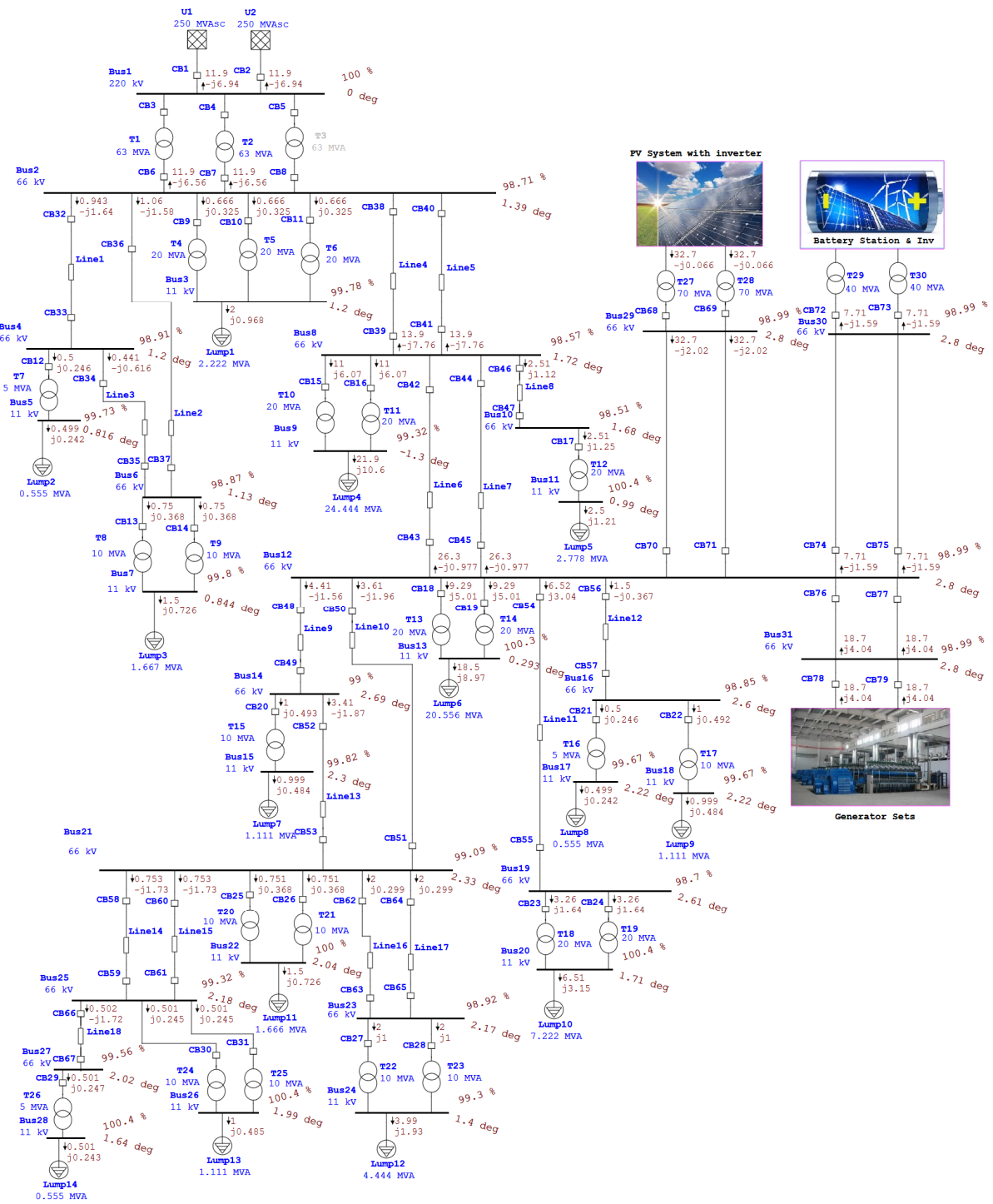


Figure 4.11 Load Flow analysis after automatic voltage regulation

Enabling counteracting in ETAP as shown in Figure 4.12(a) and (b) and Figure 4.13(a) and (b), the location of undervoltage buses can be seen clearly on the schematic diagram as well as the improved bus voltages with voltage regulation control.

Figure.4.12(a) shows power flow at maximum average load (base case), while Figure.4.12(b) shows the power flow with regulated voltage at load buses. Figure 4.13(a) shows power flow at peak load (base case), while Figure 4.13(b) shows the power flow with regulated voltage at load buses during peak load.

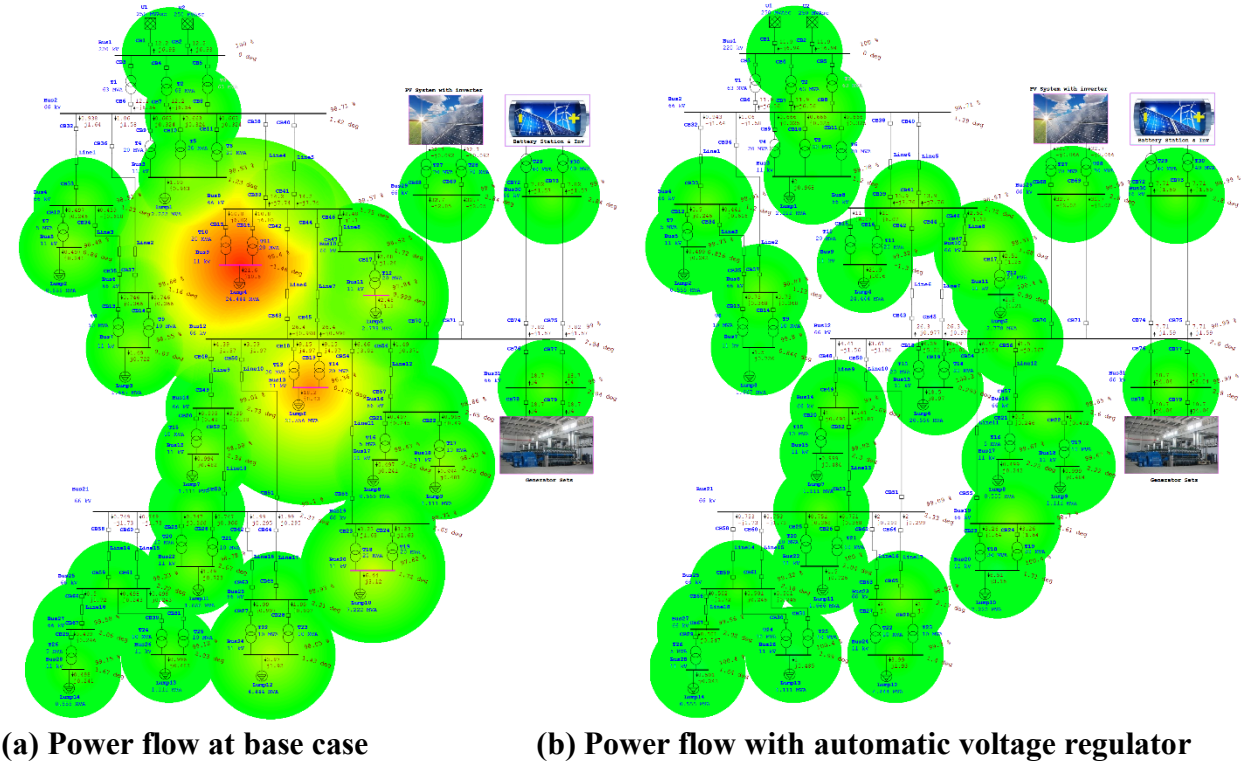
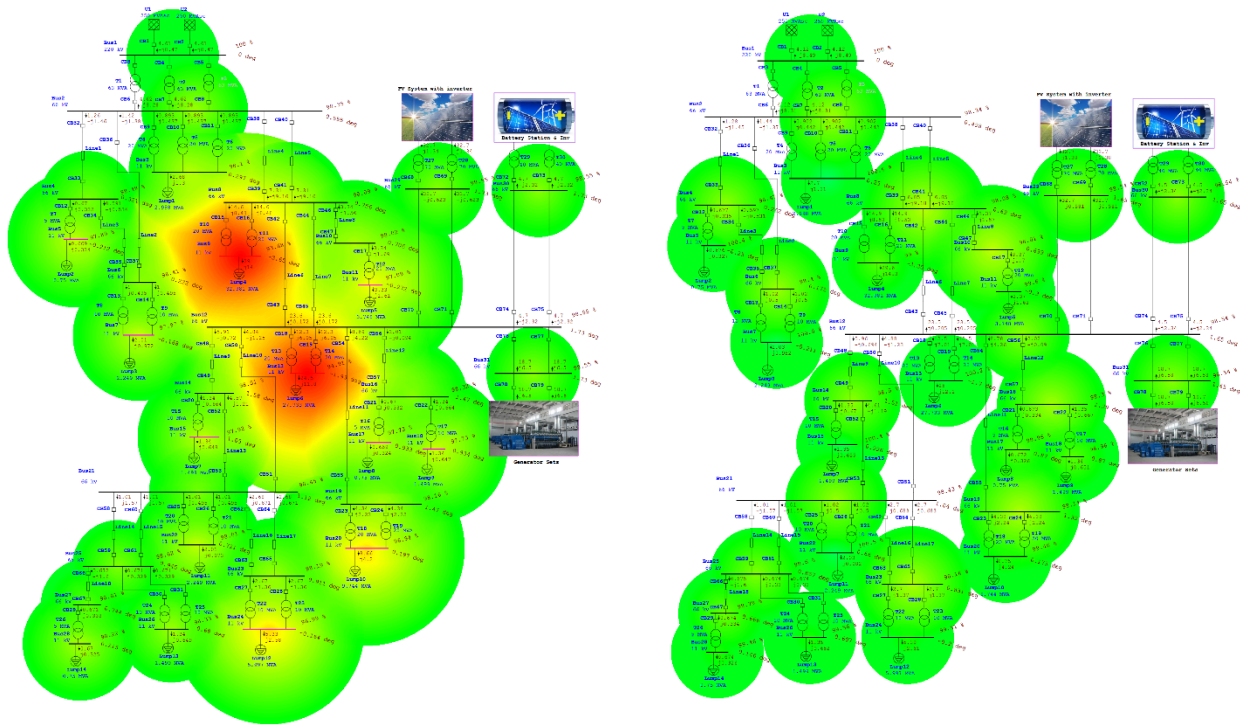


Figure 4.12 Power flow at maximum average loads



(a) Power flow at base case

(b) Power flow with automatic voltage regulator

**Figure 4.13 Power flow at peak loads**

#### 4.3.3.4 Branches loading and losses

ETAP simulation results shows that all transformers operate under the permitted limit. Maximum loaded transformers are T10 and T11 with 62.8 % each, also during peak load power flow, T10 and T11 have max loading of 85.6% each; Table.4.8 illustrates the total losses of all transformers in the system before and after voltage regulation during max average load and during peak load power flow. In both cases, total power loss for transformers is reduced to 633.515 kW at max average load and to 749.718 kW at peak load flow using the voltage-magnitude-regulating transformer.

All cables and transmission lines are loaded under the permitted limit. Table 4.9 shows the transmissions line loading summary report and Table.4.10 shows the cables loading summary report at average max load.

**Table 4.8 Total losses at transformers for different cases**

	Total losses at max average load		Total losses at peak load	
	KW	kVA	kW	kVA
Base case	641.299	12022.38	767.963	13867.15
Regulated voltage at load buses	633.515	11842.07	749.718	13487.82
Reduced loss (%)	1.21%	1.50%	2.38%	2.74%
Reduced loss (kW, kVA)	7.784	180.31	18.245	379.33

**Table 4.9 Transmission line loading report after regulating voltages at load buses**

Load flow at max average load					Load flow at peak load			
ID	MW Flow	Mvar Flow	% Loading	kW Losses	MW Flow	Mvar Flow	% Loading	kW Losses
Line1	0.943	-1.64	3.5	1.39	1.276	-1.454	3.6	1.71
Line2	1.06	-1.581	3.5	1.62	1.435	-1.374	3.7	2.28
Line3	0.441	0.66	1.5	0.143	0.597	0.734	1.8	0.271
Line4	13.945	-7.76	29.5	24.38	6.846	-9.179	21.3	12.59
Line5	13.945	-7.76	29.5	24.38	6.846	-9.179	21.3	12.59
Line6	26.338	-0.977	48.5	132.5	23.383	0.139	43.4	106.2
Line7	26.338	-0.977	48.5	132.5	23.383	0.139	43.4	106.2
Line8	2.506	1.251	5	0.616	3.371	1.702	6.7	1.14
Line9	4.413	-1.56	8.6	2.41	5.964	-0.694	11.1	4.04
Line10	3.612	-1.956	7.6	8.48	4.881	-1.234	9.3	13.73
Line11	6.516	3.282	13.5	8.37	8.763	4.477	18.3	15.47
Line12	1.499	0.739	3.1	1.46	2.019	1	4.2	2.76
Line13	3.41	-1.867	7.2	6.17	4.607	-1.186	8.8	9.86
Line14	0.753	-1.726	3.5	1.23	1.013	-1.567	3.5	1.32
Line15	0.753	-1.726	3.5	1.23	1.013	-1.567	3.5	1.32
Line16	1.999	1.001	4.1	1.79	2.701	1.369	5.6	3.43
Line17	1.999	1.001	4.1	1.79	2.701	1.369	5.6	3.43
Line18	0.502	-1.715	3.3	0.876	0.675	-1.598	3.2	0.96

**Table 4.10 Cables loading report at average max load after regulating voltages at load buses**

ID	Allowable current	MW Flow	Mvar Flow	% Loading	% Voltage Drop	kW Losses	Kvar Losses
Cable1	227.5 A	2.354	-0.0787	54.3	1.09	26.07	8.74
Cable2	227.5 A	2.353	0.0325	54.6	0.57	13.44	5.91
Cable3	227.5 A	2.353	-0.0181	54.5	0.64	15.27	6.71
Cable4	227.5 A	2.353	-0.0677	54.5	0.71	17.12	7.52
Cable5	227.5 A	2.353	-0.0792	54.5	0.79	18.95	8.33
Cable6	227.5 A	2.353	0.191	54.9	0.34	7.94	3.49
Cable7	227.5 A	2.353	0.137	54.7	0.42	9.77	4.3
Cable8	227.5 A	2.353	0.0845	54.7	0.5	11.6	5.1
Cable9	227.5 A	2.353	0.0329	54.6	0.57	13.43	5.9
Cable10	227.5 A	2.353	-0.0178	54.5	0.64	15.26	6.71
Cable11	227.5 A	2.353	-0.0674	54.5	0.71	17.11	7.52
Cable12	227.5 A	2.353	0.19	54.9	0.35	7.95	3.5
Cable13	227.5 A	2.353	0.137	54.7	0.42	9.78	4.3
Cable14	227.5 A	2.353	0.0842	54.6	0.5	11.61	5.1
Cable15	227.5 A	2.353	0.0325	54.6	0.57	13.44	5.91
Cable16	227.5 A	2.353	-0.0181	54.5	0.64	15.27	6.71
Cable17	227.5 A	2.353	-0.0677	54.5	0.71	17.12	7.52
Cable18	227.5 A	2.353	0.0838	54.6	0.5	11.62	5.11
Cable19	227.5 A	2.353	0.0322	54.6	0.57	13.45	5.91
Cable20	227.5 A	2.353	-0.0184	54.5	0.64	15.29	6.72
Cable21	227.5 A	2.353	-0.068	54.5	0.71	17.13	7.53
Cable22	227.5 A	2.353	-0.0792	54.5	0.79	19.07	8.38
Cable23	227.5 A	2.353	-0.019	54.5	0.64	15.31	6.73
Cable24	227.5 A	2.353	-0.0686	54.5	0.72	17.15	7.54
Cable25	227.5 A	2.353	-0.0792	54.5	0.79	18.98	8.34
Cable26	227.5 A	2.353	-0.0791	54.4	0.87	20.8	9.14
Cable27	227.5 A	2.353	-0.0792	54.5	0.79	18.99	8.35
Cable28	227.5 A	2.354	-0.0785	54.3	1.2	28.6	9.59

#### 4.4 Contingency Analysis

Contingency analysis plays a major role in a power grid stability. A significant change in power flow could lead to an unstable power grid system and system collapse. The main reason for the blackout in the western Libyan power grid system on July 14, 2017 was a change in power flows, because a single branch was tripped. According to the GECOL report, the cascading trip at that grid occurred due to tripping a single branch. There were three branches connecting two zones in the western Libyan power grid; one of them had already been out of service for a while. Another branch was tripped because of a fault on a Current Transformer (CT) on the branch on phase R. As a result, only one branch lasted connecting the two zones which tripped as well due to overloading, causing a cascading trip, due to a significant change in power flow in the western network, which ended with a blackout in the western Libyan power grid system [11].

To evaluate the security of the grid based on the ability of the grid to resist failures, contingency analysis has been done on the designed hybrid power system. In security of the grid is essentially voltage violation on the system and over-loading branches, which includes transmission lines, cables, and transformers when there is a failure in the system.

The basic methodology used for contingency analysis is by disabling a specific part of the system which called (N-1) or two parts at the same time which called (N-2), typically performed on transmission lines and transformers to evaluate power grid stability by using a power flow calculation. The contingency analysis (N-1) is used in this study which is generally used specially for large power grid because (N-2) takes very long time for simulation and very high capacity of memory for a large power grid. (N-2) is usually used for some restricted power grids.

#### 4.4.1 Contingency analysis results

Contingency analysis shows four alerts of overloading violations which include transformers T10, T11, T13 and T14, as shown in Table.4.11. The alerts are based on equipment rating. Xfmr is the total number of transformer loading violations. The outage of T10 causes one violation which is 130% overloading of T11 and the outage of T 13 causes 108% overloading of T14. The outage of single transmission line does not cause any loading violation. The critical loading violations has been set to 100% and bus voltage violation has been set to 1.05 pu for overvoltage and 0.95 pu for under voltage.

**Table 4.11 Loading Violations**

N-1			No. of Loading Violations	Post Contingency Violations					
N. of Contingency	ID	Type	Xfmr	ID	Condition	Rating /limit	Post Contingency (%)	% Violation	Type
9	T10	Transformer	1	T11	Overloaded	20 MVA	130.08%	30.08%	Critical
10	T11	Transformer	1	T10	Overloaded	20 MVA	130.08%	30.08%	Critical
12	T13	Transformer	1	T14	Overloaded	20 MVA	108.33%	8.33%	Critical
13	T14	Transformer	1	T13	Overloaded	20 MVA	108.33%	8.33%	Critical

Table 4.12. shows the critical voltage violations. It can clearly be seen that four transmission lines and six transformers cause voltage violation in the system as illustrated. Line 12 cause 3 under voltage buses violations as shown in Table 4.11. The post contingency analysis goes to 0.

Ten contingencies cause outage at the customer load, six transforms and 4 transmission lines. Line 12 causes two power outages as shown in Table 4.13.

**Table 4.12 Voltage Violations**

N-1			No. of Under voltage buses	Post Contingency Violations					
N. of Contingency	ID	Type		Critical	ID	Condition	Rating /limit (kV)	Post Contingency (%)	% Violation
12	Line12	Line	3	Bus16	Undervoltage	66	0	95	Critical
				Bus17	Undervoltage	11	0	95	Critical
				Bus18	Undervoltage	11	0	95	Critical
8	Line8	Line	2	Bus10	Undervoltage	66	0	95	Critical
				Bus11	Undervoltage	11	0	95	Critical
11	Line11	Line	2	Bus19	Undervoltage	66	0	95	Critical
				Bus20	Undervoltage	11	0	95	Critical
18	Line18	Line	2	Bus27	Undervoltage	66	0	95	Critical
				Bus28	Undervoltage	11	0	95	Critical
24	T7	Transformer	1	Bus5	Undervoltage	11	0	95	Critical
29	T12	Transformer	1	Bus11	Undervoltage	11	0	95	Critical
32	T15	Transformer	1	Bus15	Undervoltage	11	0	95	Critical
33	T16	Transformer	1	Bus17	Undervoltage	11	0	95	Critical
34	T17	Transformer	1	Bus18	Undervoltage	11	0	95	Critical
43	T26	Transformer	1	Bus28	Undervoltage	11	0	95	Critical

**Table 4.13 Losses during contingency analysis**

N-1			Losses		
N. of Contingency	ID	Type	Generation (MW)	Load (MW)	No. of Customer
12	Line12	Line	0.00	1.50	2
8	Line8	Line	0.00	2.49	1
11	Line11	Line	0.00	6.50	1
18	Line18	Line	0.00	0.52	1
24	T7	Transformer	0.00	0.50	1
29	T12	Transformer	0.00	2.49	1
32	T15	Transformer	0.00	0.99	1
33	T16	Transformer	0.00	0.50	1
34	T17	Transformer	0.00	0.99	1
43	T26	Transformer	0.00	0.50	1
27	T10	Transformer	0.00	0.00	0
28	T11	Transformer	0.00	0.00	0
30	T13	Transformer	0.00	0.01	0
31	T14	Transformer	0.00	0.01	0
35	T18	Transformer	0.00	0.02	0
36	T19	Transformer	0.00	0.02	0

Performance index is ranked by the voltage security index. The index number indicates the severity of the outage. From Table 4.14, it can be clearly seen that contingencies of line 12, 18, 8 and 11, and transformers T7, T12, T15, T16, T17 and T26 have a significant impact on voltage security due to the deenergization of some load buses. The outage of line 12 has the highest impact on the voltage security with a value of 12.13 due to two load buses being deenergized.

**Table 4.14 Performance index**

N-1			Losses		
N. of Contingency	ID	Type	V/Vsp	$\Delta P$	$\Delta Q$
12	Line12	Line	12.13	0.03	0.03
18	Line18	Line	8.10	0.02	0.08
8	Line8	Line	8.09	0.02	0.03
11	Line11	Line	8.09	0.03	0.21
24	T7	Transformer	4.05	0.01	0.01
33	T16	Transformer	4.05	0.01	0.01
32	T15	Transformer	4.05	0.01	0.01
43	T26	Transformer	4.05	0.02	0.01
34	T17	Transformer	4.05	0.01	0.02
29	T12	Transformer	4.05	0.02	0.03
27	T10	Transformer	0.01	0.02	0.05
28	T11	Transformer	0.01	0.02	0.05
35	T18	Transformer	0.01	0.02	0.02
36	T19	Transformer	0.01	0.02	0.02
30	T13	Transformer	0.01	0.02	0.04
31	T14	Transformer	0.01	0.02	0.04

#### 4.5 Transient stability analysis of the designed hybrid power system

The concept of power system stability is adequately defined in [46] as a “synchronous machine’s ability to shift from one steady-state operating point following a disturbance to another steady-state operating point, without losing synchronism”.

In general, power systems are rigorously nonlinear systems which must hold their functionality (i.e., stability) despite an ever-shifting operational environment. This environment includes disturbed conditions caused by constantly changing factors such as operating parameters, generator outputs and loads. A power system's stability essentially is derived from the system's movements in relation to the specific equilibrium set of initial operating conditions.

However, power systems can encounter any number or magnitude of stability disturbances. Load changes are an example of minor disturbances which occur on an almost constant basis and to which a system must respond appropriately and in a timely fashion to maintain system stability. At the same time, a power system must also be prepared to deal with major disturbances (e.g., generator loss or a transmission line short-circuit), again responding appropriately and quickly. Larger disturbances often result in the necessity to make structural changes as a means to isolate the component(s) causing the disturbance or damaged by it.

In equilibrium sets, power systems can be represented as stable during a sizeable disturbance but unstable during another type of disruption. In other words, it is next to impossible to develop systems which are universally stable, so designs must instead include contingencies with high occurrence probabilities to deal with specific problems. Hence, a stable equilibrium set must, of necessity (i.e., if it is to be successful within its operational milieu), include a finite region of attraction. Thus, as the size of the region expands, the system likewise retains its robustness in the face of disruptions.

It is worth noting that in this scenario, the power system's operational conditions can determine how and when the region of attraction must be adjusted or altered. This is because a system's reaction to disruption could include equipment malfunctions or even shutdowns. So,

for example, a fault could lead to isolation of that specific element, which in turn could cause changes to machine rotor speed, network bus voltages, or power flows. Similarly, changes or other disruptions to frequency or voltage can have an impact on system loads, while protective elements could react to changes by tripping certain components as a safety measure. All of these responses to disturbances can cause system instability which thus weakens the system's overall performance [48].

In instances of fault occurrence, the generator's rotor angles start vibrating until (depending on the configuration of the system) they either diverge or converge. These kinds of oscillations can be curtailed through applying damping procedures. Equipment which has been appropriately damped can easily return to synchronism once the disruption has been cleared from the system. On the other hand, equipment and machinery that are poorly damped are continuously unstable and suffer constant divergence of rotor angles. Even after the fault has been dealt with, improper damping causes constant increases in speed and thus constant instability of the system [49].

Transient stability takes into consideration the degree of disturbance as well as the system's initial operational parameters [50].

Power flow analysis was performed on the system using ETAP. The analysis focused on restricting the bus voltages to keep them close to the nominal values and ensuring that the branches and power equipment were not overloaded and the phase angles not too large.

In this study, the transient stability analysis involves major disturbances such as loss of generation, faults with loss of generation, and faults with load loss.

A power system stabilizer (PSS) has been used in the hybrid grid-connected power system. Transient stability analysis is performed on the system, and the effects of PSS performance and an automatic voltage-magnitude-regulating transformer during transient stability are investigated.

#### 4.5.1 Control methods

All machines use the Woodward UG-8 governor and IEEE Type AC4 exciter system, as shown in Figures 4.14 and 4.15. The Woodward UG-8 governor is used mainly for diesel generators. This model includes a representation for a ball head filter, amplifier/compensator. The parameters of the governor and the exciter are shown in the appendix A and B respectively.

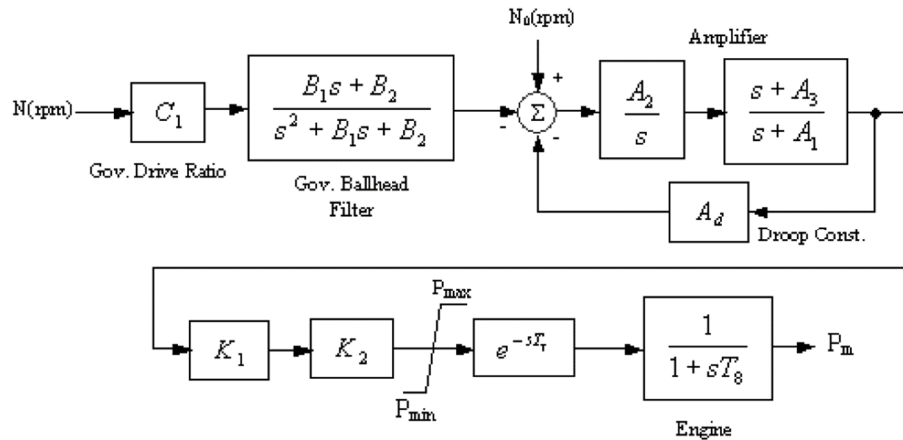


Figure 4.14 Woodward UG-8 (UG-8)

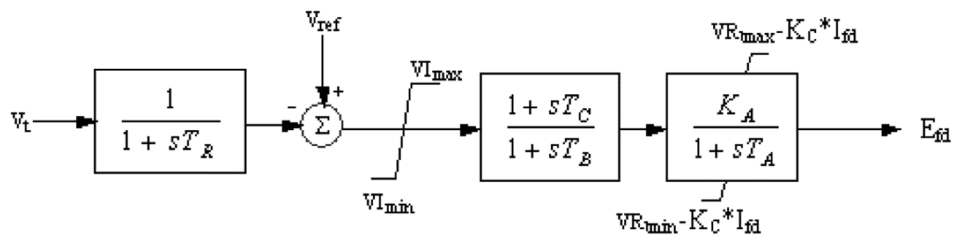
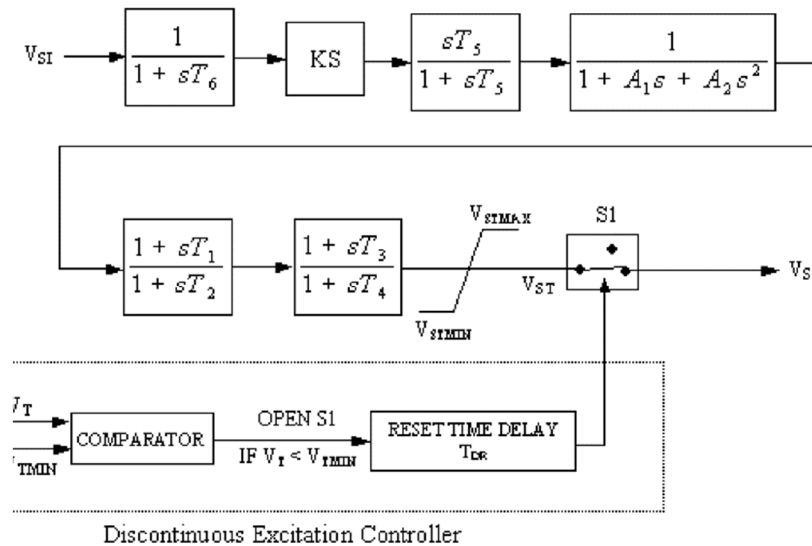


Figure 4.15 IEEE Type AC4 - High-Initial-Response Alternator-Supplied Controlled Rectifier Exciter (AC4)

A power system stabilizer (PSS) is an auxiliary device installed on the synchronous generator and tuned to help with system stability. Figure 4.16 shows the power system stabilizer IEEE standard Type 1 PSS (PSS1A). The stabilizer output,  $V_{ST}$ , is an input to the supplementary discontinuous control models. Where the discontinuous control models are not used,  $V_S = V_{ST}$  [51]. The parameters of the (PSS) are shown in the appendix C.



**Figure 4.16 IEEE Type 1 PSS (PSS1A)**

#### 4.5.2 Simulation results

A trip of the central grid, trip of the PV system, and a three-phase short circuit isolating a generation and a load are simulated for stability studies of the hybrid power system as well as the performance of the PSS and an automatic voltage-magnitude-regulating transformer on the system during transient stability is performed. The utility grid is connected to bus 2 through 220/66kV transformers. The PV system, Generator sets, and energy storage system are connected to bus 12 as shown in Figure 4.11.

#### 4.5.2.1 Trip of utility grid

In this case, the disturbance is loss of central generation by opening circuit breaker 1 and 2 after 0.2 second. The grid therefore will switch to island mode. After the circuit breakers were opened, the voltage in the system increased, since the main grid was absorbing energy from the hybrid power system. The voltage level was restored by the exciter as shown in Figure 4.17 (a). The rotor angle of Gen 1 (Gen sets group 1) and Gen 13 (Gen sets group 2) converge at a stable value, as shown in Figure 4.17 (b).

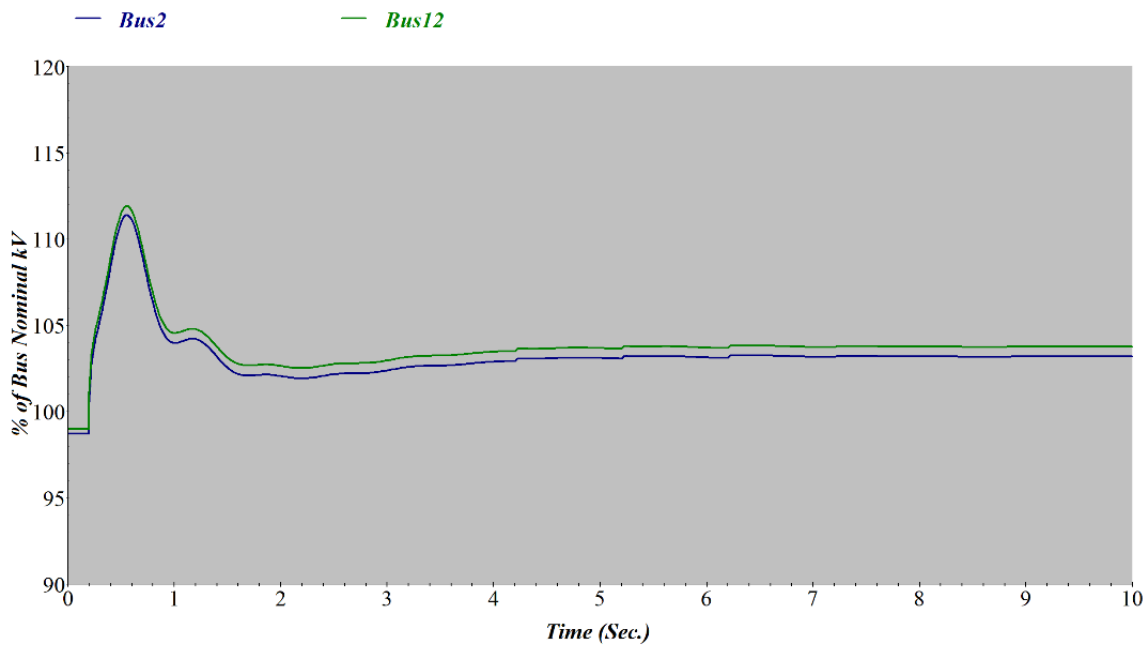
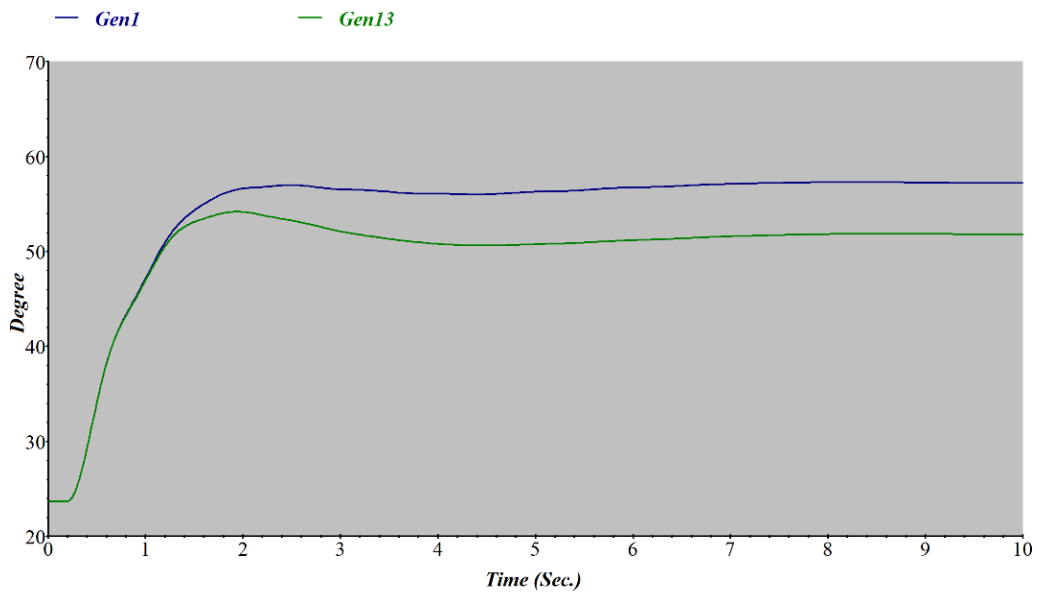


Figure 4.17 Trip of utility grid, (a) Bus 2 and Bus12 voltage (%)



**Figure 4.17 Trip of utility grid, (b) Generators absolute power angle**

#### 4.5.2.2 Trip of PV system

A trip of the PV system by opening circuit breakers 68 and 69 shows that the system is stable, as shown in Figure 4.18 (a) and (b). The rotor angle oscillated and recovered around

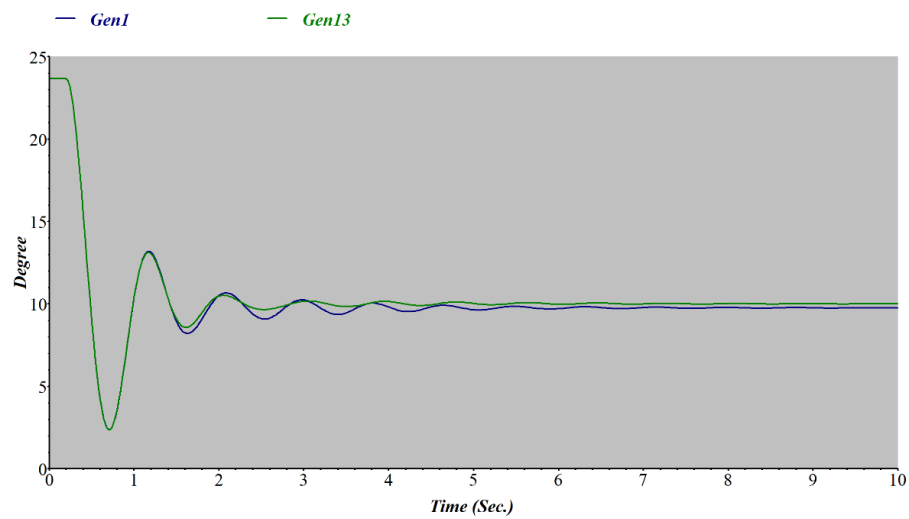


**Figure 4.18 Trip of PV system, (a) Generators absolute power angle**

a new equilibrium state, as shown in Figure 4.18 (a). The voltage dropped slightly and returned to the nominal value, as illustrated in Figure 4.18 (b).

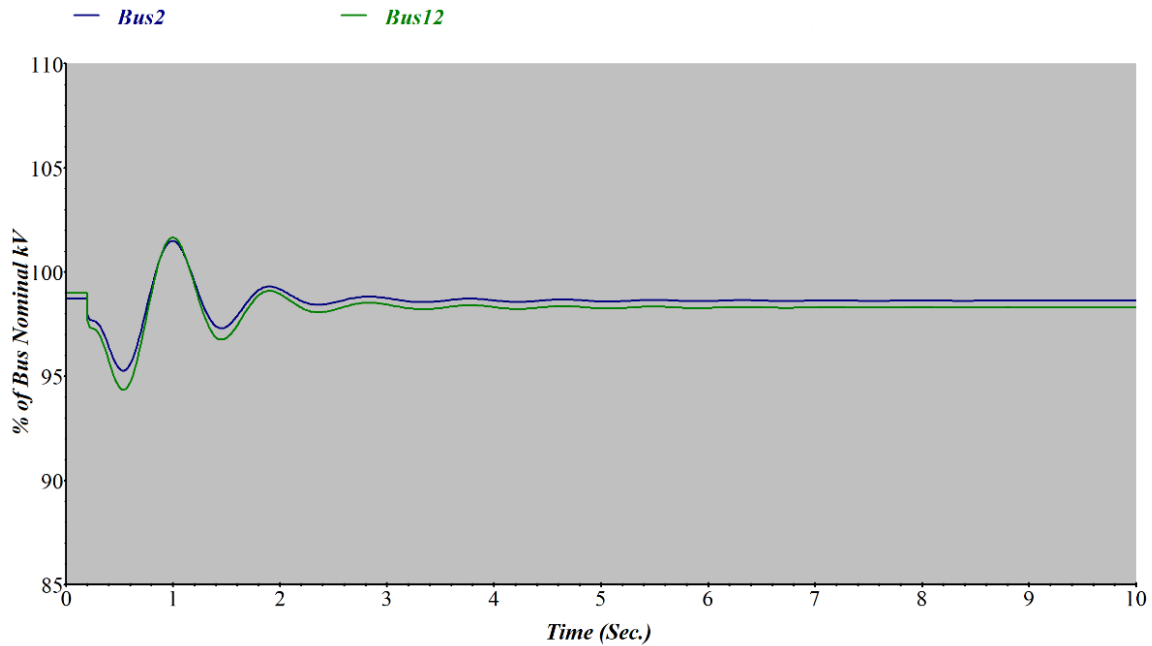


**Figure 4.18 Trip of PV system, (b) Bus 2 and Bus12 voltage (%)**

#### 4.5.2.3 Three phase short circuit at Bus 1 results in tripping the utility grid

Transient stability depends on many factors, such as the initial operating condition before the disturbance and the severity of the disturbance. In this case study, the disturbance is a three-phase fault occurring on bus 1 and clearing after 0.15 second by opening circuit breakers 1, 2, 3, 4 and 5, which isolates the hybrid power system from the utility grid and switches it to island mode.

Figure 4.19 (a) illustrates that the rotor angle recovered around a new equilibrium state and the voltages dropped significantly and settled very close to the nominal value after oscillation, as shown in Figure 4.19 (b).

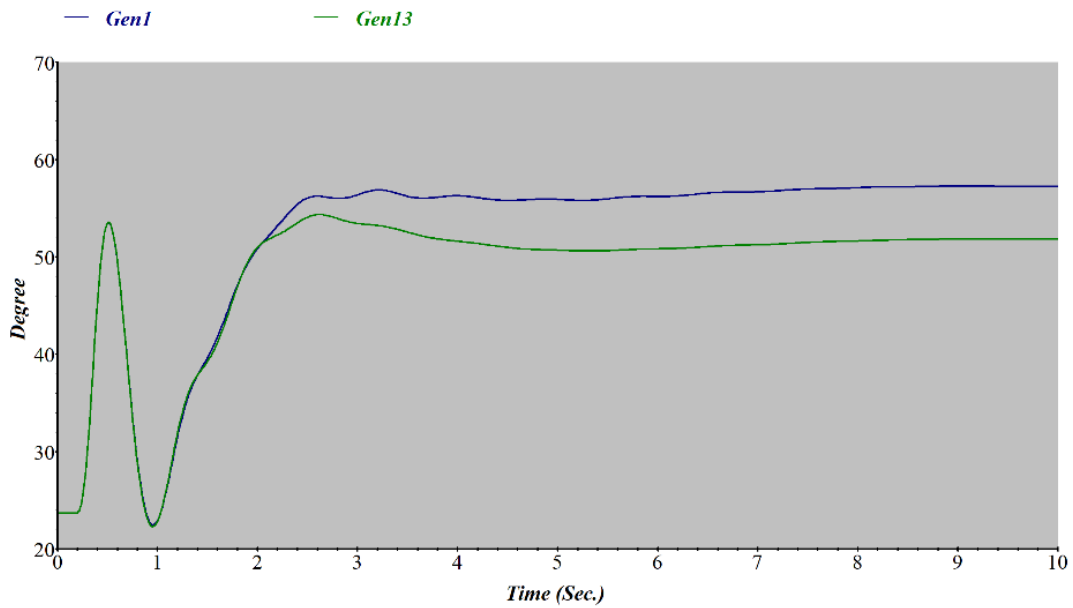


**Figure 4.19 Three phase short circuit at Bus 1, (a) Generators absolute power angle**

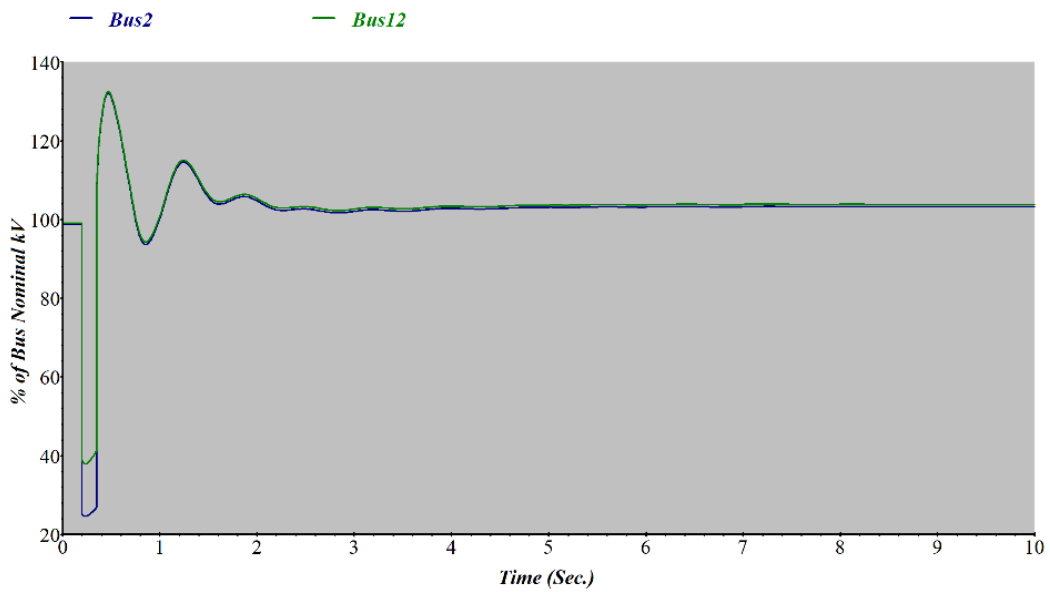


**Figure 4.19 Three phase short circuit at Bus 1, (b) Bus 2 and Bus12 voltage (%)**

**4.5.2.4 Three phase short circuit at Bus 29 results in tripping the PV system**

Tripping the PV system after a three-phase fault occurs on bus 29 shows that the system is stable. Figure 4.20 (a) shows the rotor angle of generators settled on a new angle and Figure 4.20 (b) shows voltages plot at bus 2 and bus 12.

In this case, frequency oscillated slightly and recovered to the nominal value due to the severe disturbance and its location. The fault resulted in isolating a large power source, which is the PV system. Figure 4.20 (c) shows the frequency plot at bus 2 and bus 12.

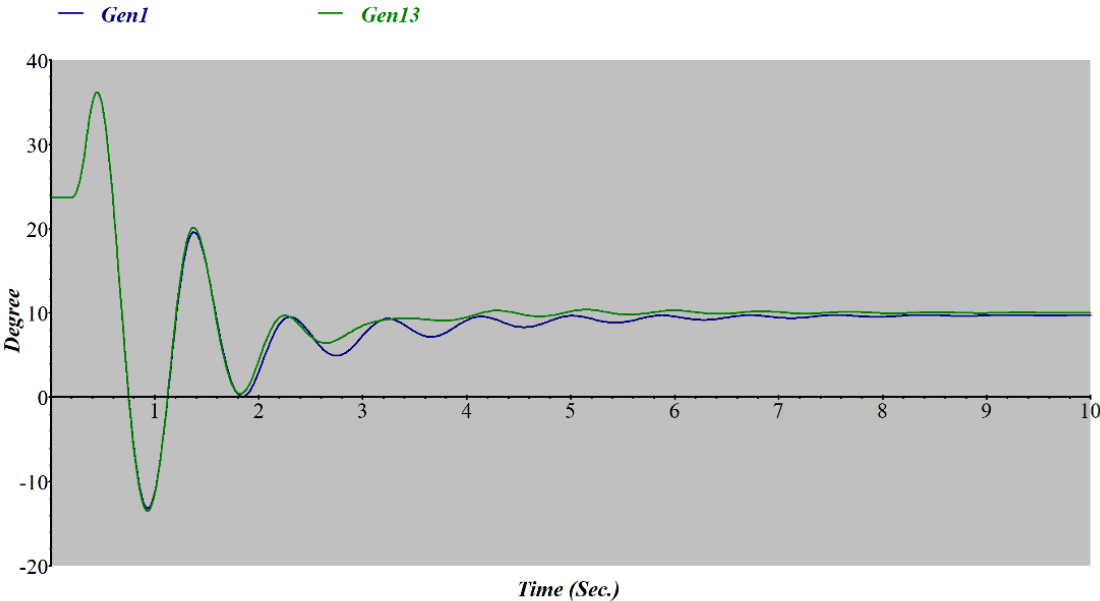


**Figure 4.20 Three phase short circuit at Bus 29, (a) Generators’ absolute power angle**

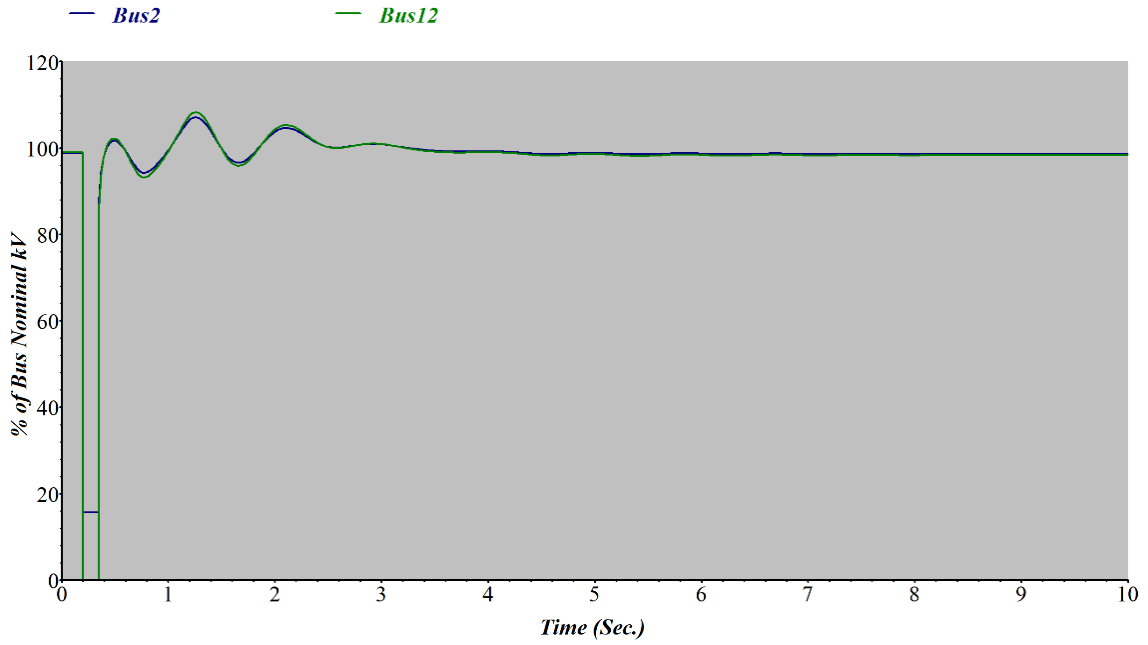


**Figure 4.20 Three phase short circuit at Bus 29, (b) Bus 2 and Bus12 voltage (%)**

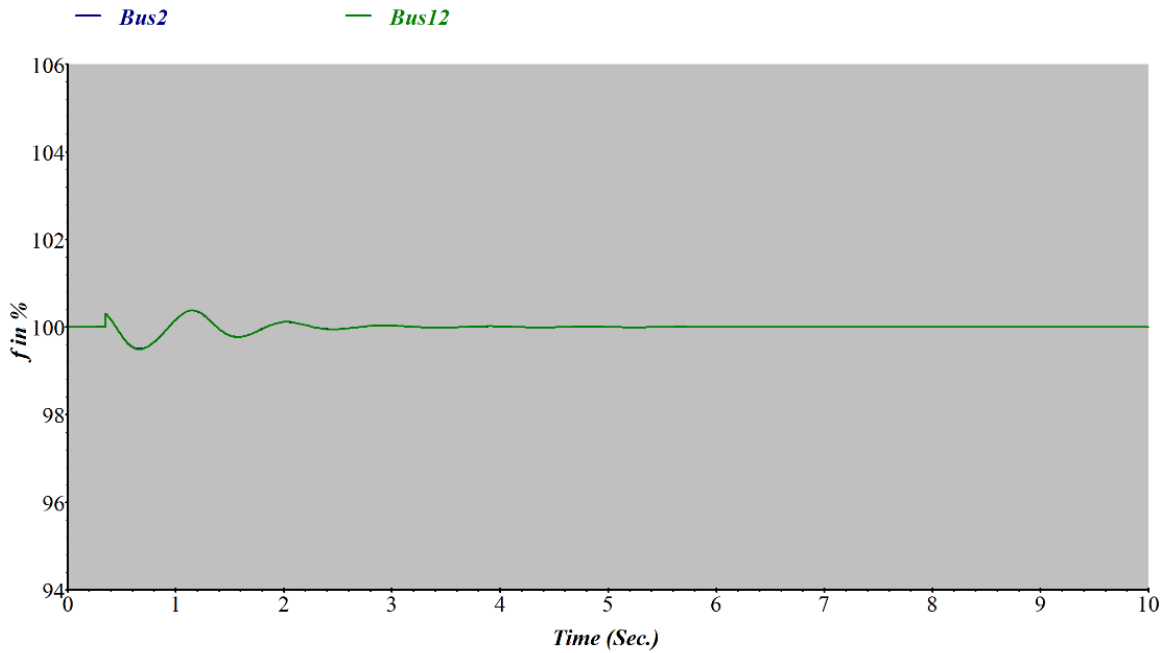


**Figure 4.20 Three phase short circuit at Bus 29, (c) Bus 2 and Bus12 frequency (%)**

**4.5.2.5 Three phase short circuit at line 11 results in tripping the load No 10 (7.222 MVA)**

The system is also stable after tripping load No 10 (7.222 MVA) after a fault on line 11.

Rotor angle and voltage plot are shown in Figure 4.21 (a) and (b).

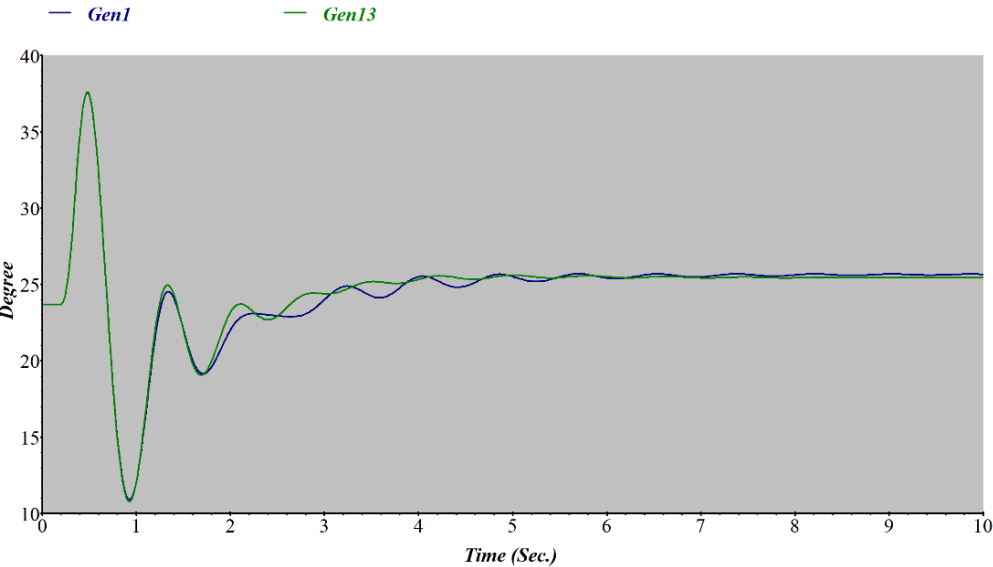


**Figure 4.21 Three phase short circuit at line 11, (a) Generators' absolute power angle**

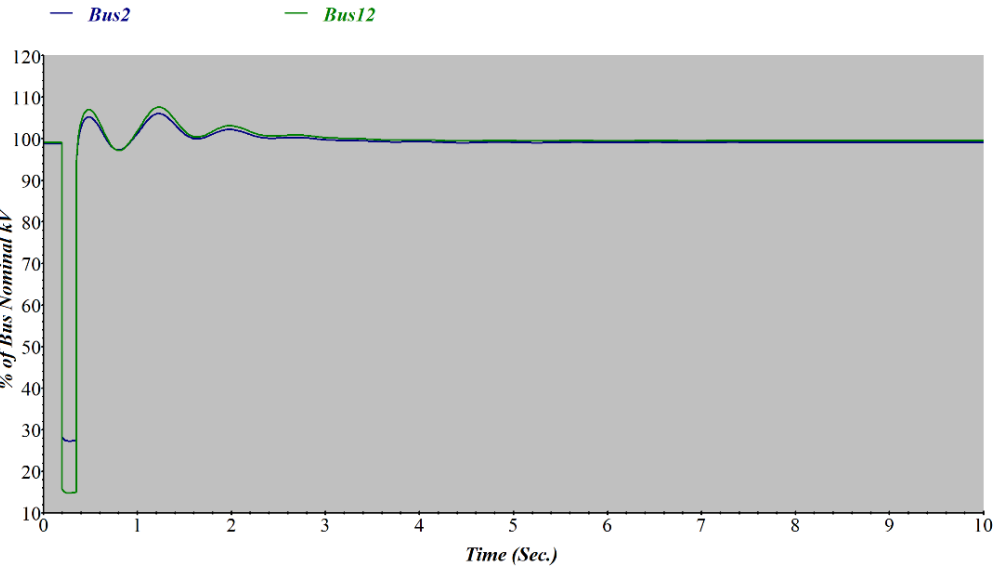


**Figure 4.21 Three phase short circuit at Bus 29, (b) Bus 2 and Bus12 voltage (%)**

**4.5.2.6 Power system stabilizer (PSS) performance during transient stability on the designed connected hybrid power system**

The (PSS) type PSS1A is employed in this hybrid power system to help with system stability. The difference between the system case with (PSS) and the system case without (PSS) can be clearly seen in Figure 4.22, which shows the rotor angle after a three-phase fault on bus 29 in both cases.

It can be clearly seen that PSS can quickly damp and improve the oscillation during transient stability.

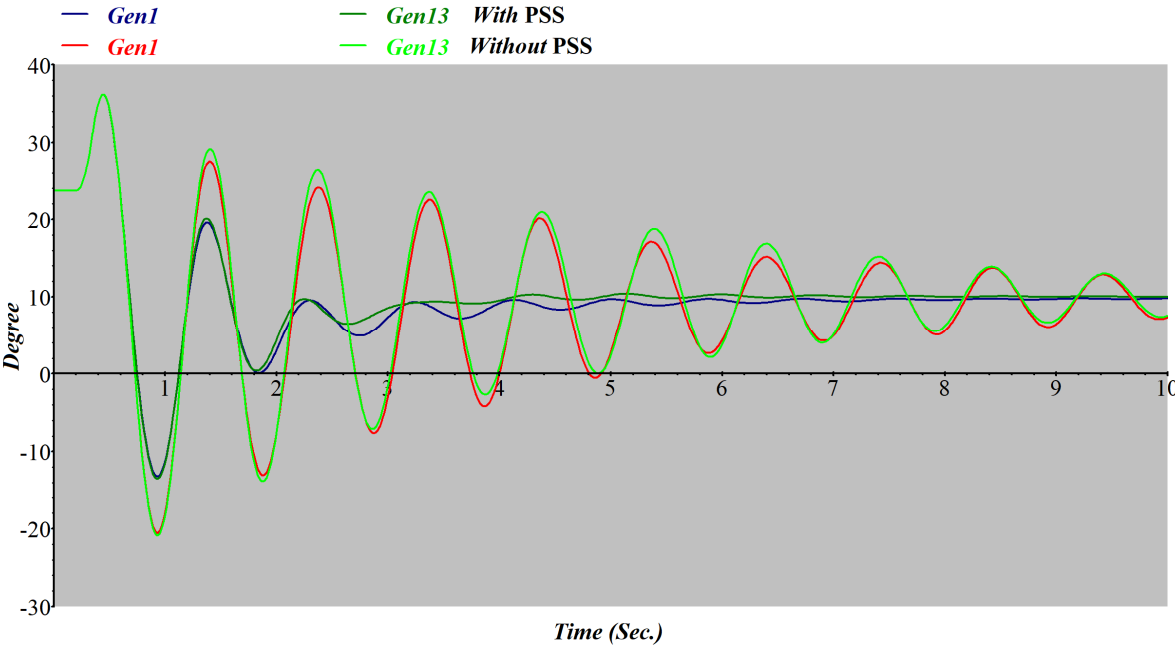


**Figure 4.22 Generators' absolute power angle with and without PSS after three phase short circuit at Bus 29**

**4.5.2.7 The performance of automatic voltage-magnitude-regulating transformer on the system during transient stability**

In case study 4.5.2.1 which is a trip of utility grid, the nominal voltage at bus 2 before the disturbance occurs was 0.987051 pu. The peak voltage at bus 2 after the disturbance was 1.11393 pu at 0.561 second and decreased to 1.03196 pu at 10 seconds. However, the nominal voltage at load bus 3 before the disturbance occurred was 0.997758 pu. The peak voltage at bus 3 after the disturbance was 1.12636 pu. and decreased to 1.00501 pu at 10 seconds. The voltage decreased to closer to the nominal value than bus 2 and also closer to the nominal value at bus 3 without using the automatic voltage-magnitude-regulating transformer, as illustrated in figure 4.23. (a) and (b). (a) shows voltage at bus 2 and load bus 3 with the automatic voltage-magnitude-regulating transformer and (b) shows voltage at bus 2 and load bus 3 without the automatic voltage-magnitude-regulating transformer. Figure 4.24 shows the voltage plot at all load buses.

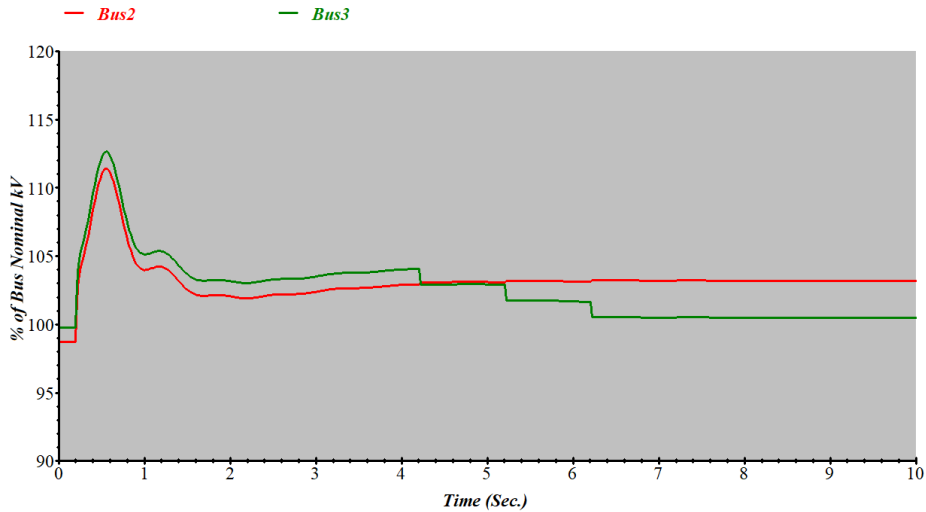


**Figure 4.23 (a) Voltages at bus 2 and load bus 3 with automatic voltage-magnitude-regulating transformer**

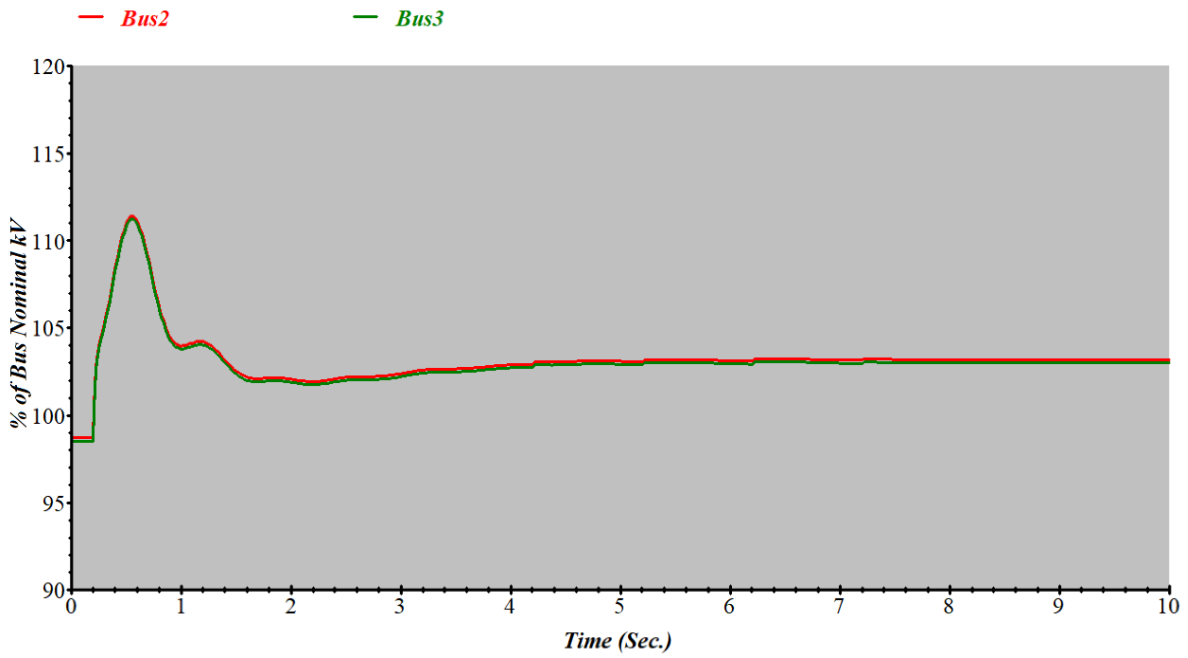


**Figure 4.23 (b) Voltages at bus 2 and load bus 3 without automatic voltage-magnitude-regulating transformer**

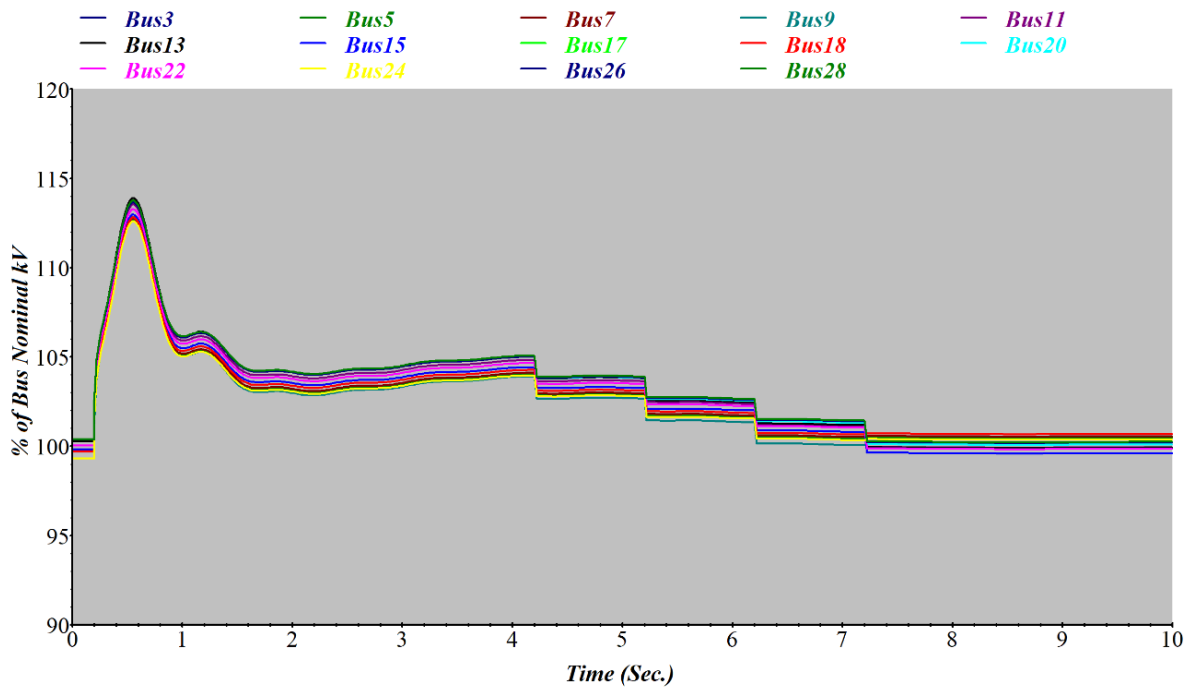


**Figure 4.24 Voltage plot at all load buses after trip of utility grid**

The automatic voltage-magnitude-regulating transformer helped to restore the voltage level to close to the nominal value during transient stability.

#### **4.6 Conclusion**

In this chapter, a hybrid grid connected power system with diesel generator, energy storage, and a large-scale PV system is designed at the proposed location in western Libya and connected to the power grid. Data have been collected for simulation to study the stability and impact of the designed hybrid power system, which has been sized as reported in chapter 3, into the existing distribution network in western Libya. However, this hybrid system is classified as an isolated network and can be hybrid grid connected.

From the simulation results, can be clearly seen that the rejection of the PV system does not have any negative impact on the system, since the load can be supplied by generator sets and an energy storage system. Also, rejection of the utility grid does not have any negative impact on the system, since the other power sources of the hybrid power system can produce plenty of energy to supply the loads.

Short circuit analysis was performed to study transient stability of the system. The objective of a transient stability study is to determine whether or not the machines will return to synchronous frequency with new steady-state power angles. The system frequency was stabilized by the generator governor and the exciter of the generator sets was able to restore voltage level. PSS can damp the rotor oscillation quickly. Using an automatic voltage-magnitude-regulating transformer can help to restore the voltage level to close to the nominal value during transient stability and improve power flow in the hybrid power grid.

## **Chapter 5**

### **5 Conclusion and Future Work**

#### **5.1 Conclusion**

This thesis proposed and designed a hybrid power system with energy storage on a real power grid with real grid data and loads in the western Libyan grid power system and improved its stability. The power sources of the hybrid power system are the PV system, ESS, and generator sets.

The study presented a steady-state stability analysis of the grid to ensure the stability of the grid before designing the hybrid power system. Reactive power has a major role in voltage stability. Q-V curve analysis is performed for monitoring voltage stability of load buses. This study is important for planning and designing a power system; the controllers in the system could behave incorrectly and cause the system to collapse if one bus in the system has negative Q-V sensitivities. The results show that all load buses are stable in the system. The designed shunt capacitor improved the voltage magnitude at all buses in the system and also reduced total MW and Mvar losses in the system. It reduced MVA loading on the transmission lines and transformers that are connected to the controlled buses which are bus 8 and bus 9. The transmission lines are between bus 2 and bus 8, and the transformers are connected to bus 9.

Designing a hybrid power system at a specific location requires a complete study of the available renewable energy sources at that location to design a suitable hybrid power system. Libya has a great potential of solar energy and wind energy; these resources vary from city to

city in Libya as Libya has a vast area. Wind speed in Bani Walid is not high enough. Therefore, designing wind turbines for a large power system is not feasible in that area.

The hybrid power system has been sized using Homer software for the best system optimization, with considering the temperature at the proposed location. The optimized system shows a large PV scale in that area. The results also include an important overview, different configurations and an evaluation of the performance of the power system. The results show that the COE is reduced to the lowest value using battery storage in the system, while using the other power sources without battery storage gives the highest COE. A comparison of using only generator sets and including renewable energy in the system has been done in chapter 3. The simple payback period is 9.02 years. This proves that including renewable energy in the system is feasible. The results also illustrate that the emissions are reduced 29% with using renewable energy in the system.

The designed approach has been scaled for different cases, as the optimization results are affected by variable inputs such as solar radiation, increasing loads and diesel price. It can be concluded that load growth and decreasing irradiance raise the COE. The PV and battery sizing are affected by the load growth. The irradiance sensitivities of -5%, 0%, 5% do not significantly affect battery sizing and have no effect on battery sizing at a diesel price sensitivity of 30% due to a high jump of the string price in such a large hybrid power system.

As renewable energy prices are decreasing and efficiency is improving every year, the results of the system optimization could be better, and the COE could be less in the future.

The configuration of the PV system has been done as well as the field design of the proposed PV system using AutoCAD software to calculate the required area for the PV system and cables' length. Cables' length is needed in ETAP software.

The designed hybrid power system is classified as an isolated network and can be grid connected to a hybrid power system. It has been analyzed using the Electrical Transient Analysis Program (ETAP) to study the impact of a large-scale PV system with battery storage and generator sets in a distribution network in Bani Walid. The analysis included power flow analysis, contingency analysis and transient stability analysis. Power flow has been improved using an automatic voltage-magnitude-regulating transformer, as presented in chapter 4. The disconnection of the PV or the utility grid does not have any negative impact on the system, since it can be supplied by the other sources in the system. The system has been tested for several disturbances (e.g., loss of a generation, short circuit with loss of a generation, and short circuit with loss of a load). The PSS was used in the system to help with system stability. The results show that the generator governor (Woodward UG-8) and the exciter (IEEE Type AC4) of the generator sets were able to recover the stability of the system and that PSS1A damped the rotor oscillation quickly.

The performance of OLTC is also presented in chapter 4. The results illustrated that OLTC improved power flow and helped to recover voltage level to close to the nominal value during transient stability.

## **5.2 Contribution**

This research contributes to the enhancement, increase and refocus of energy production across western Libya through the application of hybrid energy-producing systems and by

exploiting the benefits of local renewable energy systems in cities like Bani Walid. This research could also be implemented in cities across the world to benefit from their local renewable energy sources.

Stability analysis of the existing power grid with real data and loads in Western Libya has been performed using the PowerWorld Simulator and the results of this work were presented as a paper and published at a local NECEC conference in 2016 [52]. The proposed hybrid power system has been sized for best optimization of the system and the results and a comparison of different configurations as well as scaling the design approach for different cases have been presented in this thesis and will soon be published in a peer-reviewed journal paper. This research studied the impact of a large PV scale with ESS and generator sets in a real distribution network in Libya and improved the stability of the hybrid power system using Automatic OLTC. The PV system configurations have been done as well as the field design, using AutoCAD software for accurate results. A study of the performance of Automatic OLTC and the comparison between different cases have been done in steady-state stability, as well as the performance of automatic OLTC during transient stability, and the results will be published soon.

### **5.3 Future Work**

This thesis, demonstrates that additional work can be done for continuity. Controllers in generator sets can also be designed by using UDM as well as a master controller on the grid for transient stability analysis enhancement in hybrid power systems.

- Other energy storage options such as pumped hydro could be studied.

- Other large solar systems, e.g. a central receiver system, dish Stirling system and paraboloid reflector-based systems, could be studied for Libya.
- Economics of gas vs. oil-based generators can be studied and compared.
- Effects of dust on a PV system and dust cleaning methods can be studied and compared.

## References

- [1] Pittet, André. "An overview of technical aspects of mini-grids." (2013).
- [2] Verma, Rohit Kumar, S. N. Singh, and Alternate Hydro Energy Center. "A REVIEW OF MINI-GRID USED FOR ELECTRIFICATION IN RURAL AREA." American International Journal of Research in Science, Technology, Engineering & Mathematics 3.2 (2013): 140-144.
- [3] Mahapatra, Sadhan, and S. Dasappa. "Rural electrification: optimising the choice between decentralised renewable energy sources and grid extension." Energy for Sustainable Development 16.2 (2012): 146-154.
- [4] Peskett, Leo. "The history of mini-grid development in developing countries." Policy brief. Global Village Energy Partnership, London, UK (2011).
- [5] Inversin, Allen R. "Mini-grid design manual." (2000).
- [6] Rolland, Simon, and Guido Glania. "Hybrid mini-grids for rural electrification: lessons learned." Alliance for Rural Electrification (2011).
- [7] Maher NASR, Electric Power System of Libya and its Future., 2010.
- [8] Ramli, Naseem M., Salma AS Alarefi, and Stuart D. Walker. "Renewable power and microgeneration in Libya: Photovoltaic system sizing, wind, rainfall potentials and public response." Renewable Energy Congress (IREC), 2015 6th International. IEEE, 2015.
- [9] Khalil, Ashraf, and Ali Asheibe. "The Chances and Challenges for Renewable Energy in Libya." the Proceedings of the Renewable Energy Conference, Palermo. 2015.
- [10] T&D World. <https://www.tdworld.com/overhead-transmission/conflict-damage-and-reconstruction>. May 2017.

- [11] General Electricity Company of Libya. Annual Report, Report 2010.  
<http://www.gecol.ly/gecol/index.php>
- [12] Mohamed, Ahmed MA, Amin Al-Habaibeh, and Hafez Abdo. "Future prospects of the renewable energy sector in Libya." (2016).
- [13] Khalil, Ashraf, Zakariya Rajab, and Ali Asheibi. "The economic feasibility of photovoltaic systems for electricity production in Libya." The 7th International Renewable Energy Congress (IREC'2016), Hammamet, Tunisia. 2016.
- [14] GLOBAL SOLAR ATLAS. An innovation of the world Bank Group.2016.  
[www.http://globalsolaratlas.info](http://globalsolaratlas.info). Last access 2017.
- [15] KAMARUZZAMAN, ZETTY ADIBAH, AZAH MOHAMED, and HUSSAIN SHAREEF. "Effect of grid-connected photovoltaic systems on static and dynamic voltage stability with analysis techniques—a review." *Przeegląd Elektrotechniczny* 91.6 (2015): 134-138.
- [16] Kamaruzzaman, Zetty Adibah, and Azah Mohamed. "Dynamic voltage stability of a distribution system with high penetration of grid-connected photovoltaic type solar generators." *Journal of Electrical Systems* 12.2 (2016).
- [17] Katiraei, Farid, et al. "Modeling and dynamic analysis of a medium penetration PV-Diesel Mini-Grid system." presentation at the Proceedings of the 4th European Conference on PV-Hybrid and Mini-Grid. 2008.
- [18] Rikos, Evangelos, Stathis Tselepis, and Aristomenis Neris. "Stability in Mini-Grids with Large PV Penetration under Weather Disturbances: Implementation to the Power System of Kythnos." *PV-Hybrid and Mini-Grid 4th European Conference*. No. 1. 2008.
- [19] Lopes, L. A. C., et al. "PV hybrid mini-grids: Applicable control methods for various

- situations." IEA PVPS Task 11 (2012).
- [20] Al-Jadi, IM Saleh Ibrahim, M. A. EKhlal, and N. M. Krema. "Photovoltaic in Libya applications, and evaluation." Proceedings of the International Conference on Renewable Energy for Developing Countries. 2005.
- [21] Nassar, Yasser Fathi, and Abubaker Awidat Salem. "The reliability of the photovoltaic utilization in southern cities of Libya." Desalination 209.1-3 (2007): 86-90.
- [22] Aldali, Y., D. Henderson, and T. Muneer. "A 50 MW very large-scale photovoltaic power plant for Al-Kufra, Libya: energetic, economic and environmental impact analysis." International Journal of Low-Carbon Technologies 6.4 (2011): 277-293.
- [23] Aldali, Yasser, and Farag Ahwide. "Evaluation of A 50MW two-axis tracking photovoltaic power plant for AL-Jagbob, Libya: energetic, economic, and environmental impact analysis." International Conference on Environmental, Energy and Waste Management, UAE. 2013.
- [24] Saleh, Ibrahim M., Hamed M. Abufares, and Haitham M. Snousi. "Three-year performance evaluation of single junction amorphous solar cells grid-connected power station in Libya." Conference Papers in Science. Vol. 2013. Hindawi Publishing Corporation, 2013.
- [25] Mohamed, Ahmed MA, et al. "The significance of utilizing renewable energy options into the Libyan Energy Mix." Energy Research Journal 4.1 (2013): 15-23.
- [26] Mohamed, Ali Omar, and Abdulazez Hasan. "Effect of dust accumulation on performance of photovoltaic solar modules in Sahara environment." Journal of Basic and applied scientific Research 2.11 (2012): 11030-11036.
- [27] Roche, Robin. "Introduction to PowerWorld Simulator." Université de Technologie de

- Belfort-Montbéliard (2015).
- [28] THAKUR, NEHA PARSAI ALKA. "PV curve–Approach for Voltage Stability Analysis." *Information Technology 2012* (2015): 15.
- [29] Pakkiraiah, B., and G. Durga Sukumar. "Research Survey on Various MPPT Performance Issues to Improve the Solar PV System Efficiency." *Journal of Solar Energy* 2016 (2016).
- [30] Kawase, Masashi, Keiichi Okajima, and Yohji Uchiyama. "Evaluation of Potential Geographic Distribution for Large-Scale Photovoltaic System in Suburbs of China." *Journal of Renewable Energy* 2013 (2013).
- [31] Gairaa, Kacem, and Yahia Bakelli. "Solar energy potential assessment in the Algerian south area: Case of Ghardaïa region." *Journal of Renewable Energy* 2013 (2013).
- [32] Bonkaney, Abdoulatif, Saïdou Madougou, and Rabani Adamou. "Impacts of Cloud Cover and Dust on the Performance of Photovoltaic Module in Niamey." *Journal of Renewable Energy* 2017 (2017).
- [33] Ani, Vincent Anayochukwu. "Feasibility and Optimal Design of a Stand-Alone Photovoltaic Energy System for the Orphanage." *Journal of Renewable Energy* 2014 (2014).
- [34] Energypedia, Libya Energy Situation, [https://energypedia.info/wiki/Libya\\_Energy\\_Situation](https://energypedia.info/wiki/Libya_Energy_Situation), 2017
- [35] Khalil, Ashraf, and Ali Asheibe. "The Chances and Challenges for Renewable Energy in Libya." *the Proceedings of the Renewable Energy Conference, Palermo*. 2015.
- [36] James Diebel, Jacob Norda, Orna Kretchmer, Weather Spark, <https://weatherspark.com/y/74243/Average-Weather-in-Bani-Walid-Libya-Year-Round>,

- 2017.
- [37] Zhu, Honglu, et al. "Online Modelling and Calculation for Operating Temperature of Silicon-Based PV Modules Based on BP-ANN." *International Journal of Photoenergy* 2017 (2017).
- [38] NASA Atmospheric Science Data Centre, NASA Surface Meteorology and Solar Energy: Available from: <http://eosweb.larc.nasa.gov/>, Last Accessed 12th October 2017.
- [39] Okedu, Kenneth E., et al. "Optimization of Hybrid Energy Efficiency in Electrical Power System Design." *Energy Efficiency Improvements in Smart Grid Components*. InTech, 2015.
- [40] Paudel, Subodh, et al. "Optimization of hybrid PV/wind power system for remote telecom station." *Power and Energy Systems (ICPS), 2011 International Conference on*. IEEE, 2011.
- [41] Qi, Boyuan, and Jizheng Wang. "Fill factor in organic solar cells." *Physical Chemistry Chemical Physics* 15.23 (2013): 8972-8982.
- [42] Cubas, Javier, Santiago Pindado, and Carlos De Manuel. "Explicit expressions for solar panel equivalent circuit parameters based on analytical formulation and the Lambert W-function." *Energies* 7.7 (2014): 4098-4115.
- [43] Chaaban, Mohamed Amer, Lana El Chaar, and Mahmoud Alahmad. "An adaptive photovoltaic topology to overcome shading effect in PV systems." *International Journal of Photoenergy* 2015 (2015).
- [44] Goetzberger, Adolf, and Volker Uwe Hoffmann. *Photovoltaic solar energy generation*. Vol. 112. Springer Science & Business Media, 2005.

- [45] Electrical Technology <https://www.electricaltechnology.org/2014/12/advance-voltage-drop-calculator-voltage-drop-formula.html>. 2014.
- [46] Glover, J. Duncan, Mulukutla S. Sarma, and Thomas Overbye. Power System Analysis & Design, SI Version. Cengage Learning, 2012.
- [47] Afolabi, Olukayode A., et al. "Analysis of the load flow problem in power system planning studies." *Energy and Power Engineering* 7.10 (2015): 509.
- [48] Kundur, Prabha, et al. "Definition and classification of power system stability." *IEEE transactions on Power Systems* 19.2 (2004): 1387-1401.
- [49] Agber, J. U., P. E. Odaba, and C. O. Onah. "Effect of power system parameters on transient stability studies." *American Journal of Engineering Research* 4.2 (2015): 87-94.
- [50] Nallagalva, Swaroop Kumar, Mukesh Kumar Kirar, and Ganga Agnihotri. "Transient stability analysis of the IEEE 9-bus electric power system." *International Journal of Scientific Engineering and Technology* 1.3 (2012): 161-166.
- [51] Lee, D. "IEEE recommended practice for excitation system models for power system stability studies (ieee std 421.5-1992)." *Energy Development and Power Generating Committee of the Power Engineering Society* 95 (1992): 96.
- [52] Fathi Mosbah, Tariq Iqbal, Design and Analysis of A community Mini-grid Power System for Libya, presented at 25th IEEE NECEC conference 2016.

**Appendix A: Parameters of the governor Woodward UG-8 (UG-8)**

Parameter	Definition	Value	Unit
Mode	Droop or Isoch		
$A_d$	Permanent droop constant	58.2	rpm/in
$P_{max}$	Maximum shaft power	2.737	MW
$P_{min}$	Minimum shaft power	0	MW
$A_1$	Compensator constant	73.3	rad/sec
$A_2$	Compensator constant	0.195	rad/sec
$A_3$	Compensator constant	0.4	rad/sec
$B_1$	Ball head filter constant	4.2	
$B_2$	Ball head filter constant	110.3	
$C_1$	Governor drive ratio	1457	
$K_1$	Partial very high pressure turbine power fraction	1	deg./in
$T_7$	Engine dead time constant	0.15	sec
$T_8$	Fuel valve time constant	0.1	sec

**Appendix B: Parameters of the exciter IEEE Type AC4 - High-Initial-Response**

**Alternator-Supplied Controlled Rectifier Exciter (AC4)**

Parameter	Definition	Value	Unit
$VR_{max}$	Maximum value of the regulator output voltage	5.64	p.u.
$VR_{min}$	Minimum value of the regulator output voltage	-4.53	p.u.
$VI_{max}$	The value of excitation function at Efdmax	10	p.u.
$VI_{min}$	The value of excitation function at 0.75 Efdmax	-10	p.u.
$K_A$	Regulator gain	200	p.u.
$K_C$	Rectifier loading factor related to commutating reactance	0	p.u.
$T_A$	Regulator amplifier time constant	0.015	sec.
$T_B$	Exciter time constant	10	sec.
$T_C$	Regulator stabilizing circuit time constant	1	sec.
$T_R$	Regulator input filter time constant	0	sec.

**Appendix C: The parameters of power system stabilizer IEEE Type 1 PSS (PSS1A)**

Parameter	Definition	Value	Unit
KS	PSS gain	3.15	p.u.
$V_{STMax}$	Maximum PSS output	0.9	p.u.
$V_{STMin}$	Minimum PSS output	-0.9	p.u.
$V_{TMin}$	Terminal undervoltage comparison level	0	p.u.
$T_{DR}$	Reset time delay for discontinuous controller	0.2	sec.
$A_1$	PSS signal conditioning frequency filter constant	0	p.u.
$A_2$	PSS signal conditioning frequency filter constant	0	p.u.
$T_1$	PSS lead compensation time constant	0.76	sec.
$T_2$	PSS leg compensation time constant	0.1	sec.
$T_3$	PSS lead compensation time constant	0.76	sec.
$T_4$	PSS leg compensation time constant	0.1	sec.
$T_5$	PSS washout time constant	1	sec.
$T_6$	PSS washout time constant	0.1	sec.